DESIGN AND ANALYSIS OF PERMANENT MAGNET SYNCHRONOUS MOTORS

TIMOTHY A. LITTLE

Design and Analysis of

Permanent Magnet Synchronous Motors

by

Timothy A. Little, B.Sc.Eng.

A thesis submitted in partial fulfillment
of the requirements for the degree of
Master of Engineering

Faculty of Engineering and Applied Science
Memorial University of Newfoundland

March 1983

St. John's Newfoundland, Canada

ABSTRACT

The latest developments in high energy product permanent magnet materials have led to renewed interest in the permanent magnet (P.M.) synchronous motor. This is primarily due to the high efficiencies and power factors which may be obtained from the P.M. motor. If this device is to find its way into widespread industrial use, it is important that sufficient analytical skills be developed and detailed design information be transmitted to the motor design engineer, such that the inherent advantages of a P.M. motor are recognized and utilized.

This work, then, presents a detailed analysis of both the transient and steady state behavior of the P.M. motor. Included, as well, are the derivations of three of the important parameters of P.M. motors, namely direct axis reactance, quadrature axis reactance and open circuit voltage. The analysis is then used to predict transient and steady state performance with reasonable accuracy. Tested results of four prototype P.M. motors are presented in order to provide correlation with, and verification of, the analytical results.

Finally, a number of important parameter variations are undertaken, and important conclusions to the design, manufacture and testing of P.M. motors are presented.

ACKNOWLEDGEMENTS

The author acknowledges his dependence on Almighty God and His Son, Jesus Christ, by, and for whom all things consist, and the fear of whom is the beginning of all wisdom.

Further, I express my gratitude to Dr. M. A. Rahman, for his supervision and ever probing questioning. Throughout the duration of this work the technical and financial assistance of both N.S.E.R.C. and Canadian General Electric, in conjunction with P.R.A.I. Grant P-8003, are most appreciated.

Deserving recognition is also due Mrs. Ramona Raske for her meticulous care in typing this manuscript. Finally, to my wife and young family, without whose support and encouragement, this work would not have been completed, my sincere appreciation is expressed.

Table of Contents

LIST OF TABLES

LIST OF FIGURES

Glossary of Symbols

a	Parameter for determining permeability of motor steel
A_g	Air gap area per pole
A_{m1}	Area of magnet section 1 providing flux
A_{m2}	Area of magnet section 2 providing flux
b	Parameter for determining permeability of motor steel
B	Flux density
B_r, B_{ri}, B_{r1}, B_{r2}	Residual flux density of magnets
B_{m1}, B_{m2}	Operating flux density of magnets
B_g	Air gap flux density
B_f	Air gap flux density due to magnets
B_{f1}	Fundamental component of B_f
B_{ad}, B_{aq}	Air gap flux density due to armature currents on the direct axis and quadrature axes
B'_1, B'_2	Operating flux density on magnet faces due to armature currents only
BH_{max}	Maximum energy product of magnet material
BL1, BL2	Length of iron leakage paths; these may be different from the magnet lengths L_1 and L_2. They are defined in Figure 2.3b, page 30.
C_d	Direct axis reactance reduction factor
C_q	Quadrature axis reactance reduction factor
d	Direct axis, used as subscript or prefix

D	Diameter of rotor measured at the air gap
E_i	Internal voltage of motor
E_o	Generated back emf due to magnets
f	Frequency, normally 60 Hz
F_{dm}, F_{qm}	Direct and quadrature armature mmfs
g	Effective air gap length including Carter's coefficient and saturation factor. Subscript for air gap quantities.
h, h_1, h_2, h_3, h_d, h_q	Generalized variable for d-q transformation
h_i, h_1, h_2	Magnet dimensions
H	Magnetizing force
H_c	Coercive force of magnet material
H_g	Magnetizing force across air gap
H_f	Air gap magnetizing force due to magnets
H_{ad}, H_{aq}	Air gap magnetizing force due to armature currents on direct and quadrature axes
H_{m1}, H_{m2}	Operating magnetizing force on magnet sections 1 and 2
H_1', H_2'	Operating magnetizing force on magnet faces due to armature currents
H_q	Magnetizing force on quadrature axis steel path
HM1, HM2	One-half of the total height of the magnet sections 1 and 2 respectively. These are further defined on Figure 2.3b, page 30.
i	Current amplitude used in transient equations. Subscript for number of phases or leakage paths.

i_i, i_d, i_q, i_{2d}, i_{2q}	Current in various motor circuits
I	rms current magnitude for steady state equations
I_c	Total core loss current
I_{cd}, I_{cq}	Core loss current on direct and quadrature axis
IC1	Inertia constant for motor dynamics
I_d, I_q, $\overline{I}_d$, $\overline{I}_q$	Direct and quadrature axis currents and the core loss corrected equivalents
I_{fm}	Equivalent field current for magnet modelling
I_1, $\overline{I}_1$	Actual measured line current and core loss corrected variable
I, I_o, I_1, I_2	Solution values for Aitken delta-squared extrapolation technique
k	Waveform factor for d-q transformation
k_ℓ	Leakage factor
k_ω	Winding factor
k_1	Waveform factor for open circuit flux-density waveform
ℓ	Subscript for leakage quantities
ℓ_s	Length of stator core
L_d, L_q	Direct and quadrature inductance
L_{md}, L_{mq}	Direct and quadrature magnetizing inductance
L_{2d}, L_{2q}	Axis rotor inductance
L_1, L_2	Leakage inductance in stator and rotor
L1, L2, L3, L4	The magnet and bridge dimensions as defined in Figure 2.3b, page 30.

m	Number of stator phases
M	Inertia constant, same as IC1
N	Number of stator series turns per phase
P	Derivative operator p = d/dt
p	Number of poles
P_c, P_{core}	Power loss to iron core heating
P_e	Electrical power at air gap
P_{fw}	Friction and windage power loss
P_s	Shaft power
q	Quadrature axis, used as subscript or prefix
r	Rotor radius. Subscript for rotor quantities
R	Resistance or reluctance
R_g	Reluctance of the air gap
$R_{\ell 1}$, $R_{\ell m}$, $R_{\ell T}$, $R_{\ell 1}$, $R_{\ell 2}$, $R_{\ell 3}$	Reluctance of various leakage paths
R_q	Reluctance of quadrature flux path
t	Time
t_q	Thickness of quadrature flux path
T1, T2, T3, T4	The thickness of the iron leakage paths as defined in Figure 2.3b, page 30.
T_{cage}	Torque due to rotor cage
T_L	Load torque
T_m	Total motor torque

T_{mag}	Torque due to presence of magnets
v	Voltage amplitude used in transient equations
v_d, v_q, v_1, v_2, v_3	Various axis or phase voltages
V, V_m	rms and peak value of applied stator voltage
V_d, V_q	Resolved d and q axis voltages
W_i	Stator input power
X_d, X_q	Direct and quadrature reactance
X_{md}, X_{mq}	Direct and quadrature magnetizing reactance
X_1, X_2	Stator and rotor leakage reactance
β	Geometrical factor for magnet leakage
β_p	Pole arc
β_q	Saturation factor for quadrature axis
δ	Torque or load angle
δ_i	Internal torque angle
δ_o	Measured no load torque angle
Θ, Θ_r	Angular displacement
λ	Flux linkage
λ_1, λ_2, λ_3	Flux linkage of stator phases
λ_d, λ_{2d}, λ_q, λ_{2q}	Stator and rotor flux linkages on direct and quadrature axis
μ	Permeability of magnetic materials
μ', μ'_1, μ'_2	Recoil permeability of magnet sections

τ_p	Pole pitch
ϕ	Magnetic flux. Power factor angle.
ϕ_{aq}, ϕ_q	Quadrature axis flux from armature in air gap and rotor iron
$\phi_{\ell 1}$, $\phi_{\ell 2}$, $\phi_{\ell 3}$, $\phi_{\ell 4}$	The iron leakage fluxes of the four paths defined in Figure 3.2a and b, page 30.
$\phi_{\ell I}$	The sum of iron leakage fluxes ($\phi_{\ell I} = \phi_{\ell 1} + \phi_{\ell 2} + \phi_{\ell 3} + \phi_{\ell}4$)
$\phi_{\ell m}$	The leakage flux which is established through the magnet sections as defined by Figure 2.3a and b, page 30
$\phi_{\ell T}$	The total leakage flux (the sum of $\phi_{\ell m}$ and $\phi_{\ell I}$)
ϕ_{mT}	Total flux from magnets
ϕ_g	Flux crossing the air gap
ϕ_r	Quadrature axis flux in the rotor iron
ϕ, ϕ_i	Terminal and internal power factor angle
ω	Angular velocity
ω_r	Rotor speed
ω_o	Synchronous speed

1.0 INTRODUCTION

1.1 General Introduction

In recent years a changing technology and an increasing demand for high efficiency devices has sparked renewed interest in the permanent magnet motor. Like so many other technological innovations, the permanent magnet (hereafter abbreviated P.M.) motor is not new but another application waiting for the right economic and technical climate for it to be a widely accepted device. Its use with frequency controlled inverter supplies is well suited to meet many industrial drive requirements. Coupled with this are the inherent high efficiency and high power factor characteristics which make the P.M. motor an interesting and economically justifiable alternative to both the standard synchronous and induction motors in many applications.

P.M. motors, although they come in many and various forms, all use the same concept of employing permanent magnets in the rotor to provide a constant level of excitation flux. By contrast, the conventional synchronous motor derives its excitation from a wire wound coil on the rotor, fed through slip rings, from a separate D.C. supply. Thus the P.M. motor eliminates the need for a slip ring and brush gear assembly and its associated maintenance, as well as the need for a separate power supply. Upon comparing the P.M. motor with its induction motor counterpart, the P.M. motor has two major advantages: (1) a major portion of the magnetizing flux is supplied from the P.M.'s rather than the stator winding, thus an increased power factor results; and (2) because of synchronous operation, the slip losses associated with the induction rotor copper bars are absent, thus higher efficiencies are obtained.

One disadvantage associated with the permanent magnet synchronous motor is that the field flux, provided by the magnets, cannot be turned off. This causes difficulties in the run-up and synchronization stages, for the magnet flux produces a braking torque as the fully excited rotor generates a voltage against the source of applied voltage. This torque, shown in comparison with the rotor cage torque in Fig. 1.1, reduces the motor's overall ability to accelerate and synchronize a load, and can cause an asynchronous limit cycle with large associated torque and current pulsations.

The effects of this disadvantage can be minimized by a proper knowledge of operating principles and use of design variations, thus with inherent advantages the motor yields a useful new alternative for motor drives. The purpose of this research work, then, is to shed light on which motor parameters and design procedures are most effectively altered in order to produce an optimum design, and also how to tailor the performance of a P.M. motor to meet a given application.

1.2 History of Design

Considering that the design of P.M. motors is very closely linked with the properties of the magnets used in the design, it will be useful to review a few basic principles of permanent magnet applications.

1.2.1 Permanent Magnet Materials

Permanent magnets have been used in various applications for over 4,000 years, since the first compasses were made; but it has only been since the late nineteenth century, when the relationships between electricity and magnetism were formulated, that permanent magnets came into

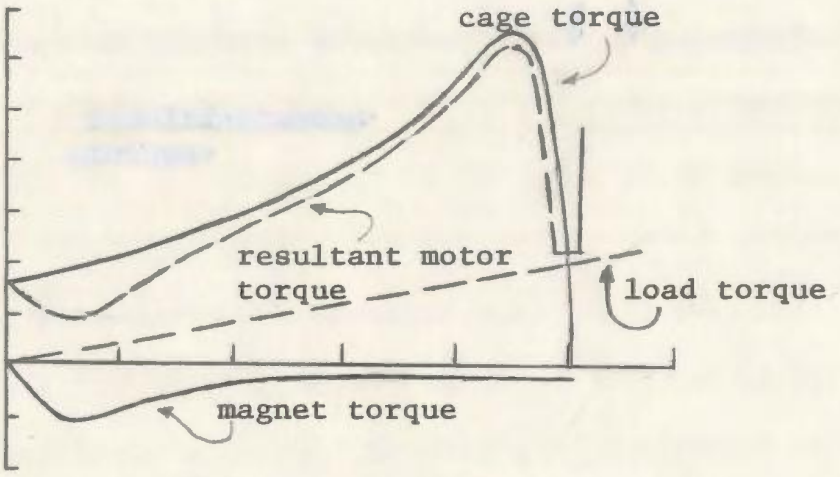

a) Small magnet flux

b) Large magnet flux

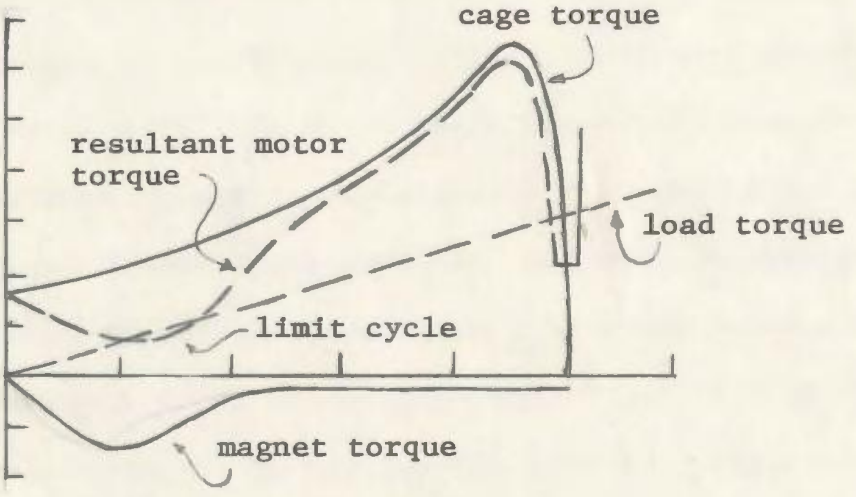

Figure 1.1 The effects of magnet brake torque on synchronizing capability

widespread use. The extent to which magnets have been used in motor and generator applications has been directly related to the advances of magnet technology. One of the most important early developments was the introduction of a series of carbon-free, precipitation hardened magnet alloys of which the ALNICO family is the most outstanding. The introduction in 1940 of the domain-oriented ALNICO V alloy climaxed a decade of phenomenal progress in permanent magnet materials [1]. However, both materials and processing are important in the performance characteristics of permanent magnets. Continued improvements of the ALNICO family were obtained by the use of both domain and grain orientation, thus producing the first anisotropic magnets. Previously, permanent magnets had been isotropic (i.e. the magnetic properties equal in all directions), but the anisotropic (i.e. the magnetic properties are optimum in a single predetermined direction) improvements allow major advances in the properties of permanent magnets. Three major figures of merit are commonly used to describe any permanent magnet [2], namely (1) Residual Flux Density (B_r) -- the magnitude of magnetic field remaining in a previously saturated magnetic material having removed all external fields, measured in Tesla; (2) Coercive Force (H_c) -- the external magnetic field required to reduce to zero the magnetic flux density within the material, measured in ampere turns per meter; and (3) Maximum Energy Product (BH_{max}) -- the point of operation wherein the magnet applies its maximum energy of field on its surrounding medium, measured in joules per cubic meter. Figure 1.2 shows a typical ALNICO V demagnetization curve illustrating each of these three figures. As can be seen from the figure, the ALNICO group

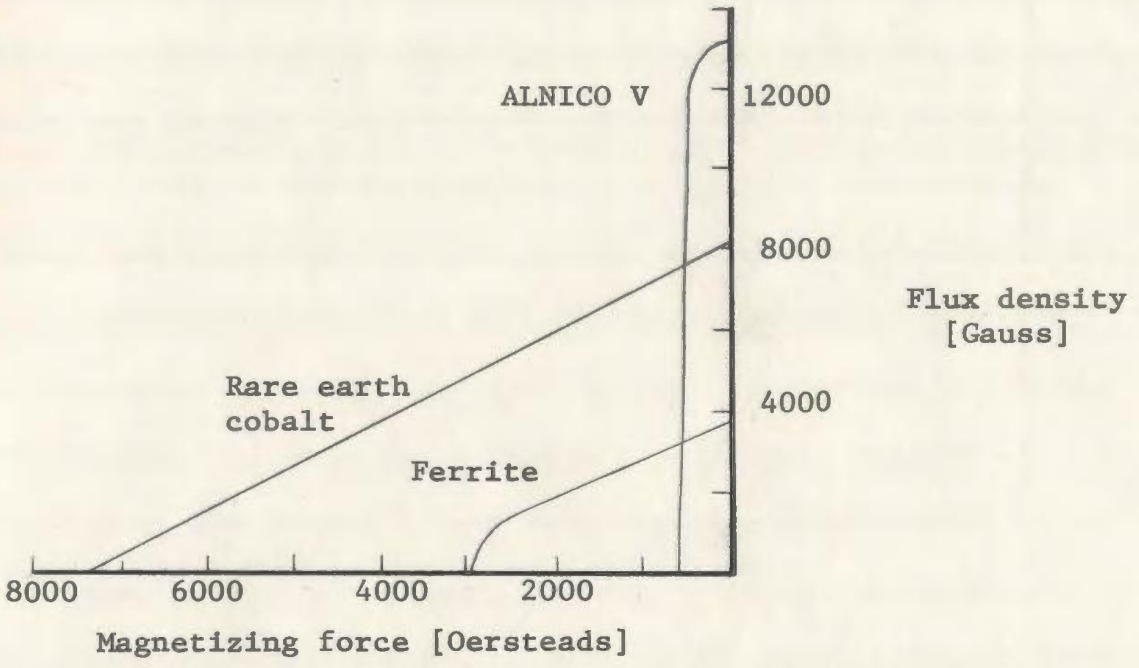

Figure 1.2 Demagnetization curves for various materials

Table 1.1 Properties and Cost of Permanent Magnet Materials

	B_r		H_c		BH_{max}		Approx. Cost
Material	(T)	(Gauss)	(kA/m)	(Oe)	(kJ/m^3)	(MGOe)	($/lb.)
Alnico 5	1.28	12800	50.90	639.6	43.76	5.61	8.50
Alnico 8	0.92	9200	127.30	1600.0	47.76	6.13	11.00
Fe-Cr-Co	1.35	13500	79.57	1000.0	63.66	8.17	4.00
Ceramic 5	0.38	3800	183.00	2300.0	27.85	3.57	1.50
Ceramic 8	0.385	3850	238.70	3000.0	27.85	3.57	1.75
Mn-Al-C	0.56	5600	238.70	3000.0	59.68	7.66	2.00
$Co_{17}R_2$	1.1	11000	397.90	5000.0	238.70	30.64	21.50
Co_5Sm	0.86	86000	636.6	8000.0	143.24	18.39	26.00

have very high residual flux density but are extremely susceptible to demagnetization forces.

Continued progress in P.M. materials produced the ferrite, or ceramic magnets, such as barrium ferrite of the early 1960's with very much higher resistance to demagnetization but with a corresponding decrease in residual flux density, also shown in Fig. 1.2. A further leap in magnet technology was taken with the introduction of the rare earth cobalt alloys in the early and mid 1970's. The magnets resulting from the combination of a rare earth transition element, usually sumarium or yttrium, and cobalt have vastly superior resistance to demagnetization and an energy product, an order of magnitude greater than the best ALNICO alloys. A typical rare earth cobalt demagnetization curve is shown in Fig. 1.2. The drawback still continues to be a lower residual flux density even though the new alloys provide a B_r of up to 75-80% of the residual induction obtained from the ALNICO's. As magnetic technology continues to advance, new magnet materials and processes will appear yielding much higher residual flux densities, coercive forces, and energy products, thus enhancing P.M. motor applications. Table 1.1 lists a variety of magnet compositions available today, comparing their demagnetization qualities as well as a price index.

One of the main factors contributing to the high price of R.E.Co. magnets, as seen in Table 1.1, is the instability of supply of cobalt. In mid 1978 political insurgents disrupted cobalt mining in Zaire, causing shock waves throughout the cobalt industry and causing cobalt prices to more than double in that year alone. Zaire produces over half

of the world's supply of cobalt [3]. Cobalt specialists at the U.S. Bureau of Mines state that prospects are good for more readily available cobalt at more reasonable prices over the long term, i.e. 1985 and beyond. This is primarily due to the substitution of more readily available materials for heavy usage cobalt applications and an increase in "at home" cobalt production. Thus the future looks good not only for reasonable rare earth magnet costs but for continued technological advances in permanent magnet materials.

1.2.2 Early Designs

Because of the low coercitivity of the ALNICO magnets, the early P.M. motor designs, larger than the fractional horsepower range, were constrained to have very large soft iron pole pieces surrounding the magnets and relatively thick magnets to prevent demagnetization. In contrast, the high residual flux density available allowed the magnet area facing the airgap to be smaller than the airgap area itself in order to get proper working fluxes. As magnet development proceeded and higher values of coercive force were obtained, the magnets were left more and more exposed to the demagnitization forces of the armature mmf. The low B_r of the ceramic magnets required "flux squeezing" or "throttling" designs to boost the airgap flux to sufficient levels. Fig. 1.3 shows several of the techniques used for increasing the airgap flux density level [4,5,6]. These flux squeezing techniques are still used with the rare earth magnets in order to minimize the required volume of magnet. Even with the "throttling" approach, the low values of B_r prevented the ceramic magnets of the 1960's from ever becoming popular for P.M. motor applications.

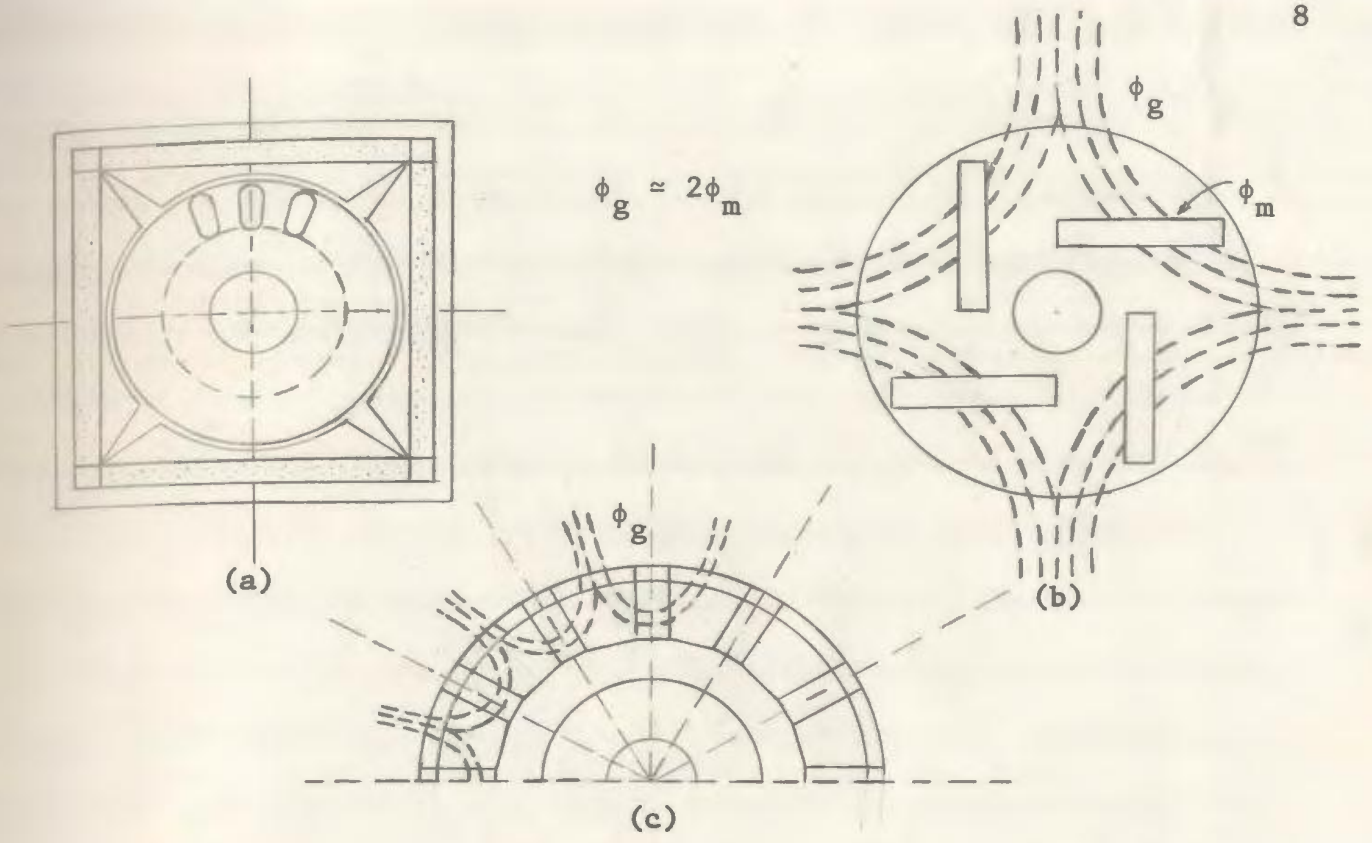

Figure 1.3 Various flux throttling techniques

g - air gap

β_p - pole pitch

L_1 - length of interior magnet

L_2 - length of peripheral magnet

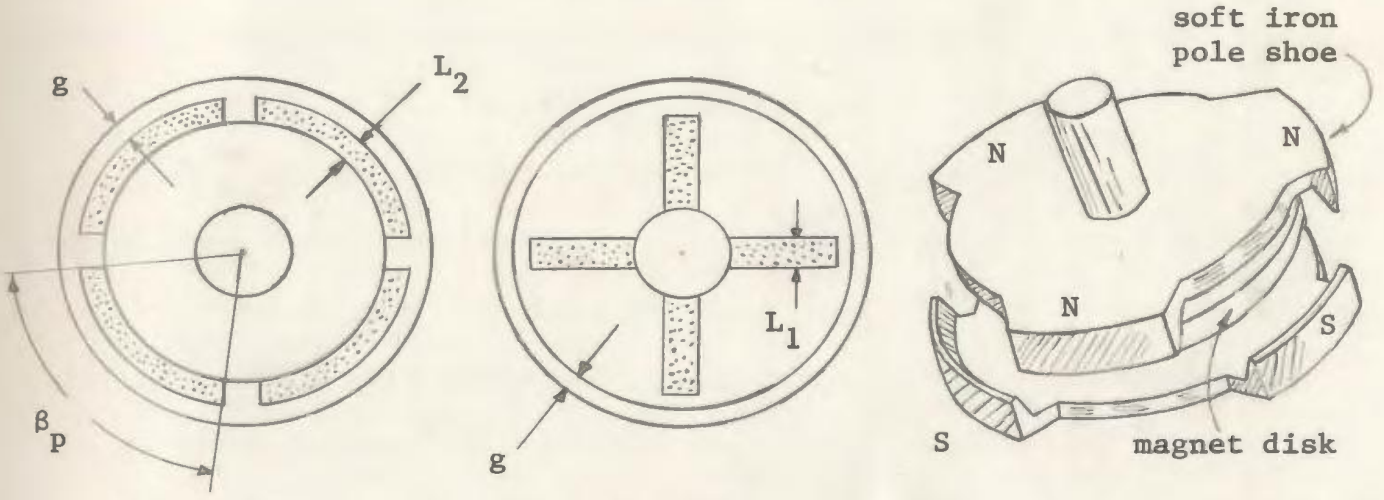

(a) peripheral (b) interior (c) claw pole

Figure 1.4 Basic P.M. motor design types

1.2.3 Modern Designs

With the advent of high energy, rare earth cobalt magnets, the higher residual flux density, combined with the large coercive force, has reduced the total magnet volume that is required for a motor application. In order to achieve a workable operating flux, it is required that the magnet area be nearly equal to the airgap area; but because of the high coercive force, a very thin magnet can withstand the full voltage starting demagnetization forces. Another feature of the modern P.M. motor design is the use of "flux barriers," that is, thin airgap slots in the rotor used to direct the magnet flux away from leakage paths onto the stator winding. Thus, most of the modern designs are characterized by their similarity to the reluctance motor. Most designers have attempted to include a large variation in the reactance of the two axis (i.e. X_d and X_q), with the P.M. motor usually having the characteristic of the quarature axis reactance larger than the direct axis reactance. This is contrary to the normal wire wound synchronous motor in which the value of X_q is typically 50 to 60% of the value of X_d for the salient pole version.

Whether the design follows that of the reluctance motor or not, there have evolved three motor design configurations for the P.M. motor [7]. These are: (1) the peripheral type -- these tend to have magnets that follow the rotor periphery and are magnetically oriented in a radial direction; (2) the interior type -- these tend to have magnets aligned radially with their axis of magnitization in a circumferential direction; and (3) claw pole type -- these are magnetic disks alligned with an axial direction of magnetization and having soft iron

pole pieces in a claw arrangement giving the pole configuration. Fig. 1.4 shows these three design types.

Like its wound rotor counterpart, the P.M. synchronous machine has no starting torque of its own and therefore requires some other means of starting. Most modern designs use some form of induction squirrel cage in order to accelerate the rotor and load to a sufficient speed whereby the magnets can synchronize the load. Although an induction cage is the most commonly used means of starting, other methods such as hysteresis rings have been investigated. As well, a frequency controlled power supply can be used to eliminate the need for a squirrel cage altogether, by ramping the frequency at a rate such that the rotor stays in synchronism throughout the run-up period. The designs studied in this work have interior magnets oriented radially and require a squirrel cage for starting torque.

1.3 Literature Review

As mentioned before, the interest in P.M. motors followed directly the progress in permanent magnet materials. This is also evident in the amount of publications dealing with P.M. machines. The first series of publications dealing with the use of permanent magnets in machines was in the late 1940's, just after the domain oriented ALNICO's were introduced for industrial use. The first mention of using P.M. materials for motor or alternator use was by Merril [8], and later by Saunders and Weakly [9]. These first designs were usually single castings attached to a shaft with no damper bars or laminated pole shoes. The first use of magnets in a large alternator was a 75KVA generator built by the U.S. Engineer Research and Development Laboratory,

a division of the U.S. Armed Forces, and reported by Brainard [10] and Strauss [11] in some detail. Some design considerations for fractional horsepower, claw pole type motors were presented by Hershberger [12], but it was Merrill [13] who made the first significant motor contribution in his paper detailing some of the work done by General Electric Co. and their Permasyn line of P.M. motors. He is the first to present the idea of using properly shaped and sized flux barriers, primarily to prevent demagnitization of the ALNICO magnets, but used in more modern designs to direct the magnet flux to the most useful path. It is most significant to note the comments of Merrill [13] in the discussion section of his paper where he predicts in what direction magnet technology needs to improve in order to improve the motor's performance. Two comments worthy of note come from that discussion: (1) The first from Alger [14] who states that the future of P.M. motors depends to a high degree on the properties and costs of P.M. materials. This comment has been proven out, for it is only the present P.M. material properties and the present economic climate which have made the P.M. motor a feasible device. (2) The second is Merrill's comment that if new magnets are produced with greater energy products than the ALNICO types, because of an increased coercive force, retaining the residual magnetism, the improvement in output, power factor and efficiency would be remarkable. These comments highlight the difficulties of the early designs in which high magnet cost and low coercive force were the major problems holding back widespread industrial use of P.M. motors. Also, they predict the major reasons for wanting larger and better P.M. motors to be higher power factor and efficiencies. J.F. Douglas [15] made a

further contribution to the P.M. motor technology with his performance evaluation using current-loci techniques. The first use of two axis theory in the performance calculations of P.M. motors came after the production of ferrite magnets and was introduced by Volkrodt [16] of Siemens and shortly thereafter by Cahill and Adkins [17] in late 1962. The barrium-ferrite magnets did not become a serious contender for P.M. application, and publications on P.M. machines virtually silenced for almost 16 years with very few exceptions. By this time the rare earth cobalt magnets had been introduced, and consequently, from 1978 and after, a large number of papers started to appear and have continued till the present. In Europe the most notable works have come from K.G. Binns, M.A. Jabar et al [4, 18-24], with a series of papers dealing with several hybrid permanent magnet-reluctance type designs, as well as many patents [25-28]. Also Weh and Boules [29-31] have made significant contributions to the disc type P.M. synchronous machine. Very few publications have emerged from Japan with the notable exception of Miyashita et al [32] from Hitachi, whose finite element techniques show good correlation between computed and predicted flux waveforms. In the U.S.A. the major effort in P.M. research has come from General Electric's Corporate Research and Development group at Schenectady, New York, with V.B. Honsinger [33-35] making the most notable advances in his presentation of the mathematics necessary for computer prediction of performance and parameters. Honsinger's work [34] was the first major presentation on asynchronous or transient operation. Others of that group, including T.J.E. Miller [36, 37] and Richter [5, 38], have made contributions in the P.M. motor field. Peter Campbell [39, 40]

has joined with D'Angelo [41] and Chari in advancing the finite element technique for axial field P.M. machines. One of the primary applications for P.M. generators has been the higher frequency aeronautical use, because of the reduced size and weight. Thus, the U.S. Air Force shows continued interest in P.M. machines as noted by recent publications by W.J. Borger [42, 43]. In Canada, M.A. Rahman et al. [7, 44, 45] have been the most outstanding with a number of papers dealing with energy efficiency and design reviews and more recently on P.M. transient simulations. G.R. Slemon et al. [46, 47] have done some work with P.M. motors also, mostly dealing with inverter drives and operations using P.M. devices.

So, as it can be seen, until very recently only the bare groundwork had been laid for analysis and design of P.M. motors, and out of that most recently published, very little involves parameter variations or optimizations which are critical to a properly designed machine.

1.4 Scope and Outline of Proposed Work

Having reviewed the history of P.M. motor design and the necessary magnetic materials in order to get a general understanding of the state of the art of P.M. synchronous motors, it is now appropriate to deal more fully with the scope of the present work. It is the objective of this research work to determine what features and motor parameters are the most important in the design of a P.M. motor, and how they can be calculated and used in order to build a P.M. motor given only its application specifications (i.e. load torque, speed, voltage, etc.). In order to do this it is important to look at the transient behavior of the motor to ensure that a good trade-off has been achieved between

steady state performance and run-up response. Finally, several prototypes have been built and these will be examined in some detail, both in transient and steady state performance, to verify the analytical results.

The following is an outline of the remaining chapters of this report: Chapter 2 presents the basic theory of operation of the P.M. motor. It begins with the full transient behavior as described by the system differential equations, then reduces these equations to steady state operation by equating the derivatives to zero and using the appropriate constants. From there the three important parameters X_d, X_q and E_o are described and derived using the magnetic circuit approach. Chapter 3 details how the equations derived in chapter 2 are solved by numerical techniques. Following that the design dimensions and parameters of the prototype motors are detailed, and then these figures are used to calculate motor performance, in both run-up and steady state modes. Finally, a summary of the computed results is shown, highlighting the critical parameters.

Chapter 4 presents the important details of the various tests conducted on the four prototype P.M. motors. This includes testing for various motor parameters as well as transient and steady state performance. A brief discussion on the difficulties related to P.M. motor testing is also included. Chapter 5 shows the correlation between computed and tested results, giving confidence in the analytical models. A section showing a number of variations of important motor parameters and the effects on performance is included in this chapter as well as a highlight of the major design features. Chapter 6 concludes the work,

restating the most important conclusions gained by the work of the previous chapters. Finally, recommendations for further study of P.M. machines are given.

2.0 THEORY OF OPERATION

2.1 Transient Behavior

One convenient way of dealing with the theory of operation for P.M. motors is to consider the complete transient behavior and then reduce these equations to examine the steady state case. This procedure allows a maximum understanding of the various phenomena associated with P.M. motors and will be the method used in this chapter.

The standard two axis theory with fixed rotor reference frame will be used. Analysis will be given for the 3-phase case since the experimental work was conducted on 3-phase motors, and since this class of motor is the most likely candidate to implement the P.M. motor on the industrial level. The analysis is similar for 1- or 2-phase motors. In transforming from the three phase variables to the fixed rotor d-q axis variables, the following are the transformation equations [48] where h can be either voltage (v), current (i), or flux linkage (λ).

$$h_d = k\left[h_1 \text{ Sin } \theta_r + h_2 \text{ Sin } (\theta_r - 2\pi/3) + h_3 \text{ Sin } (\theta_r - 4\pi/3)\right] \quad (2.1a)$$

$$h_q = k\left[h_1 \text{ Cos } \theta_r + h_2 \text{ Cos } (\theta_r - 2\pi/3) + h_3 \text{ Cos } (\theta_r - 4\pi/3)\right] \quad (2.1b)$$

where θ_r is the angular displacement of the rotor.

The constant k is associated with the waveform used in the analysis: if one uses the rms values of the phase variables (v, i, λ) then k is given as $\sqrt{2}/3$; conversely if one uses the maximum value of the sinusoidal waveform then k is given as 2/3. In this analysis the rms quantities will be used, therefore $k = \sqrt{2}/3$. Consider the derivative of the quadrature axis flux linkage obtained by differentiating equation 2.1b

with h replaced by λ (i.e. $h_q \rightarrow \lambda_q$, $h_1 \rightarrow \lambda_1$, etc.):

$$\frac{d\lambda_q}{dt} = -k\left[\lambda_1 \operatorname{Sin}\theta_r \frac{d\theta_r}{dt} + \lambda_2 \operatorname{Sin}(\theta_r - 2\pi/3)\frac{d\theta_r}{dt} + \lambda_3 \operatorname{Sin}(\theta_r - 4\pi/3)\frac{d\theta_r}{dt}\right] \qquad (2.2a)$$

$$+ k\left[\frac{d\lambda_1}{dt}\operatorname{Cos}\theta_r + \frac{d\lambda_2}{dt}\operatorname{Cos}(\theta_r - 2\pi/3) + \frac{d\lambda_3}{dt}\operatorname{Cos}(\theta_r - 4\pi/3)\right]$$

Equation 2.2a can be simplified by considering its two terms independently. To simplify the second bracketed expression, an alternate form for $d\lambda_i/dt$ is required; this comes from the phase voltage equations. These equations are:

$$v_i = \frac{d\lambda_i}{dt} + i_i R_1 \qquad i = 1,2,3;\ R_1 \text{ is the stator winding resistance per phase} \qquad (2.2b)$$

rearranging yields

$$\frac{d\lambda_i}{dt} = v_i - L_i R_1 \qquad i = 1,2,3 \qquad (2.2c)$$

The second expression of 2.2a is in the form of equation 2.1b and using the substitution of equation 2.2c it is easily simplified. Similarly, the first term of equation 2.2a is in the form of equation 2.1a where h_i is replaced by λ_i. Using these simplifications the total equation 2.2a can be written

$$\frac{d\lambda_q}{dt} = -\lambda_d \frac{d\theta_r}{dt} + v_q - i_q R_1 \qquad (2.3)$$

Now using the p operator for d/dt and noting that $\frac{d\theta_r}{dt} = \dot{\theta}_r = \omega_r$ we write the voltage equation for the q-axis:

$$v_q = p\lambda_q + i_q R_1 + \lambda_d \omega_r \tag{2.4a}$$

Following a similar procedure the d-axis voltage equation is:

$$v_d = p\lambda_d + i_d R_1 - \lambda_q \omega_r \tag{2.4b}$$

It is assumed that the actual phase voltages are balanced and given by:

$$\left.\begin{aligned} v_1 &= V_m \text{ Cos } \omega t \\ v_2 &= Vm \text{ Cos } (\omega t - 2\pi/3) \\ v_3 &= Vm \text{ Cos } (\omega t - 4\pi/3) \end{aligned}\right\} \tag{2.5}$$

Substituting equations 2.5 into 2.1a and b, yields:

$$\left.\begin{aligned} v_d &= - (3k\ Vm/2) \text{ Sin } (\omega t - \theta_r) \\ v_q &= + (3k\ Vm/2) \text{ Cos } (\omega t - \theta_r) \end{aligned}\right\} \tag{2.6}$$

Substituting the value of $k = \sqrt{2}/3$, using rms values for V and noting that $\omega t - \theta_r$ is the torque angle δ, equation 2.6 is written:

$$\left.\begin{aligned} V_d &= - V \text{ Sin } \delta \\ V_q &= V \text{ Cos } \delta \end{aligned}\right\} \tag{2.7}$$

Equations 2.4 and 2.7 combine to give the stator voltage equations. To obtain the rotor voltage equations it is noted that there is no forcing voltage in the rotor but only the induced emf in the rotor cage winding and the rotor resistance drop, thus the rotor voltage equations are:

$$\left.\begin{aligned} 0 &= \frac{d\lambda_{2d}}{dt} + R_{2d}\, i_{2d} \\ 0 &= \frac{d\lambda_{2q}}{dt} + R_{2q}\, i_{2q} \end{aligned}\right\} \qquad (2.8)$$

where the subscript 2 refers to a rotor quantity.

The above equations include the assumption of only two rotor circuits, one on each of the d and q axis. Actually the rotor cage resistance varies with every pair of cage bars and the rotor angle (θ), but the proper choice of direct and quadrature axis rotor resistances (R_{2d} and R_{2q}, respectively) gives sufficiently accurate numerical solutions, and the analysis is greatly simplified.

Having established the voltage equations for the direct and quadrature axis in both rotor and stator, the other necessary equations to deal with transient behavior are the mechanical equations as follows:

$$\frac{d\delta}{dt} = \omega_o - \omega_r \qquad (2.9)$$

$$\frac{d\omega_r}{dt} = \frac{1}{M}(Tm - T_L) - \frac{B}{M}(\omega_r) \qquad (2.10)$$

where ω_o is the synchronous speed and T_m and T_L are the available motor and applied load torques, respectively.

In equation 2.10 it can be assumed that the friction constant term, B, is small with respect to the other terms, and therefore can be neglected. Upon observing equations 2.4, 2.8, 2.9 and 2.10, it is convenient to choose the four flux linkages and the rotor torque angle and speed as the state variables. Thus, with only slight rearrangement all the equations are in standard format for solving numerically. Since flux

linkages are not measurable quantities, a number of secondary quantities such as torque, current, slip, etc., must be calculated from the six state variables in order to check the accuracy of the solution technique. It is important to note that some of the variables in equations 2.4 and 2.8-2.10 are functions of the flux linkages (such as i_d, i_{2d}, T_m, etc.) and thus must be solved in terms of the state variables before proceeding further. The quadrature axis flux linkage in both rotor and stator has only one source and that is the stator winding; conversely the direct axis flux linkage is composed of both a stator winding component and a component from the permanent magnets. Thus, the permanent magnet may be represented as if it were a rotor coil with fixed D.C. excitation current I_{fm}. The flux linkage equations can now be written:

$$\left.\begin{aligned} \lambda_d &= L_d i_d + L_{md}\, i_{2d} + L_{md}\, I_{fm} \\ \lambda_{2d} &= L_{2d}\, i_{2d} + L_{md}\, i_d + L_{md}\, I_{fm} \\ \lambda_q &= L_q i_q + L_{mq} i_{2q} \\ \lambda_{2q} &= L_{2q} i_{2q} + L_{mq} i_q \end{aligned}\right\} \qquad (2.11)$$

where L_{mq} and L_{md} are the magnetizing inductance along the two axis and:

$$L_d = L_{md} + L_1 \qquad L_q = L_{mq} + L_1$$

$$L_{2q} = L_{md} + L_2 \qquad L_{2q} = L_{mq} + L_2$$

L_1 and L_2 are the stator and rotor leakage inductances.

Solving equations 2.11 for the axis currents yields:

$$\begin{bmatrix} i_d \\ i_{2d} \end{bmatrix} = \begin{bmatrix} L_d & L_{md} \\ L_{md} & L_{2d} \end{bmatrix}^{-1} \times \begin{bmatrix} \lambda_d - L_{md} I_{fm} \\ \lambda_{2d} - L_{md} I_{fm} \end{bmatrix}$$

$$\begin{bmatrix} i_q \\ i_{2q} \end{bmatrix} = \begin{bmatrix} L_q & L_{mq} \\ L_{mq} & L_{2q} \end{bmatrix}^{-1} \times \begin{bmatrix} \lambda_q \\ \lambda_{2q} \end{bmatrix} \qquad (2.12)$$

Having solved for currents and flux linkages, all that remains is to solve for the motor torques. The motor during run-up has two components of torque, one derived from the squirrel cage winding and the other due to the presence of the magnets. The magnet torque acts as a breaking torque during run-up until synchronization takes place whereby the magnet becomes the sole source of holding torque. The total motor torque at the airgap is:

$$T_m = \lambda_d i_q - \lambda_q i_d \qquad (2.13)$$

And the torque produced by the rotor cage is:

$$T_{cage} = \lambda_{2d}\, i_{2q} - \lambda_{2q}\, i_{2d} \qquad (2.14)$$

the magnet torque being the difference:

$$T_{mag} = T_m - T_{cage} \qquad (2.15)$$

Although the magnet torque can be described in terms of flux linkages and equivalent magnet currents, it also can be described in terms of the power delivered to the source. Assuming the source presents a zero impedance source, then the torque required to turn the rotor shaft is proportional to the power dissipated in the stator winding resistance.

2.2 Steady State Behavior

From the last section the following system of equations was used in order to completely describe the P.M. motors transient behavior:

$$\left.\begin{aligned} p\delta &= \omega_o - \omega_r \\ p\omega_r &= \frac{1}{M}(T_m - T_L) - \frac{B}{M}\omega_r \\ p\lambda_d &= -V \operatorname{Sin}\delta - i_d R_1 + \lambda_q \omega_r \\ p\lambda_q &= V \operatorname{Cos}\delta - i_q R_1 - \lambda_d \omega_r \\ p\lambda_{2d} &= -R_{2d}\, i_{2d} \\ p\lambda_{2q} &= -R_{2q}\, i_{2q} \end{aligned}\right\} \qquad (2.16)$$

Upon considering the steady state behavior of this system, it is only a matter of setting the derivative terms to zero and allowing $\omega_r = \omega_o$ or synchronous speed. The first and last two equations of 2.16 reduce to trivial equations, which leaves the following set of equations.

$$\left.\begin{aligned} T_M &= T_L + B\omega_o \\ V \operatorname{Sin}\delta &= \lambda_q \omega_o - I_d R_1 \\ V \operatorname{Cos}\delta &= \lambda_d \omega_o + I_q R_1 \end{aligned}\right\} \qquad (2.17)$$

By using equation 2.11 of the previous section, a more useful form of equation 2.17 can be obtained. It was determined previously that λ_q and λ_d are as follows:

$$\left.\begin{aligned} \lambda_d &= L_d i_d + L_{md} i_{2d} + L_{md} I_{fm} \\ \lambda_q &= L_q i_q + L_{mq} i_{2q} \end{aligned}\right\} \qquad (2.11)$$

It is good to remember that i_{2d} and i_{2q} are the induced currents in the rotor cage bars derived from the relative motion between the airgap flux wave and the rotor bars. Upon synchronization both of these currents vanish such that in steady state:

$$\left.\begin{aligned} \lambda_d &= L_d I_d + L_{md} I_{fm} \\ \lambda_q &= L_q I_q \end{aligned}\right\} \tag{2.18}$$

Thus substituting equation 2.18 into 2.17b and c, the steady state voltage equations are obtained:

$$\left.\begin{aligned} V \text{ Sin } \delta &= X_q I_q - I_d R_1 \\ V \text{ Cos } \delta &= X_d I_d + X_{md} I_{fm} + I_q R_1 \end{aligned}\right\} \tag{2.19}$$

Also note that $X_{md}\ I_{fm}$ is nothing but the magnet produced open circuit voltage when the rotor is running at synchronous speed, ω_o. It is given the symbol E_o, for its likeness to the internal generated voltage of the standard synchronous machine. Equations 2.19 are identical to those arrived upon by using the phasor diagram technique, as is illustrated by Fig. 2.1 [33]. Equations 2.19 can easily be solved for the axis currents which are given as follows:

$$\left.\begin{aligned} I_d &= \frac{V\ (X_q \text{ Cos } \delta - R_1 \text{ Sin } \delta) - E_o X_q}{R_1^2 + X_d X_q} \\ I_q &= \frac{V\ (R_1 \text{ Cos } \delta - X_d \text{ Sin } \delta) - E_o R_1}{R_1^2 + X_d X_q} \end{aligned}\right\} \tag{2.20}$$

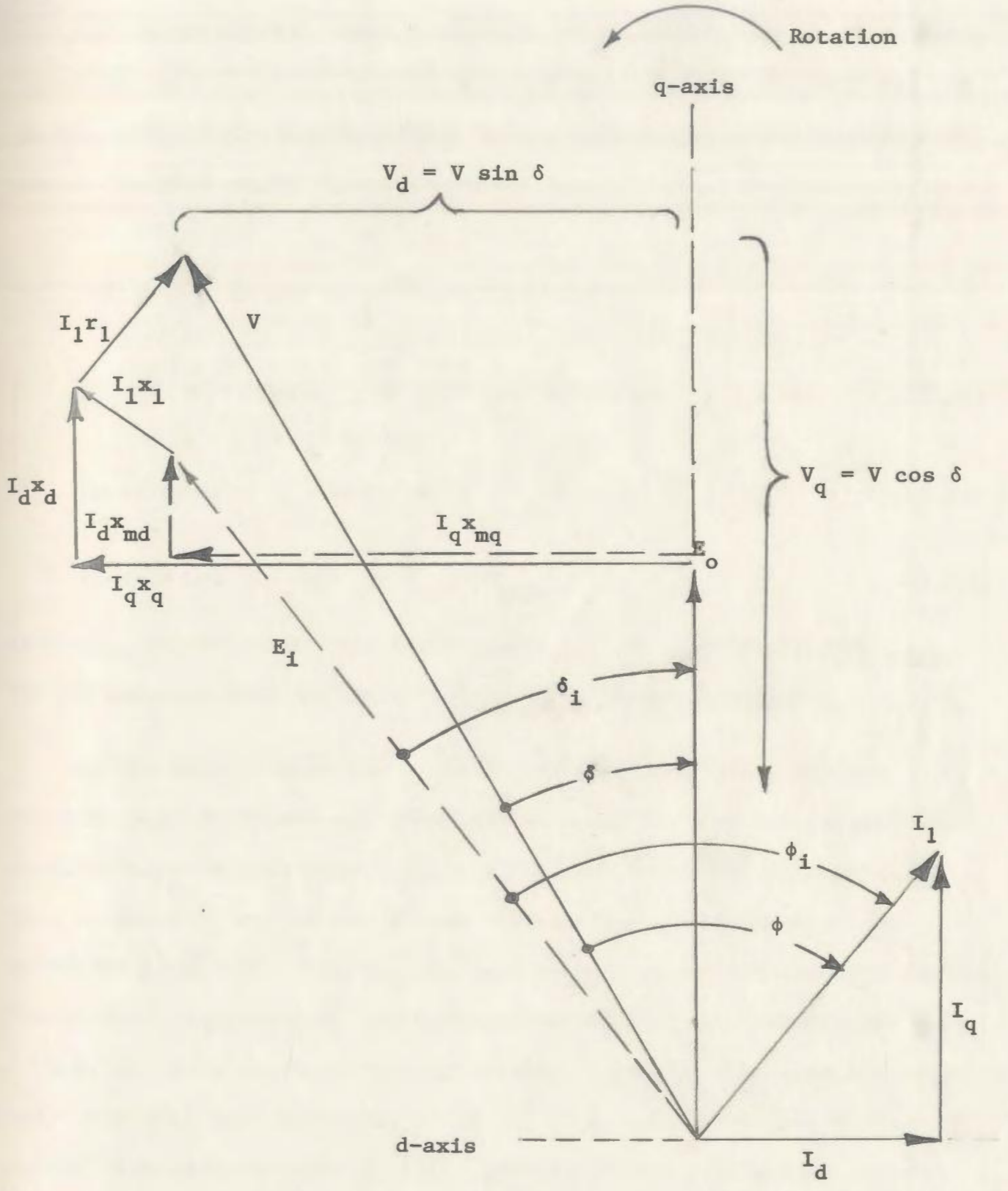

Figure 2.1 Phasor diagram of permanent magnet motor

The phase current (i.e. that which would be measured by an ammeter) is simply $I_1 = (I_d^2 + I_q^2)^{\frac{1}{2}}$. Having solved for voltages and currents, it is now easy to obtain the various power expressions needed to calculate the performance in an m-phase motor:

Air Gap Power = $P_e = m\, E_i I_i \cos \phi_i$

This can easily be put in the more familiar form:

$$P_e = m\left(\frac{E_o E_i}{X_d} \sin \delta_i + \frac{E_i^2 (X_{md} - X_{mq})}{2X_{md} X_{mq}} \sin 2\delta_i\right) \tag{2.21}$$

$$\text{Input Power} \quad W_i = mVI_1 \cos \phi = P_e + mI_1^2 R_1 \tag{2.22}$$

$$\text{Shaft Power} \quad P_s = P_e - P_{f\omega} - P_{core} \tag{2.23}$$

where $P_{f\omega}$ is the power lost to friction and windage torques and P_{core} is the magnetic loss in the iron core resulting in heating.

It has been pointed out by Honsinger [33] that the preceding analysis only considers the core loss as a lumped loss and is used only in efficiency calculations. In fact the core loss, which is modelled by a resistor R_c across the airgap voltage E_i, is very much a load dependent quantity. That is, the load increases the voltage drop across the winding resistance R_1 and leakage reactance X_1 increases, thus E_i is smaller for a constant applied voltage. When E_i decreases, the total core loss will also decrease, which can reduce the core loss by as much as 50% from no load to full load. To correct for this effect a core loss current I_c can be introduced which is in phase with E_i. Upon resolving I_c into its components I_{cd} and I_{cq}, these are added

to the d and q axis currents drawn from the secondary to give the total input currents $\bar{I}_d$ and $\bar{I}_q$ which are now corrected for core loss. Determining the power output now requires four values of current, I_d, I_q, $\bar{I}_d$ and $\bar{I}_q$, of which only I_d and I_q participate in energy conversion. Although the core loss current I_c does not directly participate in energy conversion, it does contribute to an increase in the $\bar{I}_1 Z_1$ voltage drop, a decrease in the internal voltage E_i and a decrease in power output [33]. Figure 2.2 shows the core loss corrected phasor diagram.

The core loss is now found as:

$$P_{core} = m (I_{cd}^2 + I_{cq}^2) R_c \tag{2.24}$$

Having corrected the stator current for core loss, the stator winding loss is:

$$m \bar{I}_1^2 R_1$$

and the total input power W_i becomes

$$W_i = m V \bar{I}_1 \text{ Cos } \phi = P_e + P_{core} + m \bar{I}_1^2 R_1 \tag{2.25}$$

The shaft output power can then be determined as:

$$P_s = P_e - P_{f\omega} \tag{2.26}$$

From the foregoing analysis it is clear that the complete behavior, transient and steady state, can be described from an analysis of the circuit voltage equations. The complete analysis rests on the investigator's ability to determine the various rotor and stator parameters. Of course if the parameter values are taken from actual tests done on a

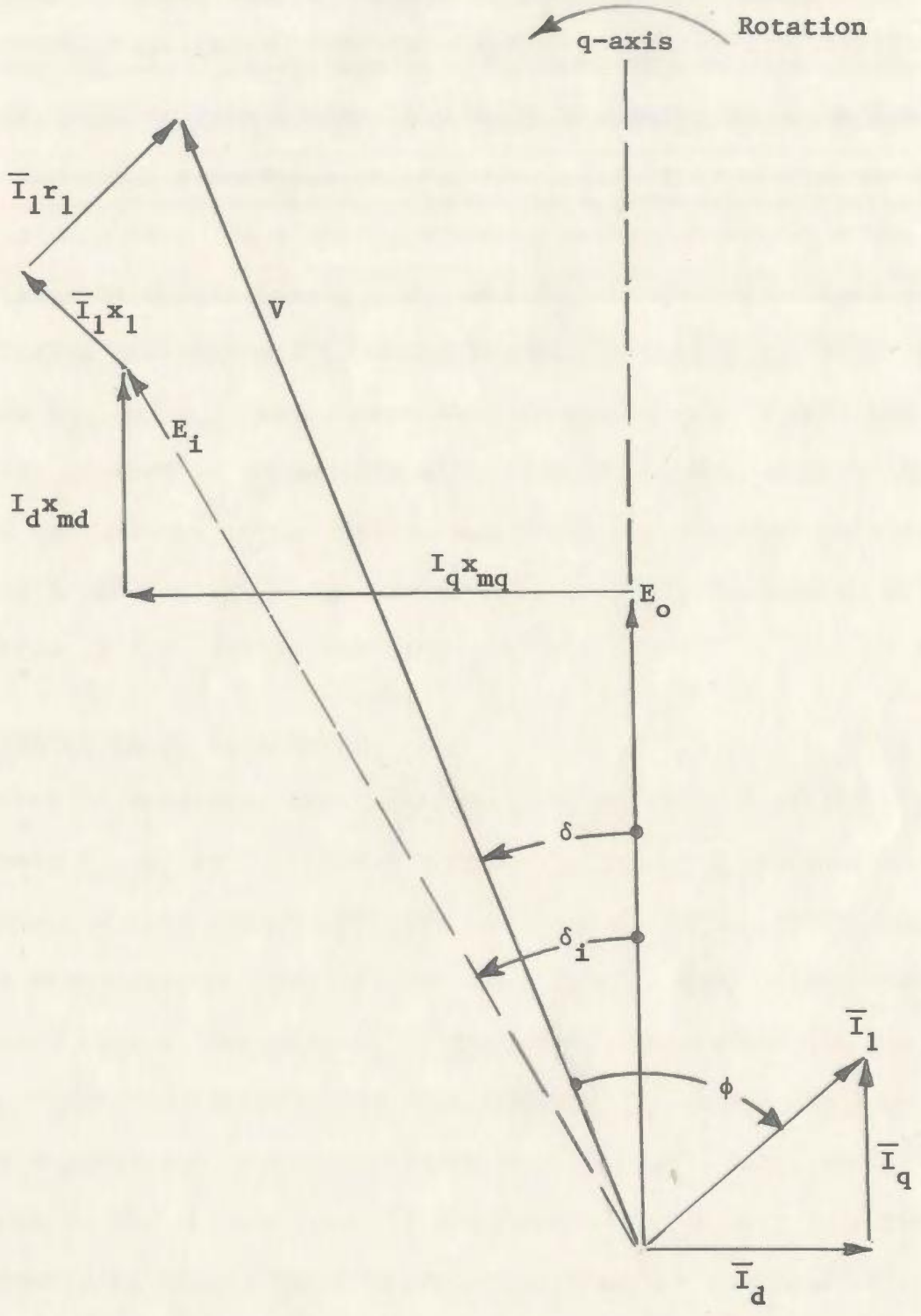

Figure 2.2 Phasor diagram of P.M. motor with core loss correction

particular motor (i.e. blocked rotor, no load, etc.), then the results will be in close agreement with the measured performance results. More importantly, and far more useful to a motor designer, is to be able to determine the motor parameters having only a knowledge of the stator and rotor geometries. Of prime interest to permanent magnet motor designers are the quantities X_{md}, X_{mq} and E_o. The other parameters, such as winding resistance R_1, stator leakage reactance X_1, rotor cage resistances R_{2d} and R_{2q}, etc., have been thoroughly dealt with and exhaustively studied in connection with standard induction motor and wire wound synchronous motor design, and therefore will not be treated at any length here except where it adds to the understanding or where peculiarities of P.M. design are involved.

2.3 Determination of Parameters

In order to determine the three critical parameters of the P.M. motor, namely E_o, X_d and X_q, the airgap flux density field must be known. This field is composed of two components: (1) the flux density due to the magnets alone, and (2) the flux density due to the armature mmf. Because of the nonlinearity of the motor iron, these two fields cannot be computed separately and then summed. To obtain the resultant field, the magnetizing force associated with each of these two fields is dependent on the permeability of the iron which in turn is dependent on the magnetizing force impressed on it. Therefore the total field is only solved by a numerical iterative routine. Nonetheless it is important to define the magnet and armature fields independently, such that they may be combined appropriately to give the total field.

2.3.1 Magnet Fields

In considering the air gap flux density produced by the magnets alone, it is essential to first have a model for the magnetic materials. The modern magnetic materials have essentially a linear demagnetization curve (see Fig. 1.2, page 5). This includes the rare earth and most of the ferrite varieties. Even the nonlinear ALNICO magnets have a linear recoil line such that the demagnetization curve may be represented by the following model:

$$B = -\mu' H + B_r \tag{2.27}$$

where the slope μ' is equal to the slope of the demagnetization curve or recoil line, and for the rare earth magnets it may be approximated by $+ B_r/H_c$. This equation considers a demagnetizing force (H) as a positive quantity for convenience. The air gap fields can be most easily determined by considering Fig. 2.3 which shows the magnet configuration used in this study as well as the various paths available to the magnet flux. Other magnet configurations are possible; these are shown in reference [35] and are analyzed in a somewhat more generalized form. For this analysis it is assumed that the iron permeability is infinite everywhere except the steel bridges surrounding the magnets. These bridges have high values of leakage flux and are thus driven into saturation; the permeability is calculated separately for each leakage path. There are two magnet sections contributing to the total air gap flux with four leakage fluxes ($\phi_{\ell 1}$, $\phi_{\ell 2}$, $\phi_{\ell 3}$, $\phi_{\ell 4}$) making up the total leakage flux $\phi_{\ell T}$. For convenience the leakage fluxes are distinguished into iron leakage paths and magnet leakage paths. The former supporting flux $\phi_{\ell I}$ and the latter supporting flux $\phi_{\ell m}$. In determining the useful

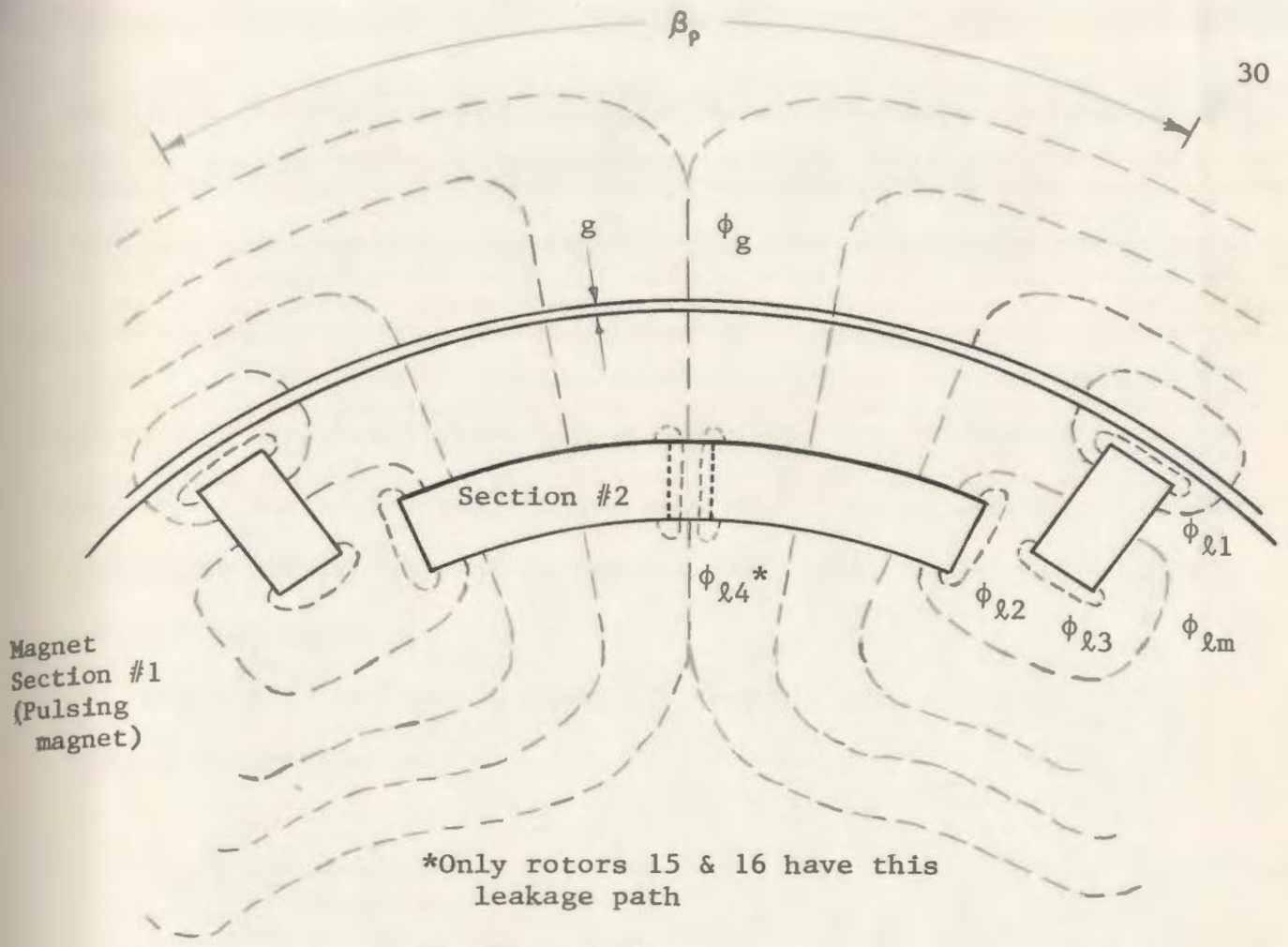

*Only rotors 15 & 16 have this leakage path

a) Flux paths

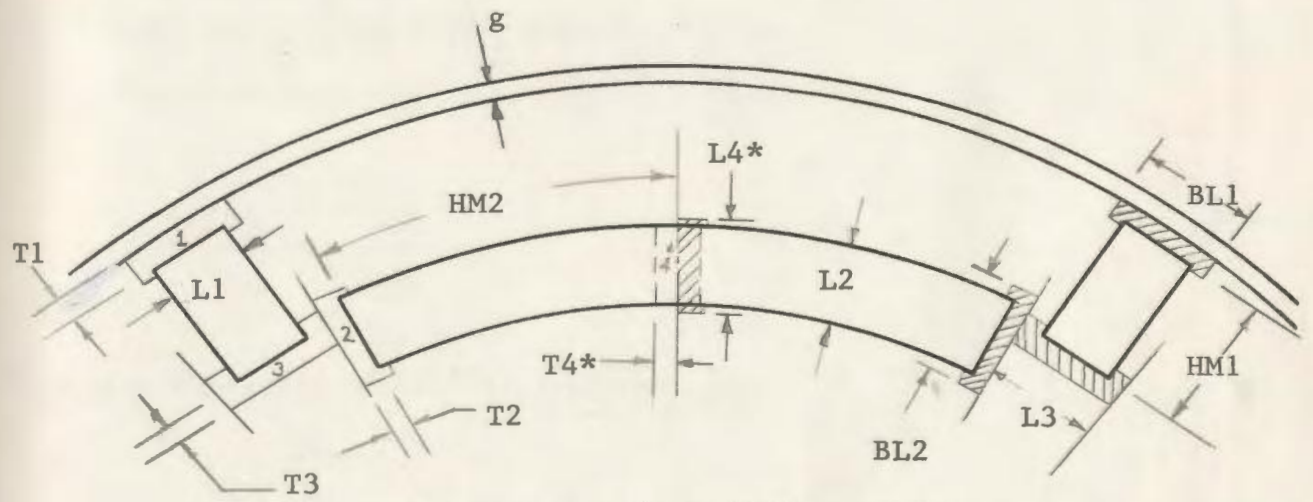

*Only rotors 15 & 16 have this leakage path

b) Dimensions

Figure 2.3 Rotor Magnet Geometry

flux (ϕ_g) crossing the air gap and cutting the stator windings, the first important equation is the flux balance equation:

$$\phi_g = \phi_{mT} - \phi_{\ell T} \tag{2.28}$$

where ϕ_{mT} is the sum of the magnet fluxes in each of the two magnet sections. Using a magnetic circuit analogy, the leakage flux can be related to the airgap flux in the same way a current divides into two resistance paths. Thus it is left to determine the reluctance of the various flux paths.

Since all the leakage paths are in parallel, the total iron leakage reluctance is:

$$R_{\ell I} = \frac{1}{\frac{1}{R_{\ell 1}} + \frac{1}{R_{\ell 2}} + \frac{1}{R_{\ell 3}}} \tag{2.29}$$

The magnet reluctance paths consist of the reluctance of section one in parallel with twice the reluctance of section two, that is:

$$R_{\ell m} = \frac{1}{\frac{1}{R_{\ell m1}} + \frac{1}{2R_{\ell m2}}} \tag{2.30}$$

Thus the total reluctance of leakage paths is:

$$R_{\ell T} = \frac{R_{\ell I}\, R_{\ell m}}{R_{\ell I} + R_{\ell m}} \tag{2.31}$$

To simplify the analysis the stator iron is considered to have an infinite permeability, or zero reluctance, thus the airgap will present the total reluctance to the flux crossing into the stator iron. (The

effects of iron saturation can be incorporated by using a slightly longer airgap.) In fact it will cross the airgap two times. Therefore using the technique of flux divider the two fluxes are found to be:

$$\phi_g = \frac{R_{\ell T}}{R_{\ell T} + 2R_g} \phi_{mT} \tag{2.32}$$

and

$$\phi_{\ell T} = \frac{2R_g}{R_{\ell T} + 2R_g} \phi_{mT} \tag{2.33}$$

Rearranging equation 2.33 and substituting it into equation 2.32, yields $\phi_{\ell T}$ in terms of ϕ_g thus:

$$\phi_{\ell T} = \left(\frac{2R_g}{R_{\ell T} + 2R_g} \right) \left(\frac{R_{\ell T} + 2R_g}{R_{\ell T}} \right) \phi_g = \left(\frac{2R_g}{R_{\ell T}} \right) \phi_g \tag{2.34}$$

If $R_{\ell T}$ is considered as having two component reluctances (iron and magnet) as in equation 2.31, the relationship between $\phi_{\ell T}$ and ϕ_g is:

$$\phi_{\ell T} = \frac{2R_g (R_{\ell I} + R_{\ell m})}{R_{\ell m} R_{\ell I}} \phi_g$$

or

$$\phi_{\ell T} = \left(\frac{2R_g}{R_{\ell m}} \right) \left(1 + \frac{R_{\ell m}}{R_{\ell I}} \right) \phi_g \tag{2.35}$$

The factors in equation 2.35 are the same factors which reference [35] calls β and k_ℓ with

$$\beta = \frac{2R_g}{R_{\ell m}} \quad \text{-- geometrical factor}$$

$$k_\ell = 1 + \frac{R_{\ell m}}{R_{\ell I}} \quad \text{-- leakage factor}$$

and

$$\phi_{\ell T} = [\beta k_\ell]\ \phi_g \tag{2.36}$$

Substituting this back in equation 2.28 gives the airgap flux as a function of magnet flux.

$$\phi_{mT} = \phi_g + \beta k_\ell\ \phi_g = (1 + \beta k_\ell)\ \phi_g \tag{2.37}$$

or

$$\phi_g = \frac{\phi_{mT}}{(1 + \beta k_\ell)} \tag{2.38}$$

The next equation of importance is the flux density equation, arrived at by integrating equation 2.37 over the magnet areas:

$$B_{m1}\ A_{m1} + B_{m2}\ A_{m2} = (1 + \beta k_\ell)\ B_f\ A_g \tag{2.39}$$

where A_g is the circumferential area of the airgap per pole

A_{mi} is the area of magnet section i, perpendicular to the direction of magnetization. i = 1,2

B_f is the airgap flux due to the magnets alone.

The third fundamental equation to determine the airgap fields due to the magnets is obtained by writing Ampere's circuital law around the main flux path which crosses the airgap. The vector direction of B and H are the same in iron or in airgaps but they are of opposite sign in the magnetic material, yielding:

$$2H_{m2}\ L_2 - 2H_f g = 0 \tag{2.40}$$

or, since $H_g = B_g$ in the most common cgs units

$$2H_{m2} L_2 - 2B_f g = 0 \tag{2.41}$$

The line integral path for magnet section 1 is:

$$H_{m1} L_1 - 2B_f g = 0 \tag{2.42}$$

Solving H_{m1} in terms of H_{m2} by use of equations 2.41 and 2.42 gives:

$$H_{m1} = \left(\frac{2L_2}{L_1}\right) H_{m2} \tag{2.43}$$

Finally, the model chosen earlier is used, relating B and H for both magnet sections

$$B_i = \mu_i' H_i + B_{ri} \qquad \text{where } i = 1,2$$

Combining all the equations necessary to solve for the airgap flux density (B_f) in one place gives:

$$\left.\begin{aligned} &B_{m1} A_{m1} + B_{m2} A_{m2} = (1 + \beta k_\ell) B_f A_g \\ &2H_{m2} L_2 = 2B_f g \\ &H_{m1} = \left(\frac{2L_2}{L_1}\right) H_{m2} \\ &B_{m1} = \mu_1' H_{m1} + B_{r1} \\ &B_{m2} = \mu_2' H_{m2} + B_{r2} \end{aligned}\right\} \tag{2.44}$$

The only factor not known in the set of equations 2.44 is the leakage factor $(1 + \beta k_\ell)$. This can be determined by calculating the reluctance

values in equation 2.35. These are:

$$R_g = \frac{g}{\mu A_g} = \frac{gP}{\mu \ell_s \pi D}$$

where g = effective airgap

ℓ_s = core length

P = number of poles

D = diameter of rotor

μ = 1.0 in air in cgs system relative permeability

$$R_{\ell m} = 1 \; / \; (1/R_{\ell m1} + 1/R_{\ell m2})$$

$$R_{\ell mi} = \frac{L_i}{\mu_i' \, 2\ell_s \, h_i}$$

L_i = width of magnet i in direction of magnetization

h_i = height of magnet i perpendicular to L_i and ℓ_s

$i = 1,2$

$$R_{\ell I} = 1 \; / \; (1/R_{\ell 1} + 1/R_{\ell 2} + 1/R_{\ell 3})$$

$$R_{\ell j} = \frac{L_j}{2\ell_s \, \mu_j \, t_j}$$

t_j = thickness of leakage path j

μ_j = permeability of leakage bridge j

$j = 1,2,3$

The difficulty in getting a solution for the set of equations 2.44 is that the permeability in the leakage bridges is directly related to the magnetizing force across that bridge and the magnetizing force is dependent on the reluctance of the paths and indirectly on permeability. Thus to find B_f, an iterative approach must be used to solve equations 2.44. The flux density waveform obtained is shown in Fig. 2.4 and is a

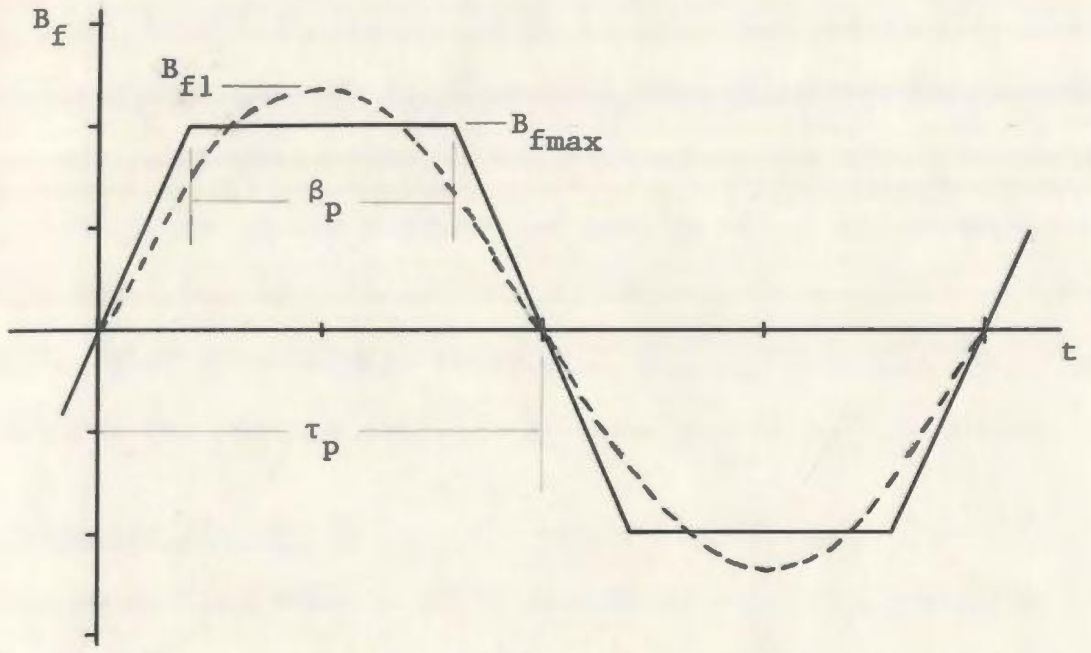

Figure 2.4 Air gap open circuit flux density due to magnets

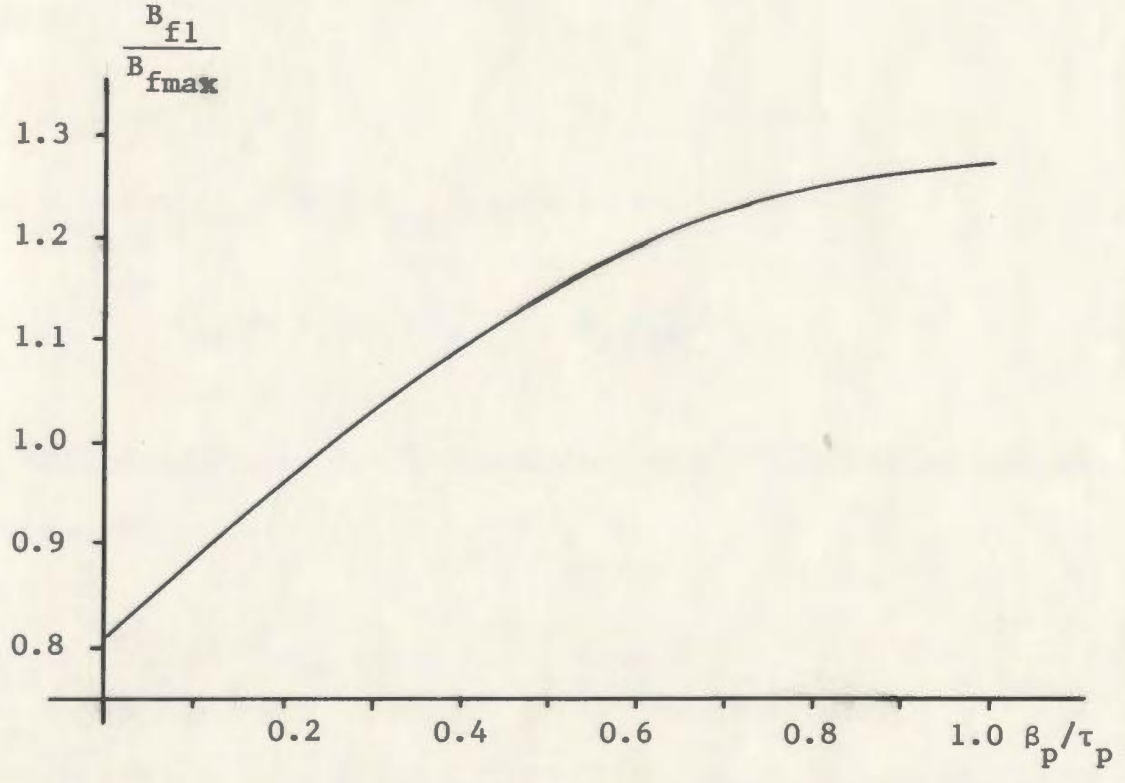

Figure 2.5 Fundamental component of B_f as a function of the pole pitch to pole arc ratio "β_p/τ_p"

trapezoidal waveform with the pole arc "β_p" being determined by the properties of magnet section 1 (both physical and magnetic). Since in determining the parameters E_o, X_d and X_q only the fundamental component is important, elementary Fourier analysis will determine the ratio of the peak amplitude of the fundamental component to the maximum value of B_f. This value varies from $4/\pi = 1.27$ for a pure squarewave to $8/\pi^2 = .810$ for a triangular flux density waveform. Fig. 2.5 clearly shows how this ratio changes for various pole arc to pole pitch (β_p/τ_p) ratios.

2.3.2 Armature Fields

The airgap flux density field caused by stator currents is resolved into its direct and quadrature axis components B_{ad} and B_{aq} respectively and solved independently. Reference [35] solves the following set of equations along the direct axis to determine the flux density along that axis:

$$\left.\begin{aligned} & H_1' L_1 - 2H_2' L_2 = 0 \qquad\qquad B_1' = \mu' H_1' \\ & 2g H_{ad} + H_1' L_1 = 0.8\pi F_{dm} \text{ Cos } (P/2)\,\theta \qquad B_2' = \mu' H_2' \\ & D\ell_s \int_o^{\pi/P} B_{ad}\, d\theta = 2\ell_s (h_I B_1' + h_2 B_2') + \phi_\ell' \end{aligned}\right\} \qquad (2.45)$$

Having solved equations 2.45, the direct axis flux density can be written thus:

$$B_{ad} = \frac{0.4\pi F_{dm}}{g}\left[\text{Cos } (P/2)\,\theta - \frac{2\pi}{1 + \beta k_\ell}\right] \qquad (2.46)$$

The very irregular shape of this waveform is shown in Fig. 2.6. The

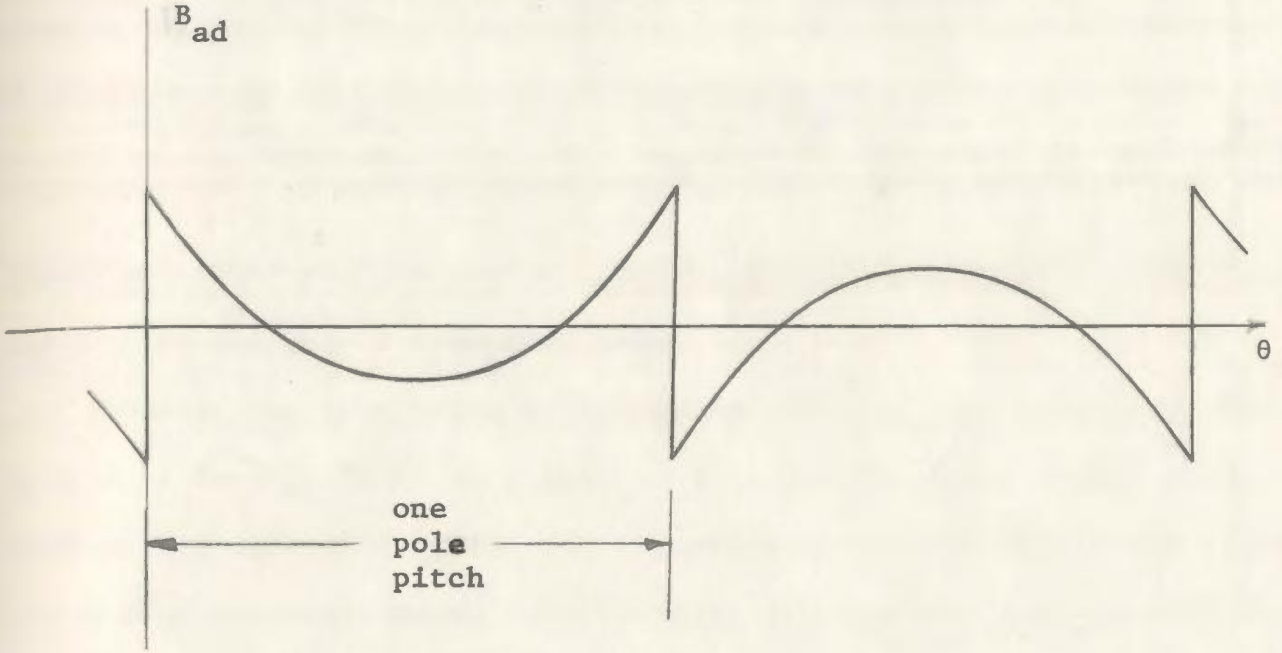

Figure 2.6 Direct axis armature field flux density waveform

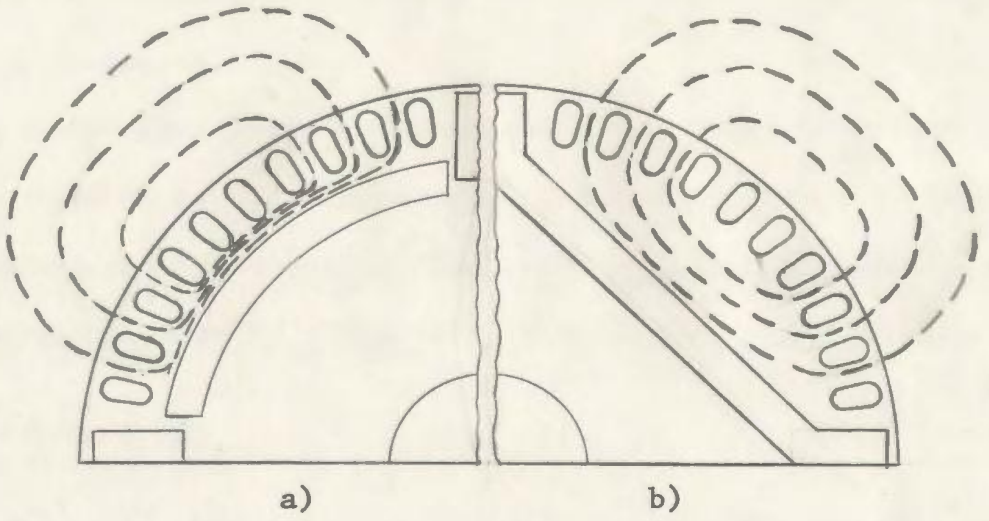

Figure 2.7 Quadrature axis flux paths for various rotor geometries

solution to equations 2.45 also lead to the flux densities upon the magnet faces. Hence

$$B_1' = \frac{\mu_1' \ 1.6 \ F_{dm}}{L_1 \ (1 + \beta k_\ell} \qquad B_2' = \frac{\mu_2' \ 1.6 \ F_{dm}}{2L_2 \ (1 + \beta k_\ell)} \tag{2.47}$$

These equations will be useful later on when determining the effects of loading on the magnet operating point.

However the conclusion of reference [35], in that the quadrature axis flux density field is simply that of the isotropic round rotor machine, is dependent on how the magnets are oriented within the rotor. The design presently under consideration differs from that of [35] in that the magnets are placed very near the induction cage bars. Consequently the quadrature axis flux must be established through the long thin bridge between the magnets and the cage bars. This bridge will tend to saturate as it must carry flux of both axes. The following analysis, which is similar to that given in [35] for the d-axis field, can be used to calculate the quadrature axis field, and thus the quadrature axis reactance.

It is clear that there is no magnet flux along the q-axis and that the stator winding is the sole source of flux. Figure 2.7 shows the rotor geometry and rotor q-axis flux paths. The total current supporting the quadrature flux is $2F_{qm}$ Sin (P/2) θ, where F_{qm} is given as: [49]

$$F_{qm} = \frac{0.9m \ I_q \ NK_w}{P} \tag{2.48}$$

and θ is any angular position measured from the direct axis. It is assumed that the leakage bridges around the ends of the magnets are

saturated and none of the q-axis flux leaks out around the back of the magnets such that the flux balance equation may simply be written:

$$\phi_{aq} = \phi_r \tag{2.49}$$

The flux ϕ_r is the flux in the rotor iron which can be determined by the following relationship.

$$\phi_r = \frac{H_q L_q}{R_q} \tag{2.50}$$

where H_q is the magnetizing force across the rotor iron path

L_q is the length of the rotor bridge

R_q is the reluctance of the path.

Also ϕ_{aq} is the flux crossing the airgap and can be determined by integrating the q-axis flux density field B_{aq} over one pole pitch:

$$\phi_{aq} = \int_{-\pi/P}^{\pi/P} B_{aq}\, \ell_s\, r\, d\theta = \int_{o}^{\pi/P} B_{aq}\, \ell_s\, D\, d\theta$$

$$= D\ell_s \int_{o}^{\pi/P} B_{aq}\, d\theta \tag{2.51}$$

Completing the set of equations by writing the line integral equation around the flux path:

$$2g\, H_{aq} + H_q\, L_q = 0.8\, \pi F_{qm}\, \text{Sin}\, (P/2)\, \theta \tag{2.52}$$

or rearranged to solve for H_{aq}

$$H_{aq} = \frac{0.8\pi}{2g} F_{qm} \text{ Sin } (P/2)\ \theta - \frac{H_q L_q}{2g} \tag{2.53}$$

Since $B_{aq} = H_{aq}$ in cgs units as before, equation 2.53 may be placed in equation 2.51 and the integral evaluated to determine ϕ_{aq}:

$$\phi_{aq} = D\ell_s \int_0^{\pi/P} \left(\frac{0.8\pi}{2g} F_{qm} \text{ Sin } (P/2)\ \theta - \frac{H_q L_q}{2g} \right) d\theta$$

$$= \frac{D\ell_s}{2g} \int_0^{\pi/P} 0.8\pi\ F_{qm} \text{ Sin } (P/2)\theta d\theta - \int_0^{\pi/P} H_q L_q\ d\theta$$

$$= \frac{\pi D\ell_s}{2g\ P} \left[1.6\ F_{qm} - H_q L_q\right] \tag{2.54}$$

Noting that $\pi D\ell_s/P$ is the airgap area per pole and that g/A_g is the airgap reluctance R_g, this can now be substituted into equation 2.50 and solved for H_q:

$$\frac{H_q L_q}{R_q} = \frac{1.6\ F_{qm}}{2Rg} - \frac{H_q L_q}{2R_g}$$

or

$$H_q = \frac{1.6\ F_{qm}}{L_q\ (1 + 2R_g/R_q)} \tag{2.55}$$

A new geometrical factor may thus be defined which is similar to the factor already defined as β. Therefore β_q is introduced as:

$$\beta_q = 2R_q/R_q \tag{2.56}$$

To determine the flux density along the q-axis, equation 2.55 is substi-

tuted into equation 2.53 to give:

$$B_{aq} = \frac{0.8\pi}{2g} F_{qm} \left[\text{Sin } (P/2)\ \theta - \frac{2/\pi}{(1 + \beta_q)} \right] \tag{2.57}$$

Note the similarity with equation 2.46 derived earlier for B_{ad}, and note also that B_{aq} has flux whorls much like those in B_{ad} and their waveforms are similar with the exception of a 90° phase shift.

Once again a simple Fourier analysis yields the value of the fundamental component of the flux density waveform as

$$B_{aq} = \frac{0.4\pi\ F_{qm}}{g} \left[1 - \frac{(8/\pi^2)}{(1+B_q)} \right] \text{Sin } (P/2)\ \theta \tag{2.58}$$

Having thus found the three major components of the airgap flux density waveform, the total field is the sum of the three. However, the field on the magnets is a function of the difference between the magnet flux and the d-axis armature flux depending on motor loading conditions. Typically a P.M. motor has a magnetizing mmf at low or light loads and demagnetizing mmf as loading increases. Thus each of the leakage and saturation factors is dependent on the loading condition of the motor and consequently the parameters E_o, X_d and X_q all vary with loading. Using the method of reference [35], the fields of the magnets and leakage bridges are determined and consequently used to predict the motor parameters.

2.3.3 Open Circuit Voltage

The open circuit voltage is found by using the fundamental transformer equation [49]

$$E_o = (4.443)\ f\ \phi_1\ Nk_w \times 10^{-8} \text{ volts} \tag{2.59}$$

where f is the frequency of operation $= \frac{2\pi N}{60}$: N = rpm

N is the number of stator turns per phase

k_w is the stator winding factor.

and ϕ_1 is the peak amplitude of the alternating flux which is found as follows:

$$\phi_1 = (2/\pi)\ B_{f1}\ A_g = (2/\pi)\ k_1\ B_f\ A_g$$

where B_{f1} is the fundamental component of the trapezoidal waveform having maximum amplitude B_f

k_1 is the factor taken from Fig. 2.5 relating B_{f1} to B_f for various waveshapes.

Therefore:

$$E_o = (2\pi/\sqrt{2})\ f\ [(2/\pi)\ k_1\ B_f\ A_g]\ Nk_w \times 10^{-8}$$

$$= (4/\sqrt{2})\ f\ k_1\ B_f\ A_g\ Nk_w \times 10^{-8} \tag{2.60}$$

Note that the value of B_f is related to the saturation and leakage by:

$$B_f = \frac{B_r\ (A_m/A_g)}{(1 + \beta k_\ell)} \tag{2.61}$$

and therefore E_o is not a fixed quantity for a given rotor but is a machine-saturable parameter depending on the saturation of the steel leakage bridges.

2.3.4 Direct Axis Reactance X_{md}

The direct axis magnetizing reactance is defined to be:

$$X_{md} = \omega_o L_{md} = \frac{\omega_o \lambda_{md}}{\sqrt{2}\ I_d} \times 10^{-8} \qquad (2.62)$$

where ω_o is the power line frequency in radians/sec.

Reference [35] relates X_{md} to the magnetizing reactance of an isotropic rotor (i.e. induction rotor) X_m and includes a multiplier C_d to account for leakage and the presence of the magnets

$$X_{md} = X_m C_d' \qquad (2.63)$$

where $$X_m = \left(\frac{1.6\ \omega_o m\ D\ell_s}{g}\right)\left(\frac{Nk_w}{P}\right)^2 \times 10^{-8} \qquad (2.64)$$

$$C_d = 1 - \frac{8/\pi^2}{1 + \beta k_\ell} \qquad (2.65)$$

2.3.5 Quadrature Axis Reactance X_{mq}

Similarly the quadrature axis magnetizing reactance is defined as:

$$X_{mq} = \omega_o L_{mq} = \frac{\omega_o \lambda_{mq}}{2\ I_q} \times 10^{-8} \qquad (2.66)$$

The value $\lambda_{mq} = Nk_w \phi_q$ where ϕ_q is the quadrature axis flux linking both stator and rotor. The flux ϕ_q is obtained by integrating the flux density waveform over the stator inner surface:

$$\phi_q = \ell_s D \int_o^{\pi/P} B_{aq}\ d\theta$$

$$= \ell_s D \int_o^{\pi/P} \left(\frac{0.4\pi\ F_{qm}}{g} \left[1 - \frac{8/\pi^2}{(1+\beta_q)} \right] \text{Sin}\ (P/2)\ \theta \right) d\theta$$

$$= \frac{0.4\pi\ F_{qm}\ \ell_s D}{g}\left[1 - \frac{8/\pi^2}{(1+\beta_q)}\right]\int_0^{\pi/P} \text{Sin}\ (P/2)\ \theta\ d\theta$$

$$= \frac{0.8\pi\ F_{qm}\ \ell_s\ D}{gP}\left[1 - \frac{8/\pi^2}{(1+\beta_q)}\right] \qquad (2.67)$$

Substituting the value for F_{qm} derived earlier into equation 2.67 gives:

$$\phi_q = \frac{0.8\pi\ \dfrac{0.9\ m\ I_q\ N\ k_w}{P}\ \ell_s D}{gP}\left[1 - \frac{8/\pi^2}{(1+\beta_q)}\right]$$

$$= \frac{0.72\pi\ I_q\ m\ \ell_s D}{g}\left(\frac{N\ k_w}{P^2}\right)\left[1 - \frac{8/\pi^2}{(1+\beta_q)}\right] \qquad (2.68)$$

Multiplying ϕ_q by Nk_w gives λ_{mq} which can be used in equation 2.66 to find X_{mq}:

$$X_{mq} = \omega_o\left\{\frac{\dfrac{0.72\pi\ I_q\ m\ell_s D}{g}\left(\dfrac{Nk_w}{P}\right)^2\left[1 - \dfrac{8/\pi^2}{(1+\beta_q)}\right]}{2\ I_q}\right\} x\ 10^{-8}$$

$$X_{mq} = \omega_o\left(\frac{1.6\ m\ell_s D}{g}\left(\frac{Nk_w}{P}\right)^2\left[1 - \frac{8/\pi^2}{(1+\beta_q)}\right]\right) x\ 10^{-8} \qquad (2.69)$$

which is easily put in the form:

$$X_{mq} = X_m\ C_q$$

where X_m is as before (see equation 2.64) and

$$C_q = 1 - \frac{8/\pi^2}{(1+\beta_q)} \qquad (2.70)$$

C_q accounts for saturation along the quadrature flux path. In reference [35] Honsinger refers to C_q as being unity which does not account for any saturation along the q-axis. However, the magnets in the present work are placed very much closer to the rotor cage than in Honsinger's motor which would account for the higher saturation.

3.0 CALCULATED PERFORMANCE

3.1 Performance Prediction Routines

In the previous chapter a set of equations were derived which adequately modelled both the transient and steady state behavior of a P.M. motor. This chapter deals with the technique of obtaining a solution from the equations with the machine parameters as input.

Since the transient formulation involves a set of six nonlinear differential equations, a closed form of solution is virtually impossible, and therefore a numerical integration routine is used to obtain a solution. Many such routines exist, such as Runge-Kutta, predictor-corrector, trapezoidal, etc., but because the set of transient equations tend to be stiff they are quite sensitive to errors arising from the computational procedure. Care must be taken therefore to obtain a sufficiently good numerical technique. It was found however that the solution to the present set of equations was far more sensitive to the step size used in the integration procedure than to the method or order of the integration routine. Figure 3.1 illustrates this, showing the run-up solution for a small P.M. motor using both a modified Euler and Runge-Kutta routine for various step sizes. In considering step size, Rafian and Laughton [50] under similar circumstances state that a step size of 0.3ms is sufficiently small to cause errors of not more than 1.0%. In verifying this, the author generated a series of solutions by a repeated halving of the step size and used an Aitken, delta-squared extrapolation technique [51] in order to achieve a more accurate solution. Figure 3.2 illustrates this procedure showing that the solutions having a step size of 0.25ms or less lie within 2% of the extrapolated

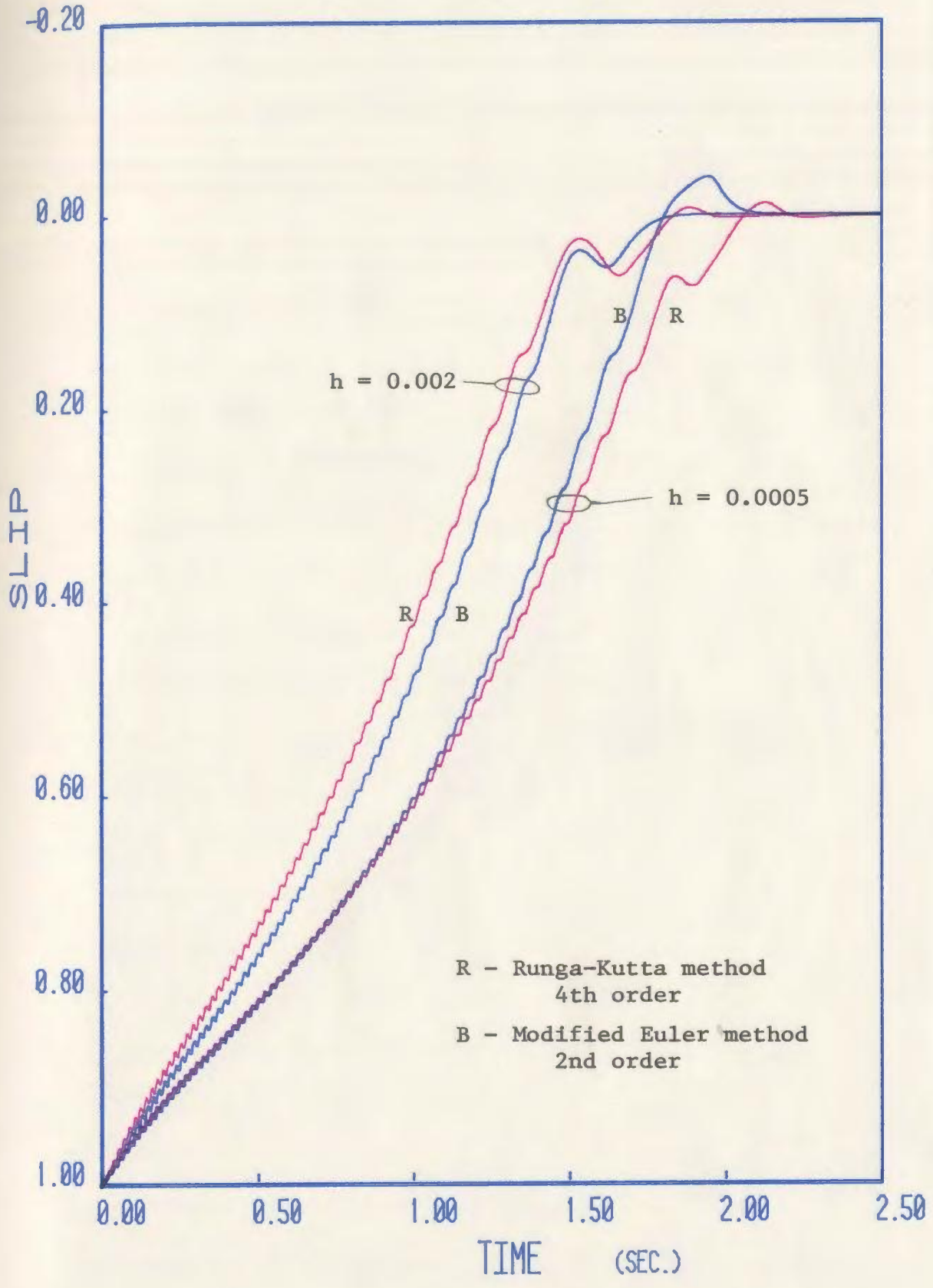

Figure 3.1 Transient solution showing method and step size variation in the numerical routine

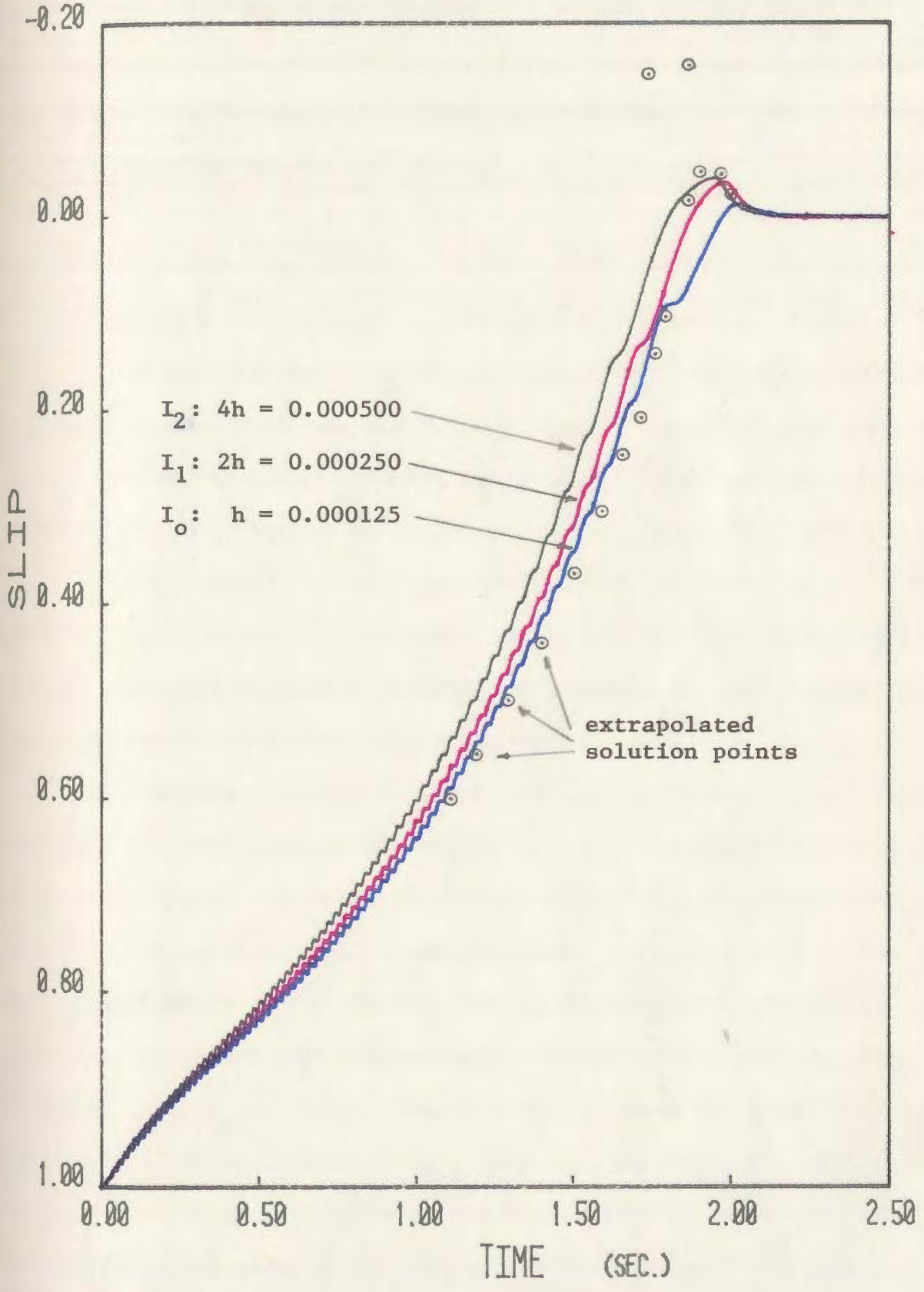

Figure 3.2 Using the Aitken, delta-squared extrapolation procedure to verify the solution accuracy

solution curve for the majority of the points. Considering I_o, I_1 and I_2 to be the solutions generated with step sizes h, 2h, and 4h respectively, the Aitken, delta-squared technique gives a more accurate solution by the following extrapolation formula:

$$I = I_o - \frac{(I_o - I_1)^2}{(I_o - 2I_1 + I_2)} \tag{3.1}$$

As can be seen from the figure, points near the region of synchronization are such that the denominator term of equation 3.1 goes to zero and so the extrapolated solution is erratic. Nevertheless, the extrapolated solution is closer to the true analytic solution, for the majority of the curve. Hence, it was concluded that a step size of 0.25ms or less will give acceptably accurate results. Throughout the remainder of this work all transient results are computed by a 4th order Runge-Kutta routine with a step size of 0.25ms.

The code used to give transient run-up performance is given in Appendix A. This program is written to receive various motor parameters in per-unit form. In order to normalize the torque expressions it was necessary to normalize all speed dependent variables by dividing by the synchronous speed "ω_o". Thus it was necessary, when writing the voltage equations, to normalize all voltages induced by the rotating mmf wave by dividing by ω_o as well. When the state equations were formed the various inductances, given by L_{xx} (where xx is the appropriate subscript md, mq, etc.) were transformed into reactances at the line frequency. Furthermore, the program allows for the saturation of the d and q axis reactances (X_d and X_q respectively) by considering them to be direct

functions of the axis currents (i_d and i_q). The functional relationship $X_q = f(i_q)$ is approximated by the piecewise linear curve shown in Figure 3.3. The details shown on the figure are taken from the curves given by Miyashita et al [32] and Honsinger [35]. Although the direct axis reactance saturation can also be modelled in the same way, it is not done so in the given program for the following reason. Honsinger [35] shows a wild variation in the value of X_d, but this variation, caused by the changes in the steel leakage bridge permeabilities, takes place for values of direct axis current less than the no-load level. However, since the transient program is used primarily to obtain start-up information, at which time the currents tend to be larger than full-load levels, the d-axis saturation was considered unnecessary. Secondly, the total change in the value of X_d is proportionately much smaller than the q-axis variation.

Appendix A also contains the numerical routine which solves for steady state performance. This routine solves a set of six nonlinear equations as well. Note that these are algebraic equations and that the nonlinearity is primarily a result of the saturation of the ferromagnetic materials.

To solve these equations a Gauss-Seidel type routine is employed, although not in matrix formulation as is common. An initial guess is made for the magnet flux leakage factor k_ℓ and the saturation factor β_q. The calculation then proceeds to adjust the various machine parameters for core loss as described previously, and then to solve the steady state voltage equations in order to determine the axis currents. Having determined the axis currents and thus the mmf's behind the axis fluxes,

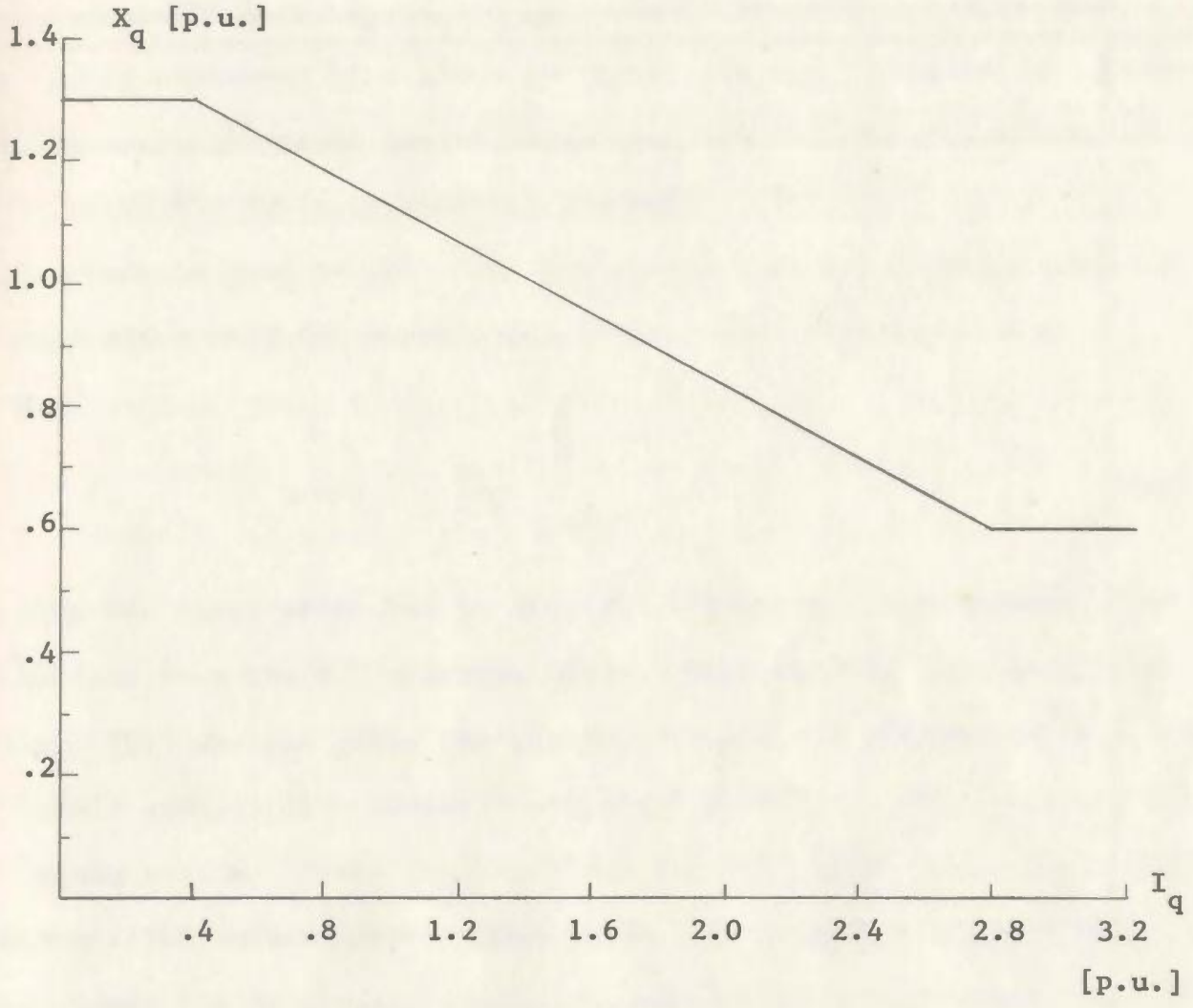

Figure 3.3 Approximation of the q-axis saturation

a better estimate can now be determined for k_ℓ and β_q. The iterative procedure continues until the change in k_ℓ is less than a specified tolerance. When the tolerance is met the program calculates the desired output quantities (e.g. I_d, I_q, P_{out}, Efficiency, etc.), the torque angle "δ" is increased by a given increment and the procedure is repeated until the output power no longer increases with increasing load angle. That is until the pull-out power is reached.

The formula used to calculate the permeability of a section of the iron path given only the magnetizing force across that path is as follows:

$$\mu = 1 + \frac{a}{b + H} \tag{3.2}$$

This form was first presented by Frölich [52] where the constants a and b were derived from the B-H characteristic. This form is also used by Honsinger [35] who has given the constants to be a = 20 000. and b = 3.2 which yield acceptable accuracy for typical 0.0025 in. or 0.0019 in. motor grade steels. These constants are found to give reasonable results for magnetizing forces greater than 10 Oe. In general, the steel bridges operate under fields greater than 10 Oe,except for a very short transition period,when the increasing armature flux cause the fields in the iron bridges to go virtually to zero. During this transition the permeability is held at a value of about 4000.

These two programs, while maintaining a fair degree of simplicity, give good flexibility for determining which parameters are the most critical to achieving a desired motor performance.

3.2 Specifications of Prototypes

Having derived the necessary equations to predict the performance of a P.M. motor, and having organized a numerical routine to generate a realistic solution, it is left but to procure the correct input data for the programs.

Before proceeding with the machine dimensions of the prototype models, it may be convenient to designate the rotors (of which,four are of particular interest) with a code number to facilitate reference of the types. Each of the four rotors is given an identification of the following format : "Rotor Type xi" where "x" is a 1 or 2 and refers to whether the rotor is a two or four pole version respectively. The "i" is a one-digit number denoting the order of assembly for that particular pole structure. For example, a type "16" rotor would be the sixth rotor assembled of the two pole variety. Of a number of rotors built,only four will be dealt with in this report; these are the rotors which provide the most insight into P.M. motor behaviour. Table 3.1 lists these rotors and some pertinent information about each.

The steady state performance program uses the rotor and magnet dimensions as input data. In order to show the magnet holes and the dimensioning details of the four prototype models, Figures 3.4 and 3.5 have been included. One important point to note is the use of small air gap at the base of the "pulsing" magnet of rotors 15 and 21, and beside the arced magnets of rotor 22. This air gap,or "flux barrier", is used to confine the magnet flux to the direct axis path and to minimize the area of the steel leakage paths. All of the necessary input data to determine the motor steady state performance, for each of

Table 3.1 Prototype Identification Codes

	Rotor Type	Description
General	1i	2-pole, 1-hp, 575-V, three-phase, 60 H_z motor. Frame size - 30.
	2i	4-pole, 1-hp, 575-V, three-phase, 60 H_z motor. Frame size - 143T.
Specific	15	6 magnet sections, including 2 "pulsing" or "boosting" magnets, all of rare earth cobalt ($Sm-Co_5$), rotor has no skew.
	16	4 magnet sections with no pulsing magnets, pulsing section is left as a void. All rare earth cobalt magnets, rotor has no skew.
	21	8 magnet sections, including 4 pulsing magnets of rare earth cobalt type. Again rotor is not skewed.
	22	4 magnet sections of rare earth cobalt type. Rotor has no pulsing magnets and area of pulsing magnets is not left void. Rotor cage is not skewed.

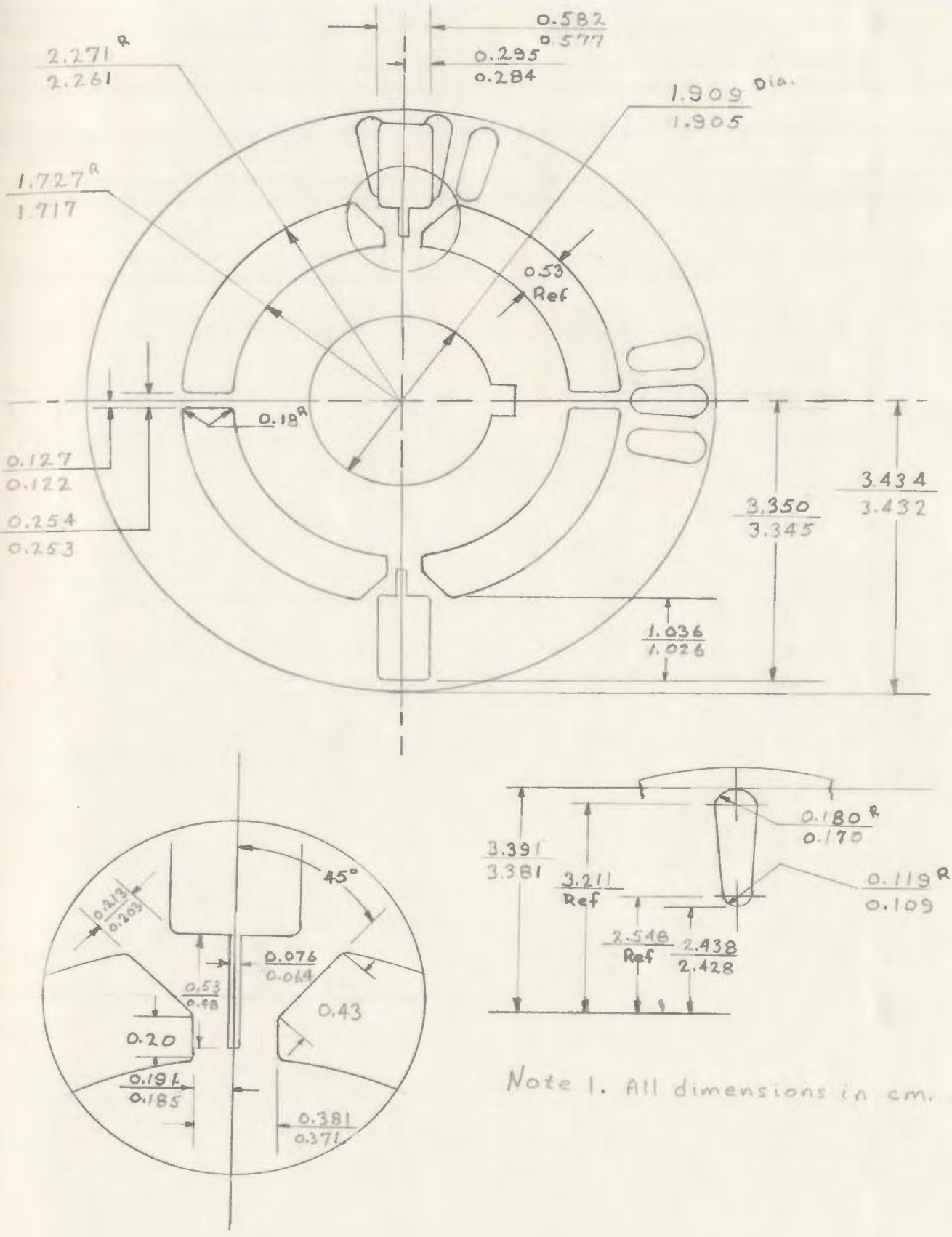

Figure 3.4 Specifications of type 1 rotor

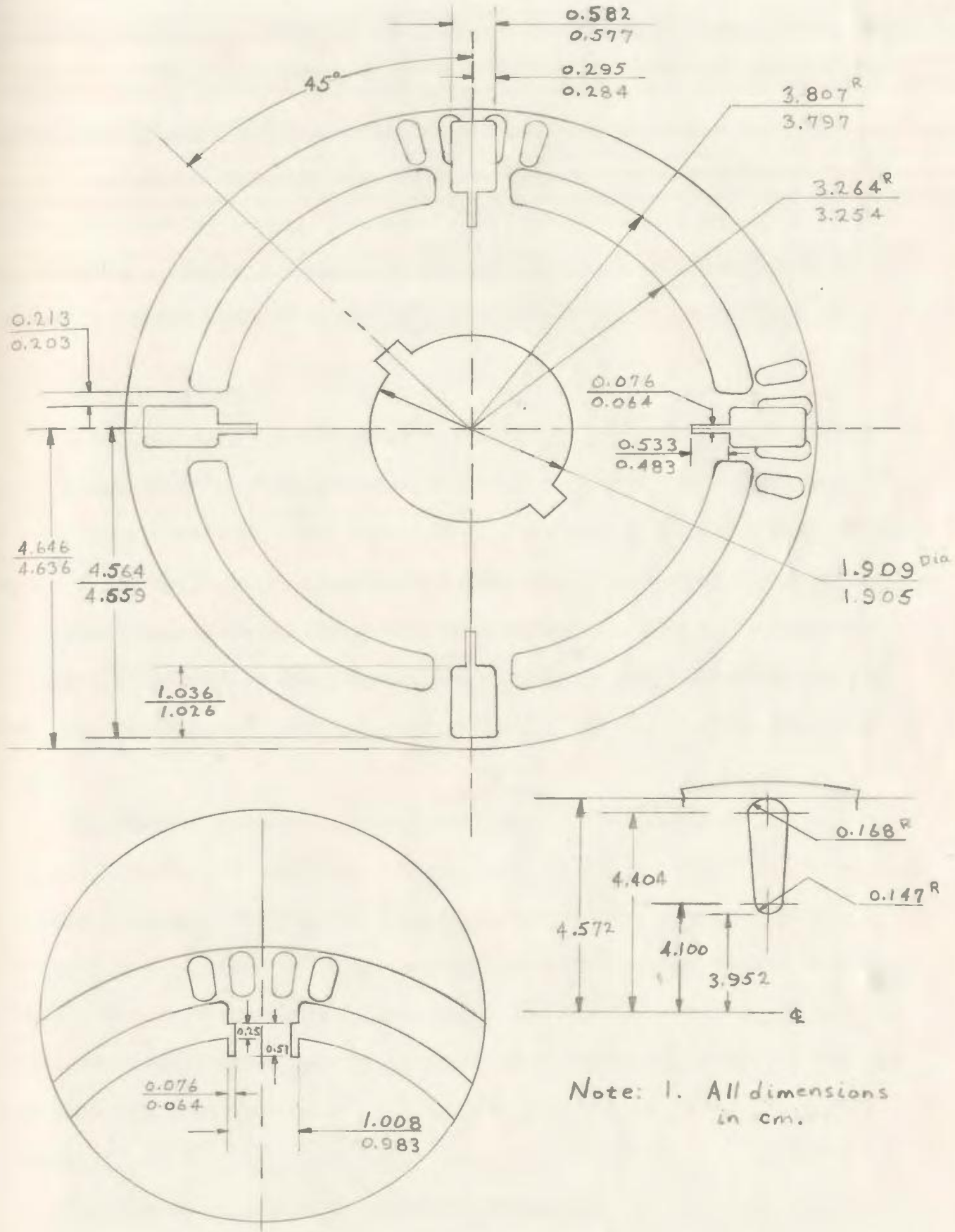

Figure 3.5 Specifications of type 2 rotor

the prototypes, is listed in Table 3.2. For the most part, these quantities have been calculated from Figures 3.4 and 3.5, but some of the data has come from the manufacturer's data sheet.

Using the steady state prediction routine outputs and some data from actual motor tests, the input data for the transient program can be obtained. Table 3.3 shows the actual input quantities for each of the four rotors used in predicting the transient motor response.

3.3 Computer Outputs

Using the data from Figures 3.4 and 3.5 and from Tables 3.2 and 3.3, a number of performance predictions, both transient and steady state, were executed. The following tables and figures are representative of the total performance and correspond closely with the conditions from which measured results could be obtained. The outputs are constrained to rotors 15 and 21, for these are the two rotors which have the best performance, and are representative of the two and four pole types.

The steady state results are presented first in Tables 3.4, 3.5 and 3.6. Table 3.4 compares the computed and predicted results for open circuit voltage. This table also shows the saturation and leakage factor $1 + \beta k_{\ell}$, which is a measure of the flux shunted by the leakage paths. Note how almost half the useful magnet flux is lost. The air gap open circuit flux density level is also included. Figures 3.5 and 3.6 show the predicted load test results for rotors 15 and 21 respectively.

The transient results are shown, primarily, by the run-up characteristic for differing load conditions, as this is the most easily

measured characteristic for comparison. The run-up curves for rotor 15, for no load, a large inertial load (with no other friction load), and the largest friction load the prototype motor could synchronize (about 0.3 p.u.) are shown in Figures 3.6 and 3.8. Similar curves for rotor 21 are shown in Figures 3.7 and 3.9.

The dynamic torque vs. slip curve during a lightly loaded (0.15 p.u.) run-up is shown in Figure 3.10 for rotor 21. This shows the pulsating nature of the accelerating torque and the synchronizing cycle.

Finally, the effects of reduced voltage on starting capability are demonstrated by Figure 3.11. This shows that at voltages reduced by as little as 20%, the motor's synchronizing capability is drastically reduced.

Table 3.2 Machine Dimensions and Parameters Input values for the steady state performance routine. All dimensions in cgs. units

Symbol	Description	Rotor 15	Rotor 16	Rotor 21	Rotor 22	Units
Motor Parameters:						
G	Effective air gap length including Carter's coefficient and saturation	0.0330	0.0321	0.0323	0.0323	cm.
D	Rotor outside diameter	6.849	6.851	9.296	9.296	cm.
LS	Length of rotor core	7.620	7.620	5.107	5.107	cm.
N	Stator series turns per phase	440	440	744	744	
KW	Winding factor = $k_d\ k_p$	0.8293	0.8293	0.831	0.831	
P	Number of poles	2	2	4	4	
M	Number of phases	3	3	3	3	
PFW	Mechanical loss to friction and windage (measured)	34	34	34	34	W.
R1	Stator winding resistance (measured)	18.26	18.26	14.02	14.02	Ω
X1	Stator leakage reactance (measured)	16.5	16.5	23.2	26.0	Ω
RC	Effective core loss resistance	3500	3500	3500	3500	Ω
Magnet Parameters:						
BR1 BR2	Residual flux density for magnet sections 1 and 2	8150	8150	8150	8150	Gauss
HC1 HC2	Coercive force for magnet sections 1 and 2	8070	8070	8070	8070	Oe.

....continued

Table 3.2 (continued)

Symbol	Description	Rotor 15	Rotor 16	Rotor 21	Rotor 22	Units
Magnet Parameters (cont'd):						
U11 U12	Relative permeability of magnet sections 1 and 2	1.014	1.014	1.014	1.014	
HM1	Dimension of magnet section 1 perpendicular to useful flux	0.9906	--	0.9906	--	cm.
HM2	Dimension of magnet section 2 perpendicular to useful flux	2.680	2.680	2.095	2.095	cm.
L1	Length of magnet #1 in direction of flux	0.559	--	0.559	--	cm.
L2	Length of magnet #2 in direction of flux	0.508	0.508	0.508	0.508	cm.
Rotor Geometry:						
BL1	Length of leakage bridge above magnet section 1	0.565	--	0.565	--	cm.
BL2	Length of leakage bridge above magnet section 2	0.553	0.553	0.553	0.553	cm.
L3	Length of leakage bridge under magnet section 1	0.085	--	0.085	--	cm.
L4	Length of leakage bridge in middle of magnet section 2	0.553	0.553	--	--	cm.
T1	Thickness of bridge corresponding to BL1	0.039	0.039	0.074	0.074	cm.
T2	Thickness of bridge corresponding to B12	0.104	0.104	0.104	0.104	cm.
T3	Thickness of bridge #3	0.556	--	0.556	--	cm.
T4	Thickness of bridge #4	0.124	0.124	--	--	cm.
LQ	Length of quadrature flux path	5.75	5.75	4.30	4.30	cm.
TQ	Thickness of quadrature flux path	0.15	0.15	0.15	0.15	cm.

Table 3.3 Input Data for Transient Program
All figures given in per unit
unless otherwise stated

Symbol	Description	Rotor 15	Rotor 16	Rotor 21	Rotor 22	Units
Base Values:						
P_b	Base kVA	1195	1195	1593	1593	W
V_b	Base voltage (1-1)	575	575	575	575	V
I_b	Rated current	1.2	1.2	1.6	1.6	A
Z_b	Base impedance	276.6	276.6	207.5	207.5	Ω
Parameters:						
XD	Direct axis reactance	1.8800	1.8077	0.6265	0.5783	
XMD	d-axis magnetizing reactance	1.8200	1.7479	0.5147	0.4530	
X2D	Damper winding d-axis reactance	1.8671	1.7951	0.6099	0.5783	
XQ	Quadrature axis reactance	0.6508	0.7592	0.7229	0.9639	
XMQ	q-axis magnetizing reactance	0.5911	0.6995	0.6111	0.8386	
X2Q	Damper winding q-axis reactance	0.6552	0.7636	0.7359	0.9639	
IFM	Equivalent magnet field current	1.1361	0.7364	0.9320	0.8300	
R1	Stator winding resistance	0.0660	0.0660	0.0675	0.0675	
X1	Stator leakage reactance	0.0597	0.0597	0.1118	0.1253	
R2D	Damper winding d-axis resistance	0.0282	0.0168	0.1358	0.1839	
R2Q	Damper winding q-axis resistance	0.0312	0.0182	0.1483	0.1550	
X2	Rotor leakage reactance	0.0597	0.0597	0.1118	0.1253	
WO	Synchronous speed	377.0	377.0	377.0	377.0	r_{ad}/s
IC1	Rotor moment of inertia	0.0014	0.0014	0.0030	0.0030	$kg\text{-}m^2$
V	Applied stator voltage	1.0	1.0	1.0	1.0	

Table 3.4 Predicted Values of Open Circuit Voltage

	Rotor 15	Rotor 16	Rotor 21	Rotor 22
E_o	171.8v l-n	119.1v	194.1v	156.5v
B_f	2592.7 G	2267.1 G	3756.8 G	3261.6 G
Saturation factor	2.09	1.73	1.76	1.40
Measured E_o	170.0	133.4	193.9	159.3

Table 3.5 Steady State Performance for Rotor 15

δ [°]	I_a [A]	Pout [W]	Efficiency [%]	Power factor	X_d [Ω]	X_q [Ω]
3.9	0.61	7.3	2.9	.419	554.0	195.3
11.4	0.78	232.9	47.9	.629	554.0	155.2
21.3	1.13	526.8	65.0	.721	554.0	137.7
31.3	1.48	713.8	68.6	.705	554.0	133.2
41.3	1.81	787.2	67.4	.648	552.4	130.8
51.2	2.04	1125.0	72.6	.762	264.5	130.0
61.2	2.31	1195.1	71.2	.730	240.3	129.5
71.2	2.54	1189.4	68.7	.684	226.9	129.1

Table 3.6 Steady State Performance for Rotor 21

δ [°]	I_a [A]	Pout [W]	Efficiency [%]	Power factor	X_d [Ω]	X_q [Ω]
2.5	1.08	238.5	51.8	.428	93.9	61.8
12.5	1.76	1023.7	77.7	.753	100.7	55.8
22.4	2.64	1610.6	78.2	.782	111.8	54.8
32.4	3.53	1904.7	74.0	.732	127.4	54.4
42.4	4.35	1848.8	66.6	.642	146.7	54.2

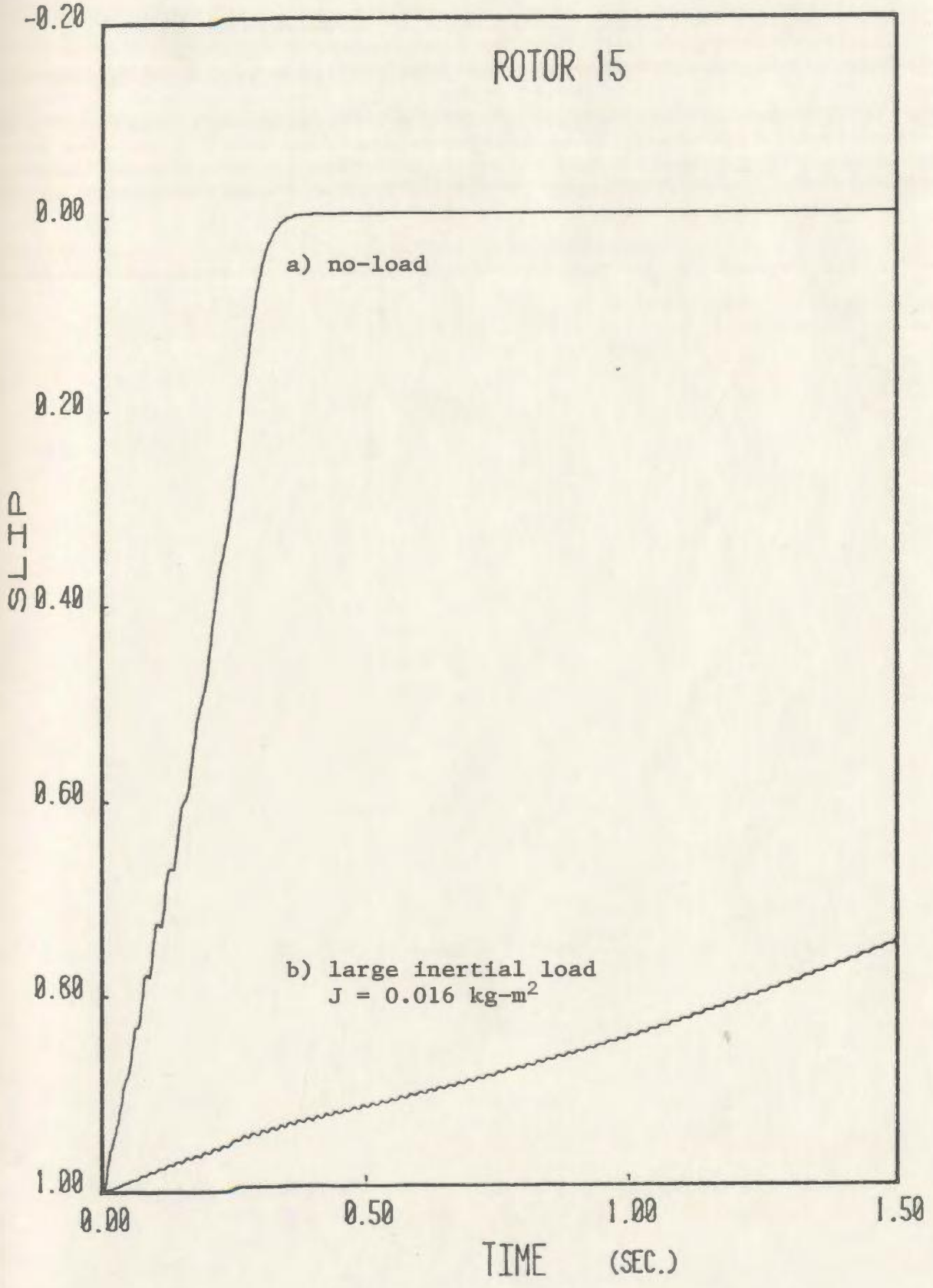

Figure 3.6 Various run-up responses for rotor 15

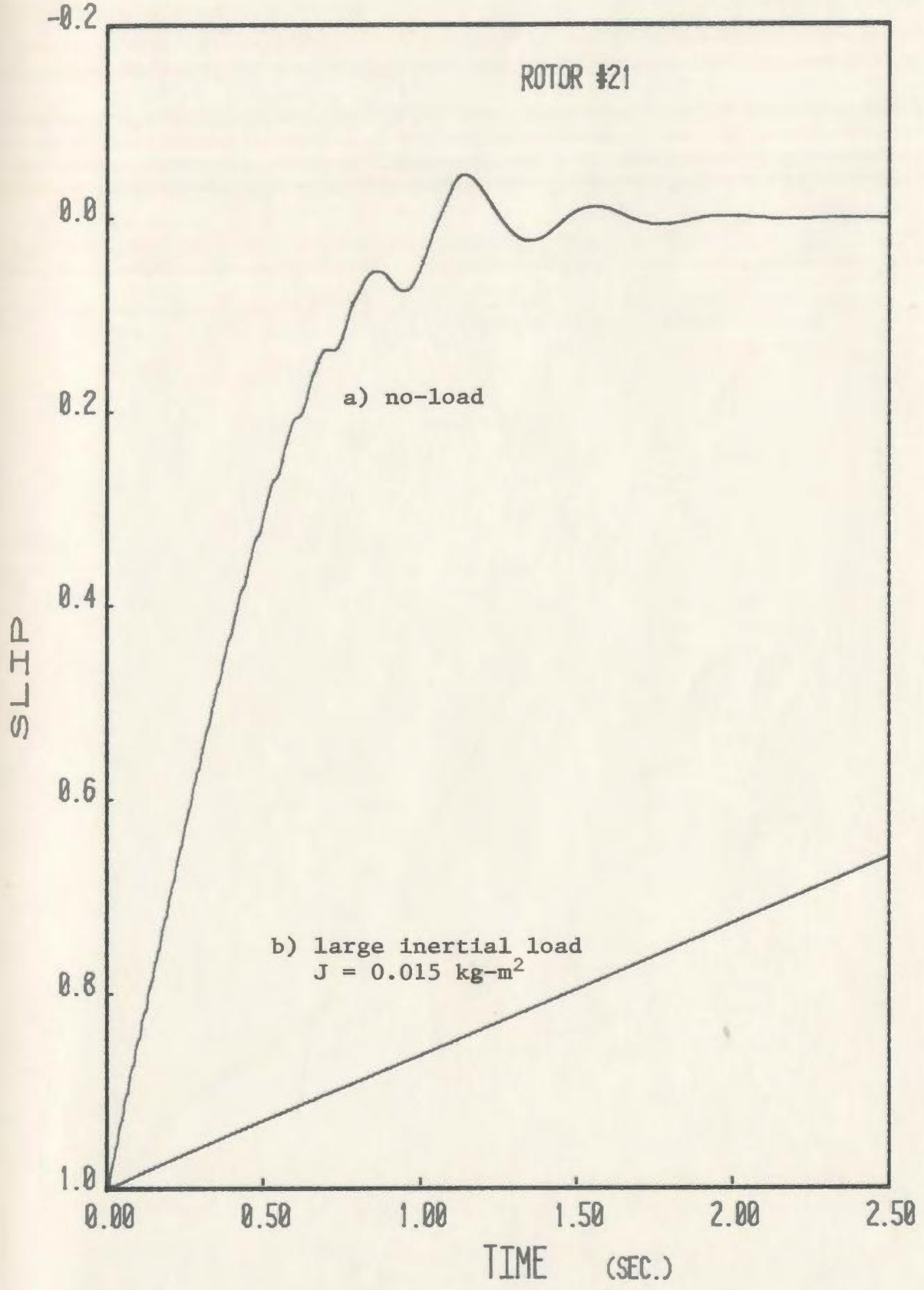

Figure 3.7 Various run-up responses for rotor 21

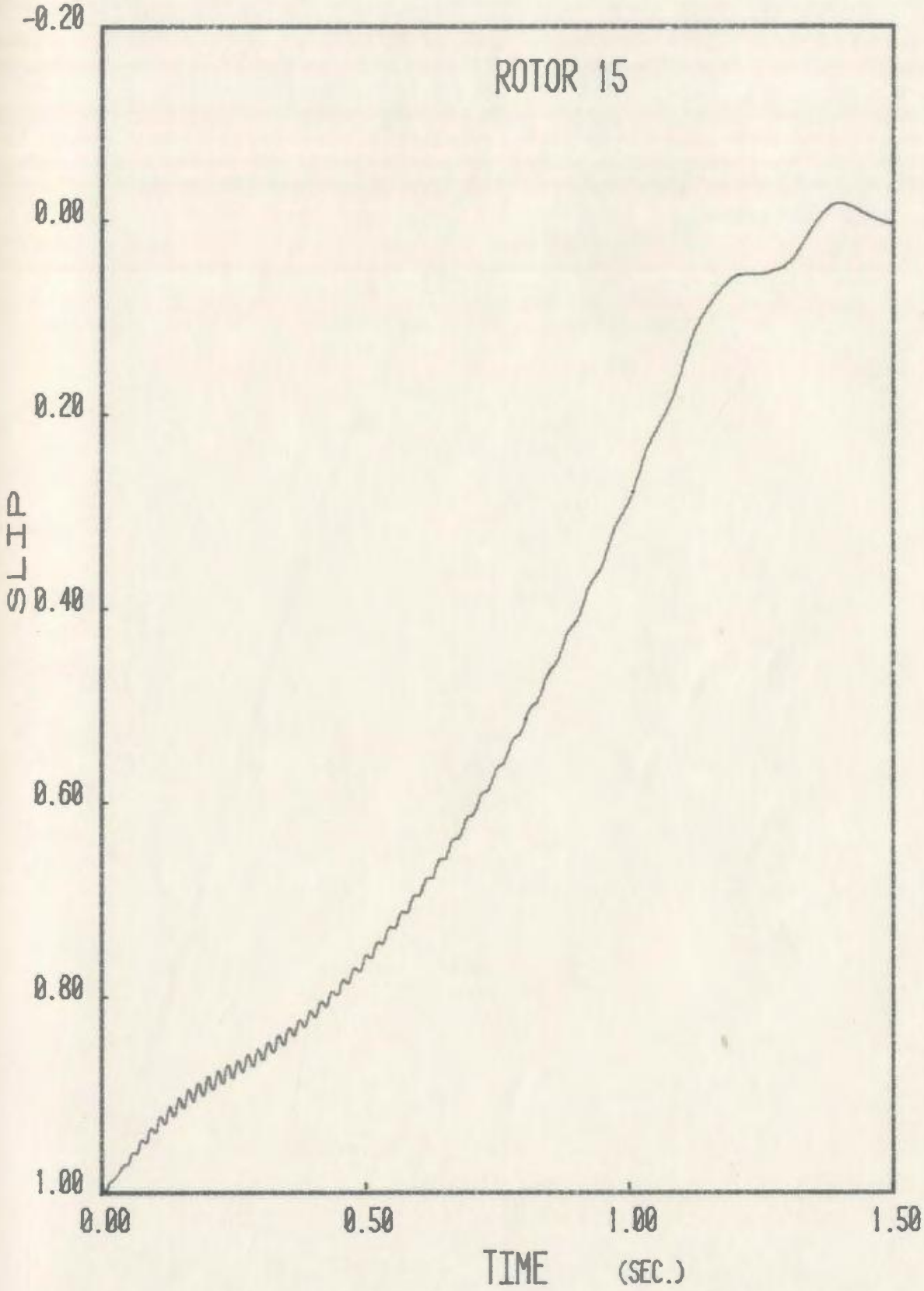

Figure 3.8 Rotor 15 run-up for large friction load

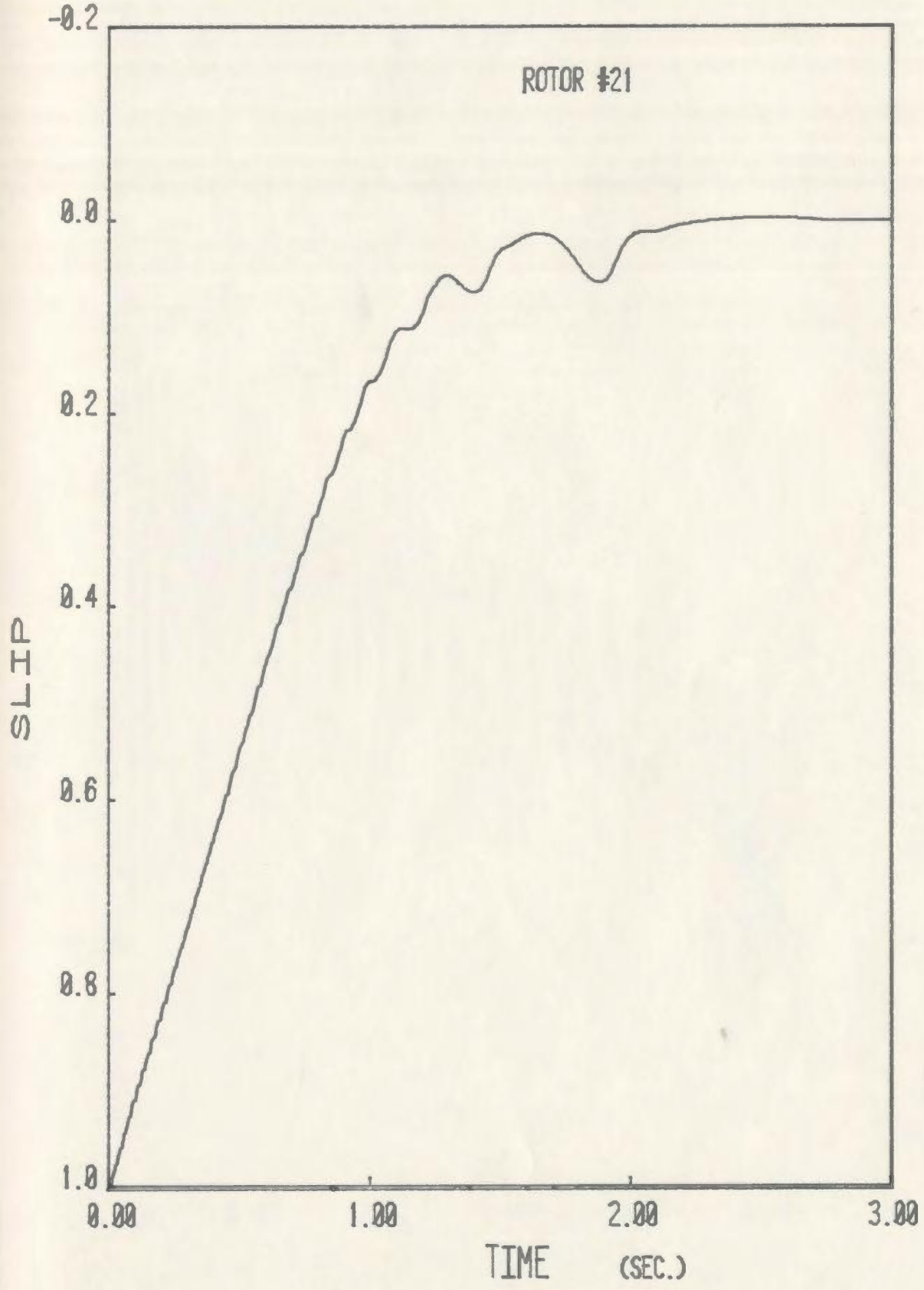

Figure 3.9 Rotor 21 run-up for large friction load

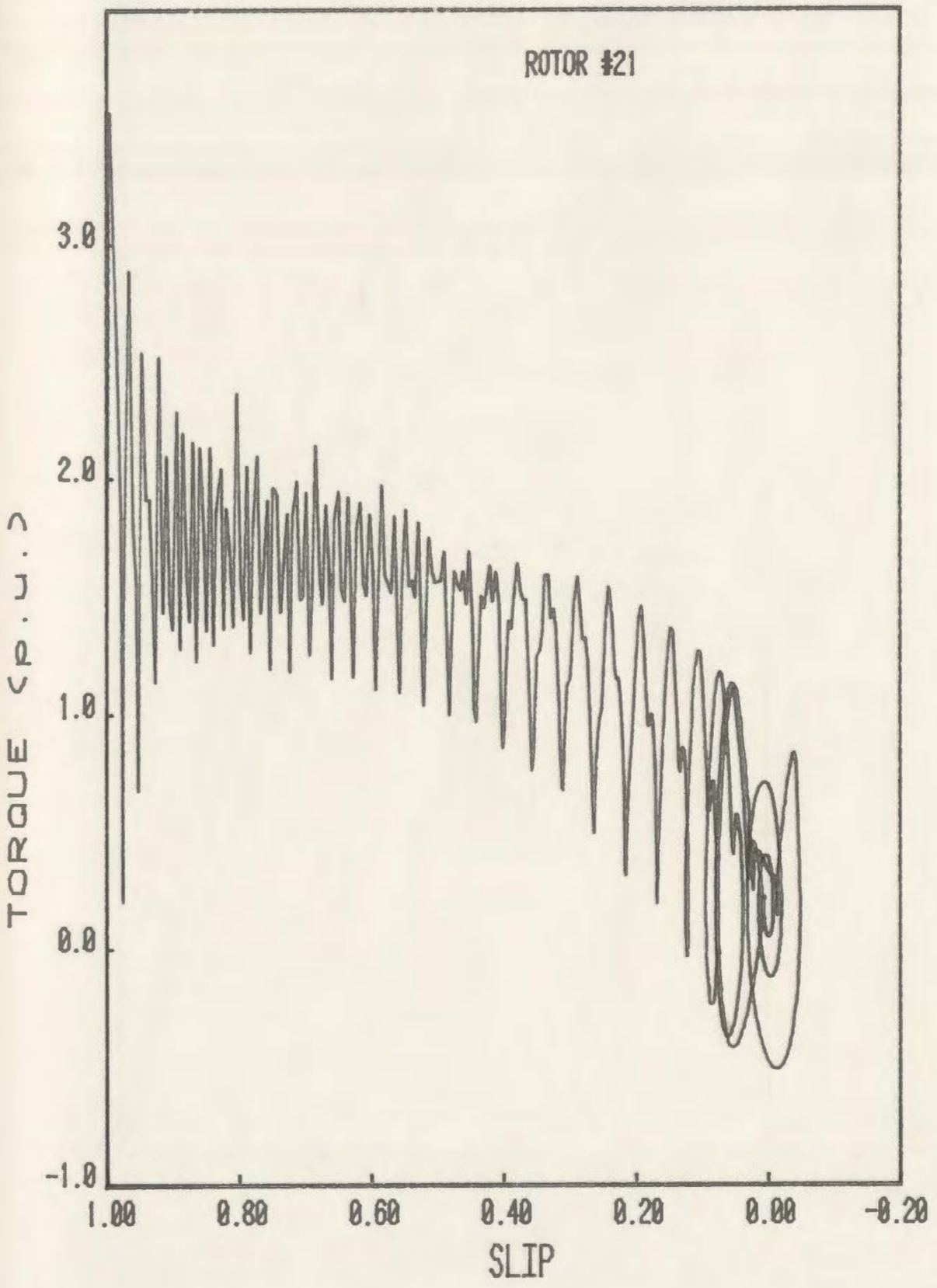

Figure 3.10 Rotor 21, torque as a function of slip

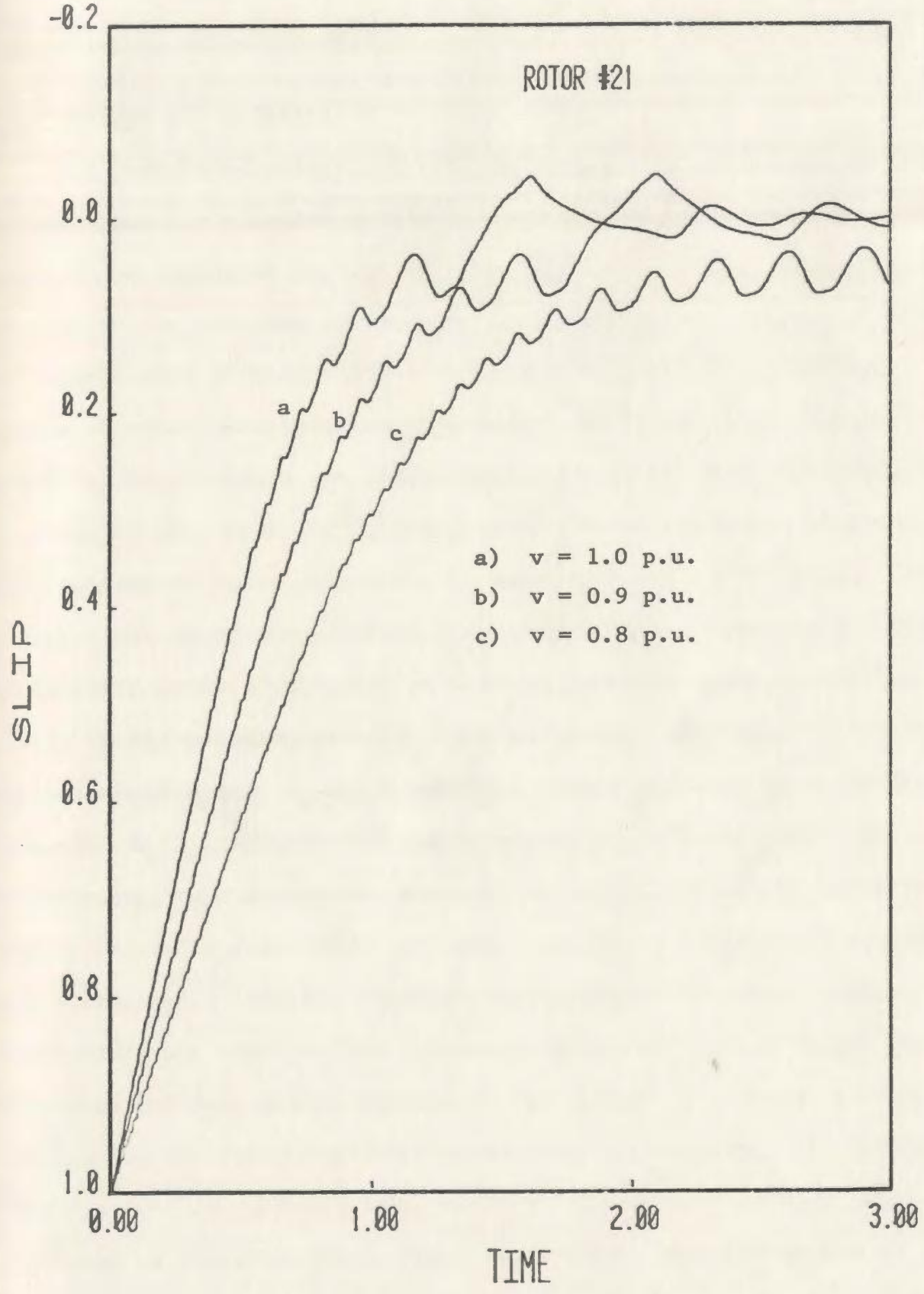

Figure 3.11 Rotor 21, starting at reduced voltage

4.0 MEASURED PROTOTYPE RESULTS

4.1 Testing Difficulties

The calculated results of the previous chapter, although giving insight into the behavior of the P.M. motor, hold little weight unless they can be supported by test results which show sufficient similarity to confirm the computed performance characteristics. In this chapter an attempt will be made to provide that confidence by presenting a series of test results, taken by standard test procedures, where possible, which detail the actual prototype performance and parameters.

It has been stated [35, 36, 53] that there are some particular difficulties in the measurement of parameters for a P.M. motor. For example, the rotor is permanently excited, thus all the conventional tests which require the rotor excitation to be reduced to zero (particularly in the measurement of X_q) are no longer applicable. Secondly, the values of E_o and X_d are inseparably linked via the machine saturable parameter E_o/X_d. Thus it becomes a matter of estimation, and not measurement, that determines the separate magnitudes of E_o and X_d by test. It can be shown that only the value of $E_o - I_d X_d$ can be determined uniquely. Finally, because of the size of the steel bridges surrounding the magnets, the phenomena of saturation can become very prominent and have marked effects on the values of measured parameters. Considering the foregoing constraints, the test data will be presented under the following three categories: a) static tests, which are conducted on the motor parts while there is no relative motion of the parts with respect to each other; b) steady state tests, which are conducted while the motor is running at or near synchronous speed; and

c) dynamic tests, which are taken during the time the motor is in a transition stage between one steady state condition and another. The following sections will briefly outline the test procedure, most of which is standard, with the results for the four prototypes where available.

4.2 Static Testing

With one exception, these static tests have been done on all of the motors of interest and include: a) stator winding resistance test, b) blocked rotor test, c) flux linkage test (only carried out on rotor 15), and d) pendulum swing test. These tests give estimates for the winding resistances of both stator and rotor, i.e. R_1, R_{2d}, R_{2q}, leakage reactances for both stator and rotor, X_1 X_2, the moment of inertia, M, the value of starting torque T_{st}, and information on the variance of the direct axis reactance X_d. Only the calculated values and the most important test results will be presented in the main body of this work; more detailed results may be obtained by consulting Appendix B. This will be the case for all forthcoming sections which deal with experimental results.

4.2.1 Stator Winding Resistance Test

This test is designated to give the value of the stator winding resistance, R_1, and is conducted on a stator after the rotor has been removed. The stator is then excited with various levels of balanced three phase currents, not exceeding the rated value, while recording the input voltage, power and current. A simple calculation yields the value of winding resistance. This value is then compared to that given

by an ohmmeter (or d.c. bridge) as a check on the first method. An appropriate constant has been applied to the ohmmeter reading to account for the skin effect at 60 Hz.

Since only one stator was used for each motor type, 1 or 2, only two tests were necessary. Table 4.1 shows the results of this test.

Table 4.1 Stator Winding Resistance

	Stator type 1	Stator type 2
Avg. a.c. resistance	18.25 Ω	14.02 Ω
d.c. resistance per phase	16.72 Ω	13.40 Ω
Skin effect factor	1.092	1.046

4.2.2 Blocked Rotor Test

The blocked rotor test, as with most of the other tests, was carried out in compliance with the appropriate standard test procedures [54-57] as closely as existing equipment would permit. This test consisted of applying sufficient load torque to the shaft in order to maintain a shaft rotation of less than 5 rpm while a reduced voltage was applied to give rated armature current. The minimum and maximum values of current and power were recorded and used to calculate R_{2d} and R_{2q}, the maximum readings relating to the direct axis and the minimum readings to the quadrature axis.

Included in this test is a measurement of the motor torque produced at the various reduced voltages. Knowing that the torque varies with a somewhat greater than the second power of the voltage, a value of starting torque can be extrapolated for the full voltage condition according to the procedure given by Pospisil [58]. Table 4.2 shows the calculated

leakage impeadances from the blocked rotor test while Figures 4.1 and 4.2 show the starting torque extrapolation. The leakage reactances are divided into rotor and stator in the proportions given by Matsch [59].

Table 4.2 Blocked Rotor Test Results

	Rotor 15	Rotor 16	Rotor 21	Rotor 22
Total leakage reactance	32.18	32.12	46.35	52.0
X_1	16.09	16.06	23.2	26.0
X_2	16.09	16.06	23.2	26.0
R_{2d}	5.72	5.03	26.8	38.17
R_{2q}	4.75	4.65	19.5	32.17

4.2.3 Flux Linkage Test

Jones [60] describes the flux linkage test for use in measuring the inductance of a coil or winding. Later this test was applied to the measurement of the direct axis inductance "L_d" of P.M. motors by Miller [36], who also expanded it to account for the presence of a quadrature axis current.

With the rotor and stator aligned along the direct axis, a d.c. current is used to establish a field in the stator winding. If the current is then changed suddenly, a measure of the resulting change in the voltage across the inductor, integrated over time, gives an indication of the inductance along the axis of alignment. This test, although yielding acceptable results, is very difficult to perform due to the instability of the bridge components. For sufficient accuracy these elements must be non-inductive resistors of low ohmic value, capable of

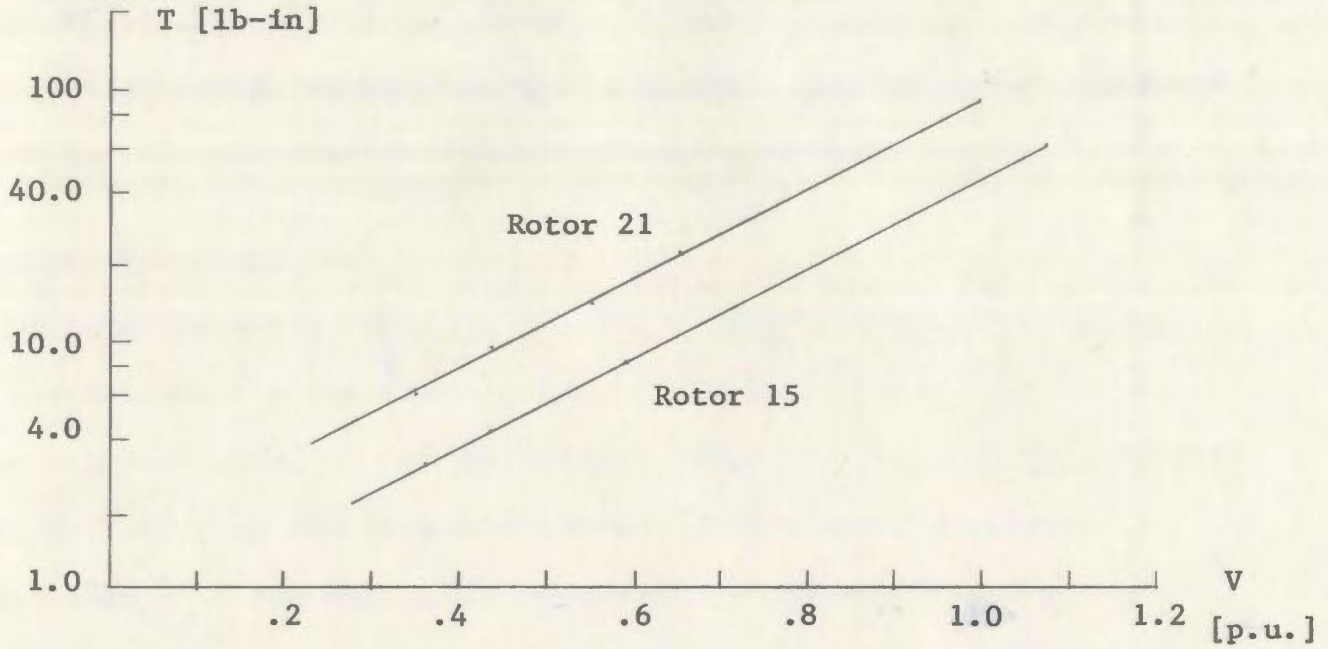

Figure 4.1 Full voltage starting torque for rotors 15 and 21

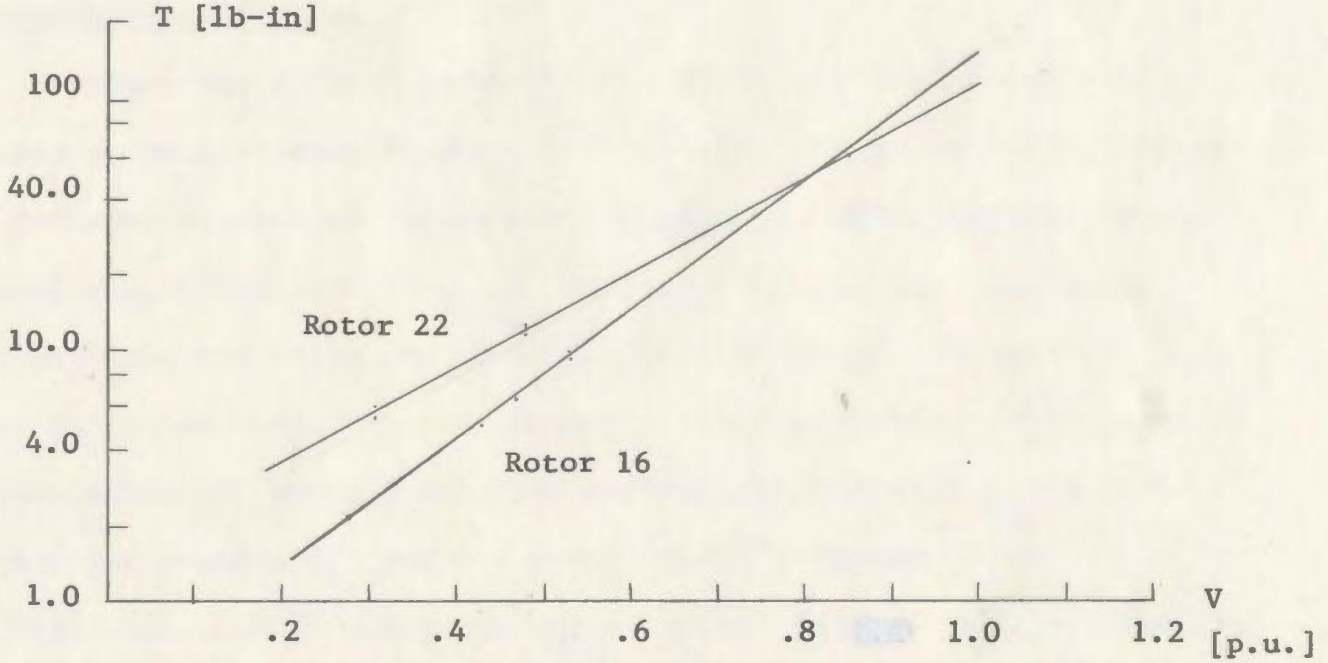

Figure 4.2 Full voltage starting torque for rotors 16 and 22

handling large d.c. currents. Problems arise when large currents are present and the bridge resistors start to heat up, changing the ohmic value and disturbing the balance of the bridge. This test was conducted on rotor 15 only and the results are shown in Figure 4.3.

4.2.4 Pendulum Swing Test

The pendulum swing test, or auxiliary pendulum test, is a common means for determining the rotor moment of inertia, and is reported in various standards [54, 57] and by Pospisil [58]. It requires an auxiliary mass to be placed on the circumference of the rotor and displaced by not more than 8°. The period of oscillation is measured and, with the known weights and measurements of the system, the rotational moment of inertia can be determined. The measured moment of inertia for rotor type 1 is 0.0015 $kg\text{-}m^2$ and for type 2 is 0.00284 $kg\text{-}m^2$.

4.3 Steady State Testing

The steady state tests were carried out on the prototypes while operating at or near synchronous speed and at a steady condition. These tests include: a) open and short circuit tests, which includes wave-form analysis, b) no load test, c) load test, d) pull-out torque test, and e) one heat run which was carried out on rotor 22. These tests are used to determine various motor parameters such as direct and quadrature axis reactances, X_d and X_q, friction and windage losses, P_{fw}, no load core loss resistance, R_c, and the open circuit voltage, E_o. As well, these tests are used to determine the motor performance characteristics such as: full load power factor and efficiency, pull-out torque and thermal capability.

4.3.1 Open and Short Circuit Tests

The open and short circuit tests performed on a P.M. motor are similar to those normally performed on the wire wound synchronous motor with the exception that the field excitation cannot be varied. The open circuit voltage is a primary indication of the amount of useful flux crossing the air gap. As with the wire wound motor, the higher the value of the open circuit voltage, the higher the motor's efficiency. The short circuit current is primarily used to determine the motor's saturated direct axis reactance X_d, which is approximated by the ratio E_o/I_{sc}. The values of E_o, I_{sc} and X_d are given in Table 4.3 for each of the four motors. Figure 4.4 also shows the short circuit current vs speed characteristic for each of the prototypes. Note that under short circuit conditions the current reaches approximately 90% of its saturated value at near 1/4 the rated speed, showing the quick saturation of the leakage paths under demagnetizing mmf.

Table 4.3 Open and Short Circuit Measurements

	E_o (1-1) [V]	I_{sc} [A]	X_d [Ω]
Rotor 15 (3600 rpm)	294.4	1.80	94.4
Rotor 16 (3600 rpm)	231.	1.47	90.7
Rotor 21 (1800 rpm)	335.8	2.68	72.3
Rotor 22 (1800 rpm)	276.0	2.16	73.8

As to the manner of test, both the open and short circuit characteristics are measured while the P.M. motor is operating as a generator being driven at rated speed. (Note: due to the high torque required to

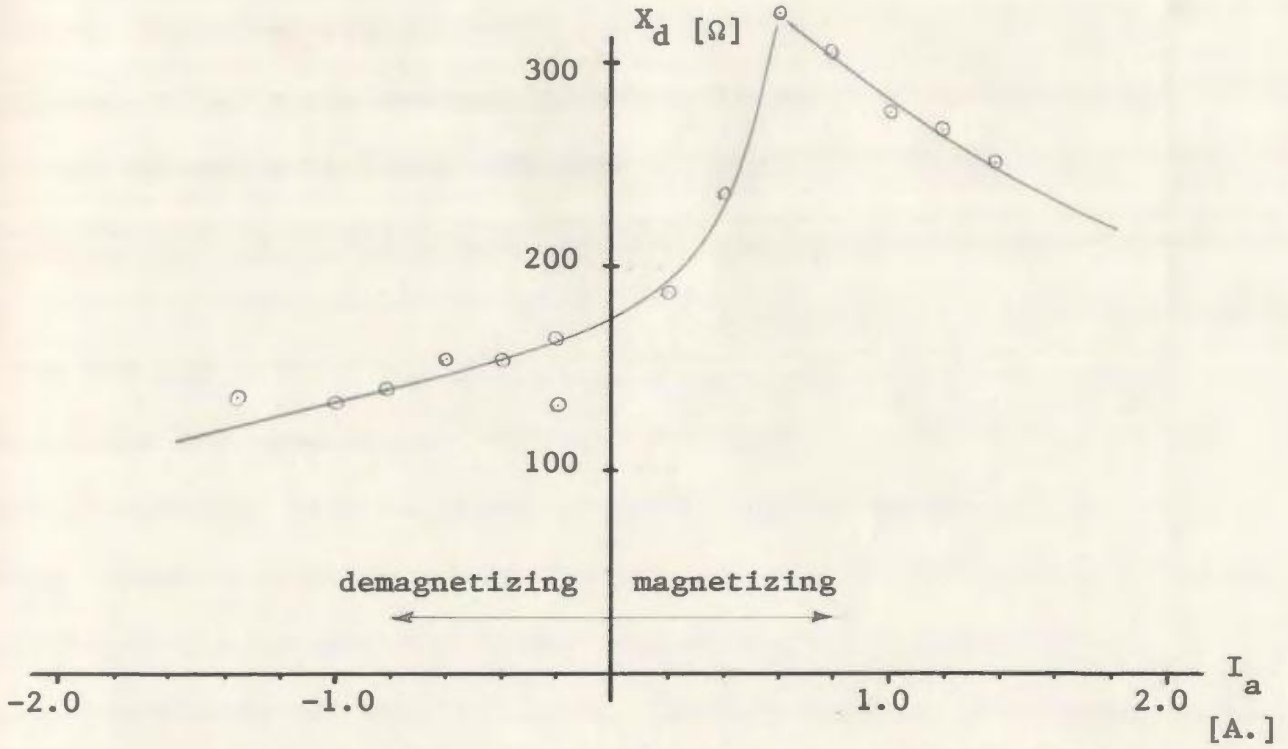

Figure 4.3 Measurement of X_d by flux linkage test

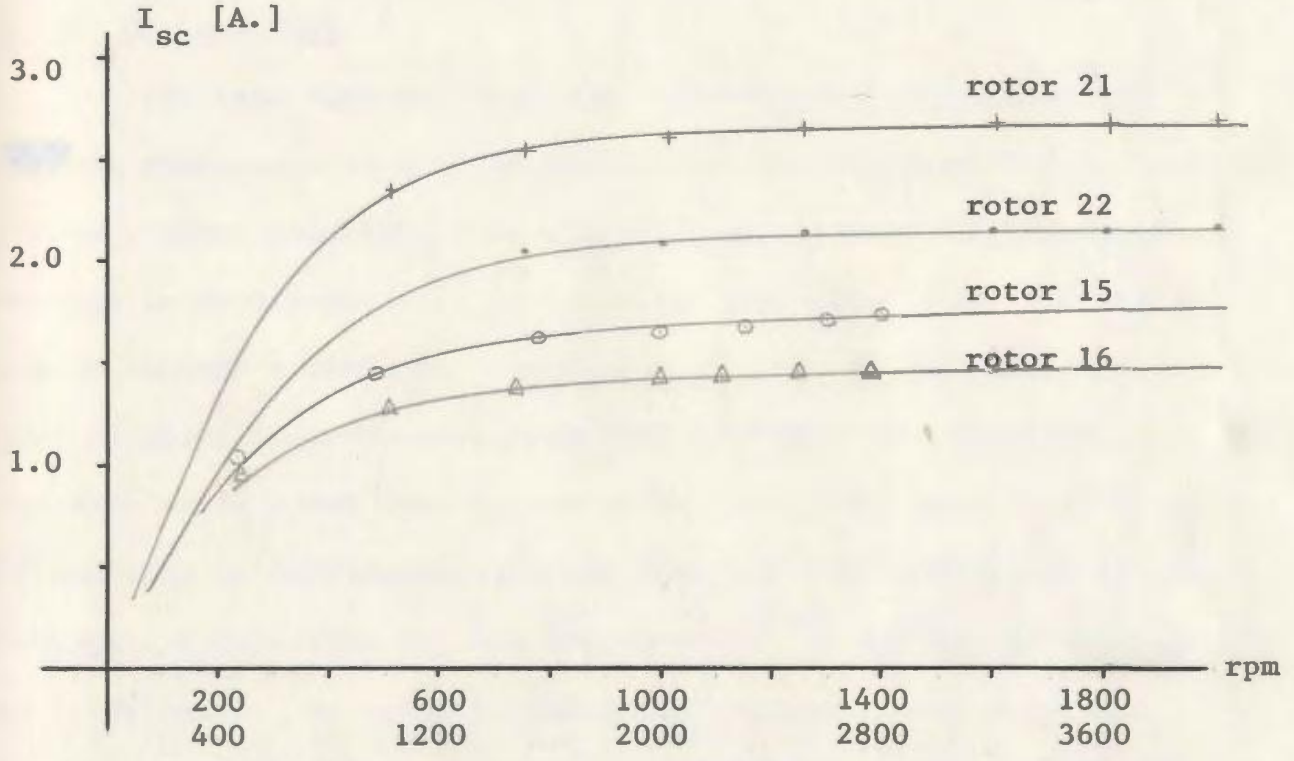

Figure 4.4 Short circuit current as a function of speed

drive the type 1 rotors under short circuit conditions, it was not possible to obtain the reading at 3600 rpm; but readings exceeding 2700 rpm are ample to fully saturate the machine.) Upon receipt of the prototype stators it was deemed necessary to insert a search coil in the face of the stator laminations. Therefore small slots were machined in the air gap side of the stator teeth and a full pitch winding of three turns was epoxied in. Using this search coil the air gap flux density waveforms were recorded for both open and short circuit conditions. Figure 4.5 shows normalized open circuit waveforms and a Fourier analysis of the various waveforms, while Figure 4.6 shows the short circuit waveforms for type 1 rotors. These waveforms, which are similar to those presented by Miyashita [32], reveal much about the magnet geometry and will be discussed in more detail in the next chapter.

4.3.2 No Load Test

As the name implies, this test is conducted while the motor is running synchronously with no attached load. Measurements of voltage, current, power and shaft load angle "δ" are taken as the terminal voltage is decreased. Various readings are taken until the current passes through a minimum. These results are then extrapolated to zero applied volts in accordance with IEEE standard test practice [54]. From the zero volts power reading the mechanical power loss to friction and windage can be determined and from that the full voltage core loss. Moreover, a reference for the torque angle "δ" can be obtained for use in later tests. By using a stroboscope and reference markings, it is observed that δ passes through a minimum angle at reduced voltage and the minimum angle "δ_o" is assumed to be approximately $\delta_o = 0°$. For

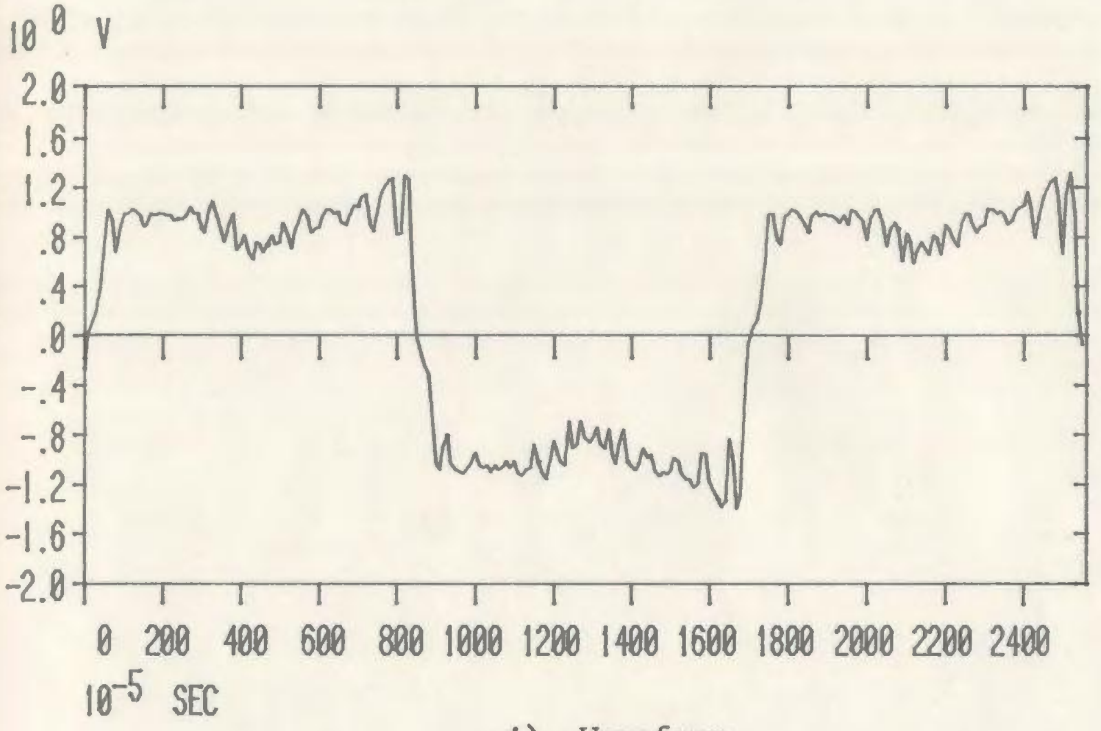

i) Waveform

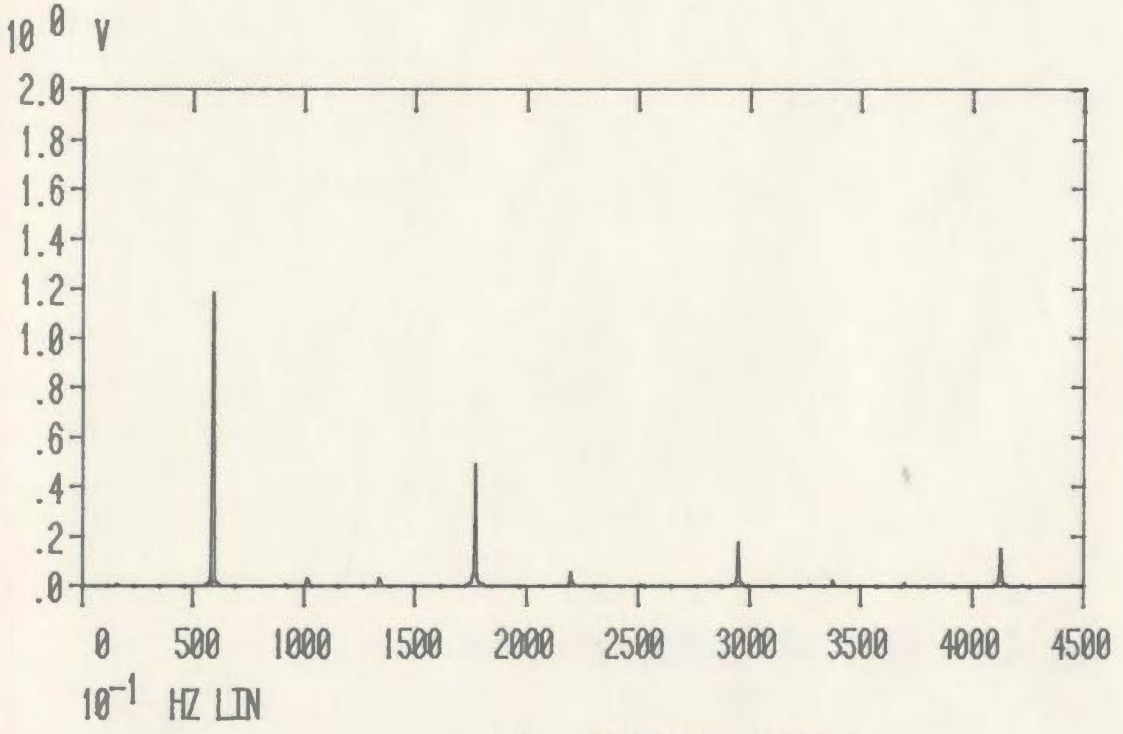

ii) Harmonic content

Figure 4.5a Rotor 15 open circuit waveform and spectrum

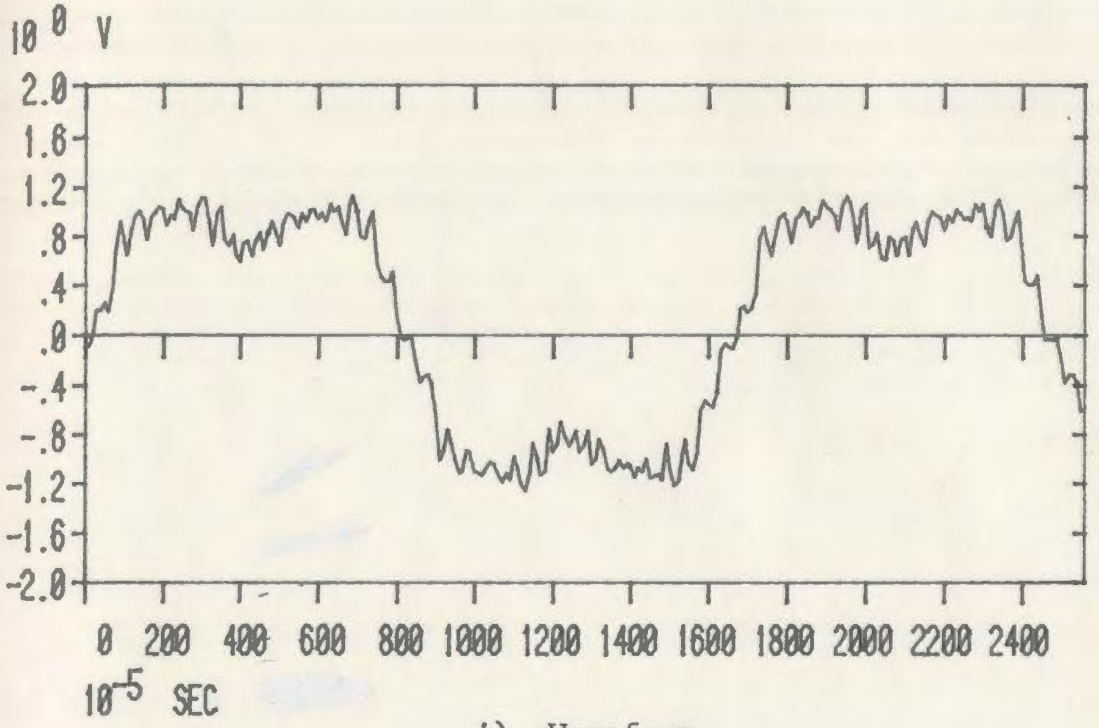

i) Waveform

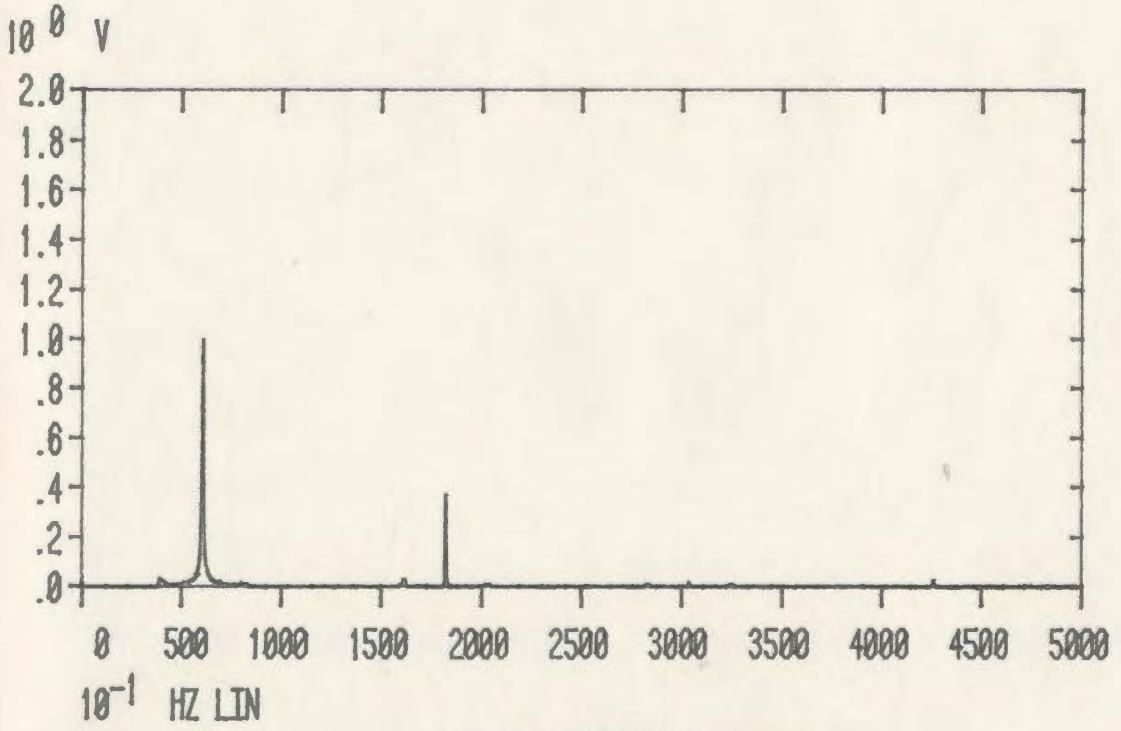

ii) Harmonic content

Figure 4.5b Rotor 16 open circuit waveform and spectrum

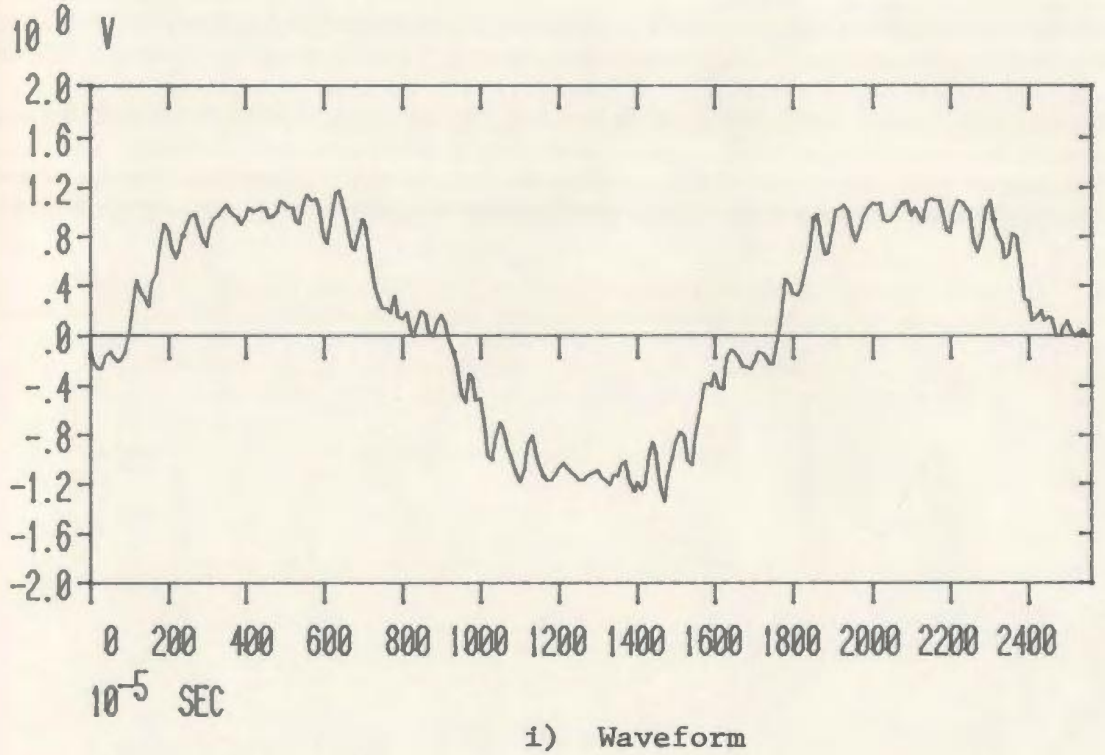

i) Waveform

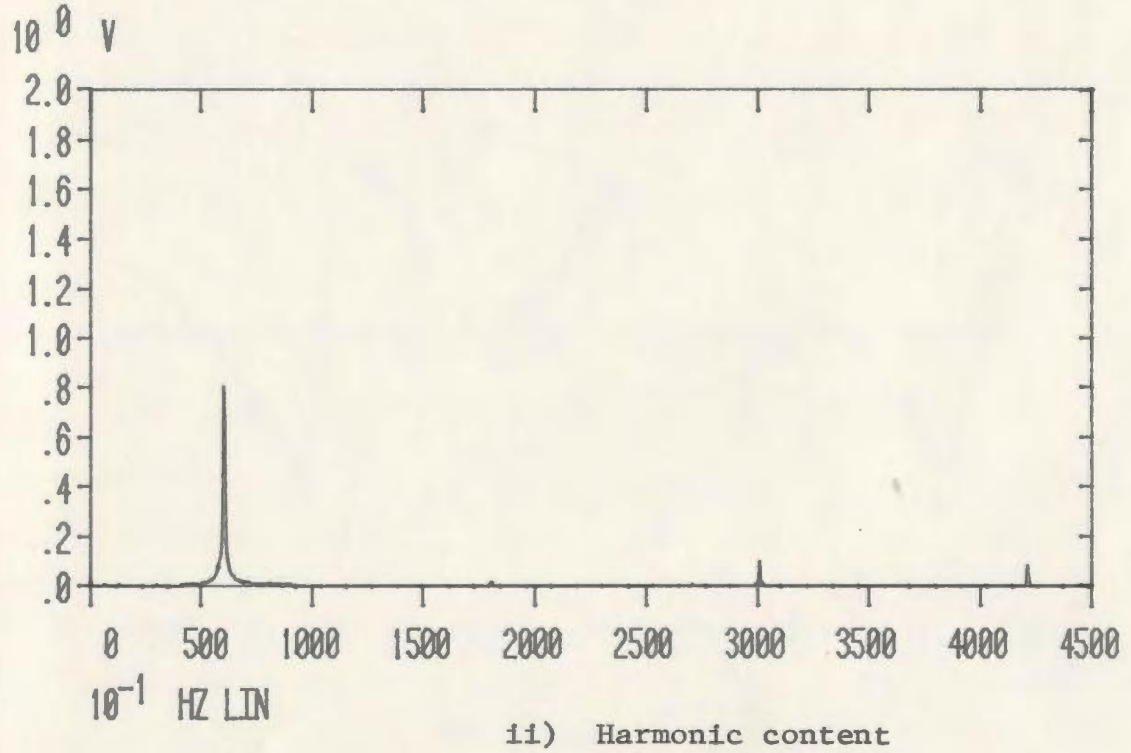

ii) Harmonic content

Figure 4.5c Rotor 22 open circuit waveform and spectrum

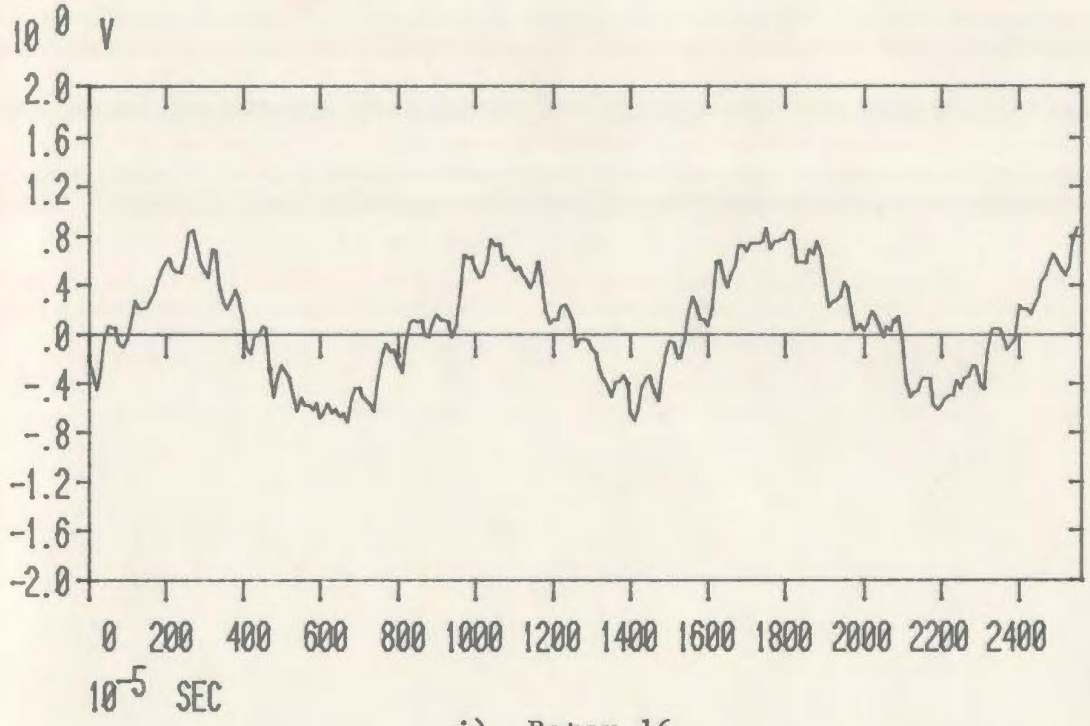

i) Rotor 16

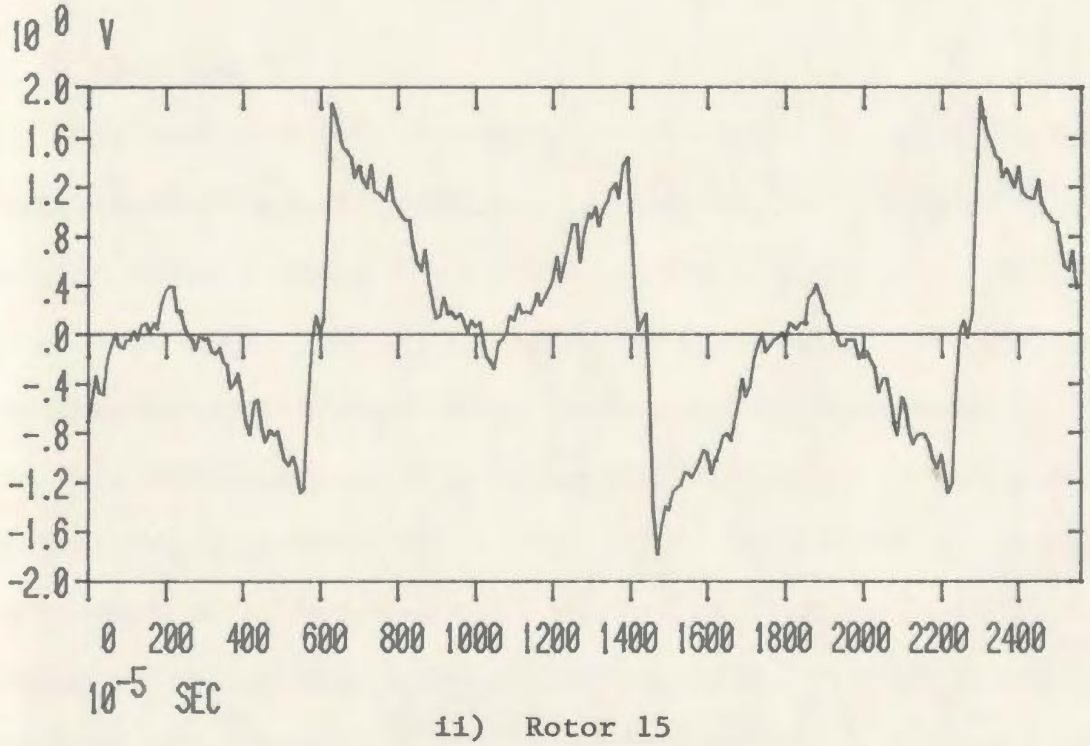

ii) Rotor 15

Figure 4.6 Short circuit waveforms for type 1 rotors

comparative purposes, Table 4.4 shows the two loss figures for the prototypes as well as the core loss values for the associated induction rotor designated as rotors 10 and 20 for types 1 and 2 respectively.

Table 4.4 Mechanical, Friction and Windage Losses for P.M. Rotors

Rotor	Friction and Windage Loss "P_{fw}"	Core Loss "P_c"
10	31.5 W	77.4 W
15	38.0	79.6
16	31.0	94.0
20	19.0	155.0
21	32.0	108.0
22	16.5	97.0

4.3.3 Load Test

This test involves loading the P.M. motor by means of calibrated dynamometers in equal steps to a loading as near as possible to the pull-out value. Using the reference torque angle "δ_o", obtained from the no load test, the torque angle can be measured for any load and consequently used to calculate values for the parameters X_q, X_d and E_o. This calculation can be done in several ways, two of which include using the measured data points to arrive at values for the parameters for every point using the equations derived in Chapter 2, or by using various curve fitting techniques on the power vs torque angle curve to arrive at average values. The present work uses the former method as is shown in Tables 4.5 a-d, which give the load test results.

Furthermore, the load test is the only means of determining the performance characteristics of the motor. Power factor and efficiency are two of the important characteristics. These two critical parameters are necessary for determining the feasibility of the P.M. motor replacing the induction motor in energy saving applications. They are included in the load test results in Tables 4.5 a-d.

4.3.4 Pull-out Torque Test

This test, although done in conjunction with the load test, is considered a separate entity to determine the motor's pull-out capability. The tested motor is loaded, by means of dynamometers, until the rotor looses synchronism with the stator mmf-wave, for various conditions of reduced voltage. Using the method previously shown for determining the starting torque [58], the pull-out torque can similarly be determined. The pull-out torque is a useful performance indicator and is used in determining what horsepower rating should be given to the prototype motor. Table 4.6 lists the various pull-out torque values.

Table 4.6 Pull-out Torque Levels

	Pull-out Torque	
Rotor	[lb-in]	[N-m]
15	41.5	4.69
16	34.9	3.94
21	149.0	16.83
22	99.0	11.18

Table 4.5 Load Test Results

a) Rotor 15 (voltage held constant at 575V.)

I_a (amps)	P_{in} (watts)	Load (lb-in)	δ (°)	Power factor	EFF. (%)	X_q (Ω)
.738	359	2.0	18	.489	23.7	189.2
.893	561	6.0	23	.631	45.5	164.2
1.088	761	10.0	27	.703	55.9	145.9
1.328	975	14.0	31	.737	61.2	131.4
1.595	1188	18.0	35	.748	64.5	120.2
1.917	1437	22.0	40	.753	65.2	111.3
2.48	1760	26.0	48	.727	62.9	101.9
2.869	2115	30.0	56	.740	60.4	98.7
3.428	2680	34.0	68	.785	54.0	103.4

b) Rotor 16 (voltage held constant at 575V.)

I_a (amps)	P_{in} (watts)	Load (lb-in)	δ (°)	Power factor	EFF. (%)	X_q (Ω)
1.03	420	2.0	29	.412	20.3	195.7
1.18	636	6.0	35	.543	40.2	174.8
1.34	824	10.0	38	.619	51.7	157.4
1.57	1046	14.0	41	.671	57.0	140.1
1.90	1318	18.0	48	.695	58.2	129.6
2.46	1669	22.0	56	.675	56.1	112.0
2.85	1887	24.0	63	.661	54.2	106.6
3.06	2155	26.0	69	.702	51.4	109.8
3.34	2442	28.0	76	.729	48.8	114.0

....continued

Table 4.5 (continued)

c) Rotor 21 (voltage held constant at 575V.)

I_a (amps)	P_{in} (watts)	Load (lb-in)	δ (°)	Power factor	EFF. (%)	X_q (Ω)
1.23	507	8.0	20	.414	33.6	131.8
1.30	681	16.0	20	.524	50.0	111.4
1.42	857	24.0	24	.608	59.6	108.3
1.54	1049	32.0	28	.684	65.0	106.9
1.70	1220	40.0	36	.720	69.8	115.9
1.88	1417	48.0	40	.759	72.2	113.5
2.05	1601	56.0	44	.783	74.5	113.0
2.28	1833	64.0	50	.809	74.4	114.9
2.52	2057	72.0	54	.820	74.5	112.8
2.77	2270	80.0	58	.822	75.1	110.6

d) Rotor 22 (voltage held constant at 575V.)

I_a (amps)	P_{in} (watts)	Load (lb-in)	δ (°)	Power factor	EFF. (%)	X_q (Ω)
1.23	427	8.0	20	.350	39.9	142.6
1.32	610	16.0	26	.464	55.8	136.8
1.40	770	24.0	30	.553	66.4	132.6
1.52	945	32.0	32	.624	72.1	122.7
1.66	1124	40.0	34	.680	75.8	114.9
1.84	1317	48.0	40	.718	77.6	116.2

4.3.5 Heat Run Test

One of the critical features of any motor design is the motor's thermal capability. The full load temperature rise indicates what insulation class (B, F, etc.) can be used on the motor windings. A class B insulation system allows for an 80°C rise over a 40°C ambient with the maximum temperature not to exceed 135°C in any one location. In order to ensure that the P.M. motor prototypes were operating within class B limits a heat run was conducted on rotor 22. Two resistance temperature detectors (RTD's) were imbedded in the stator core and a thermometer was secured to the frame exterior, then the motor was loaded to deliver a 1 hp shaft load to a dynamometer and temperature readings were recorded at 5 minute intervals until a steady temperature was achieved. Upon completion of the test, the d.c. resistance of the stator winding was taken to determine the average winding temperature rise by resistance method (RRM). Table 4.7 and Figure 4.7 illustrate the results.

Table 4.7 Full Load Temperature Rise for Rotor 22

Detector (see Fig. 4.7)	Temperature Rise
Thermometer	17°C
RTD #1	51.7°
RTD #2	50.5°
RRM	61.7°

Ambient temperature = 25.1°C

$$RRM = \frac{R_{hot}}{R_{amb}} (\theta_{amb} + 234.5) - \left(\theta_{amb} + 234.5\right)$$

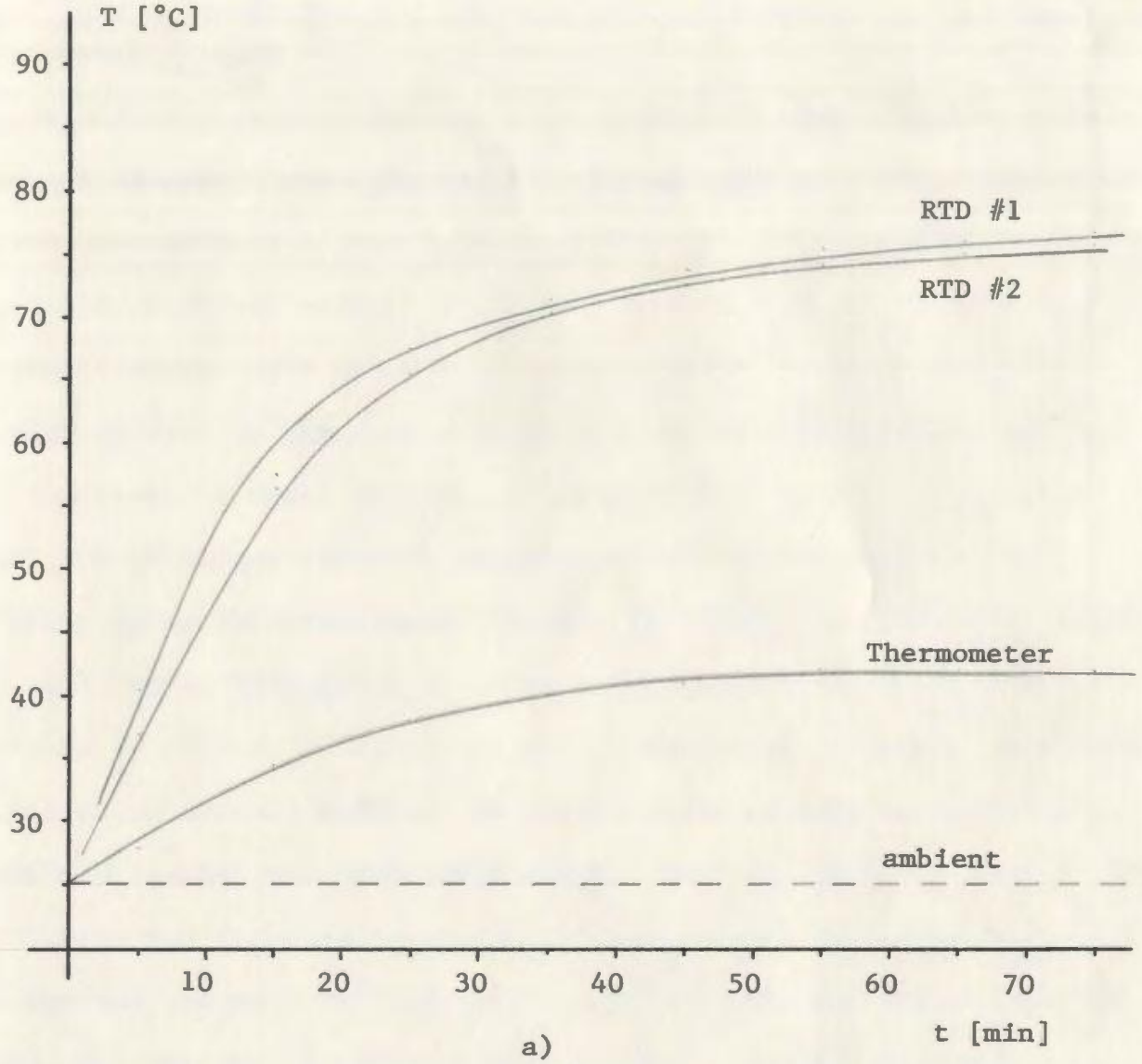

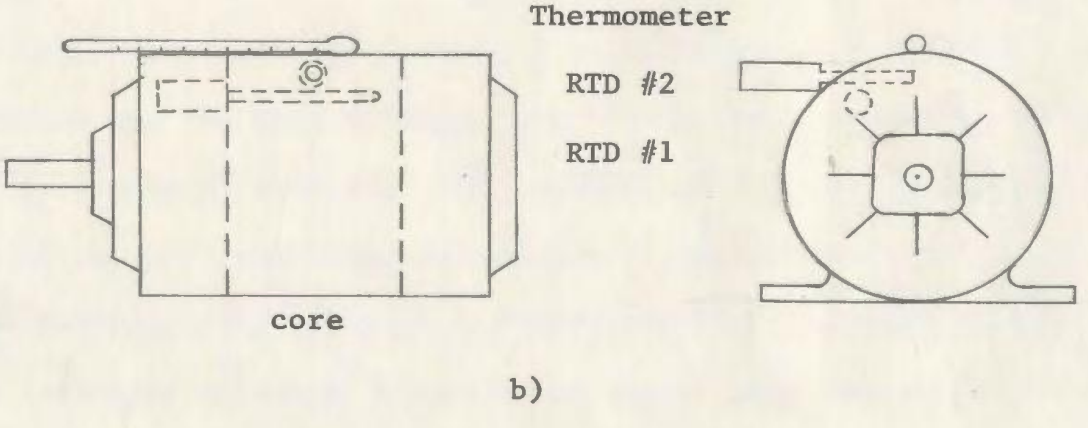

Figure 4.7 Full load temperature rise: a) as a function of time; b) RTD placement

4.4 Dynamic Testing

To a lesser extent the prototypes have been tested while in the transient stages between two steady state conditions. This testing includes measurement of the run-up speed under various loading conditions and of the speed variations as a sudden load torque is applied while running at synchronous speed. These test conditions provide useful correlation for the transient prediction routine shown in Chapter 3.

Two separate speed transducers were used to provide the speed signal for transient response curves each of which were used for different operating conditions. A small aircraft type P.M. d.c. generator with linear voltage vs speed characteristic was used as a tacho-generator to provide a voltage signal proportional to speed. A simple R-C filtering circuit reduced the tacho output voltage to acceptable levels and removed the commutator noise. This system was used to measure the run-up curves where an accurate signal was required from zero rpm and upward. For the small speed perturbation signal from the sudden load testing, an elementary digital tachometer was used. A clear plexiglass disk with alternate opaque striping was used in conjunction with a light and sensor to produce a pulse train at 1 Hz/rpm. This pulse train was fed into a phase locked loop (pll.) which had a tuned center frequency of 1.8k Hz. Thus when the motor was synchronized the output of the pll. was zero, but during speed perturbations due to load changes the output was directly proportional to the speed change. Figure 4.8 shows a layout of the speed measurement system, and Appendix C gives the details of the schematics and design values.

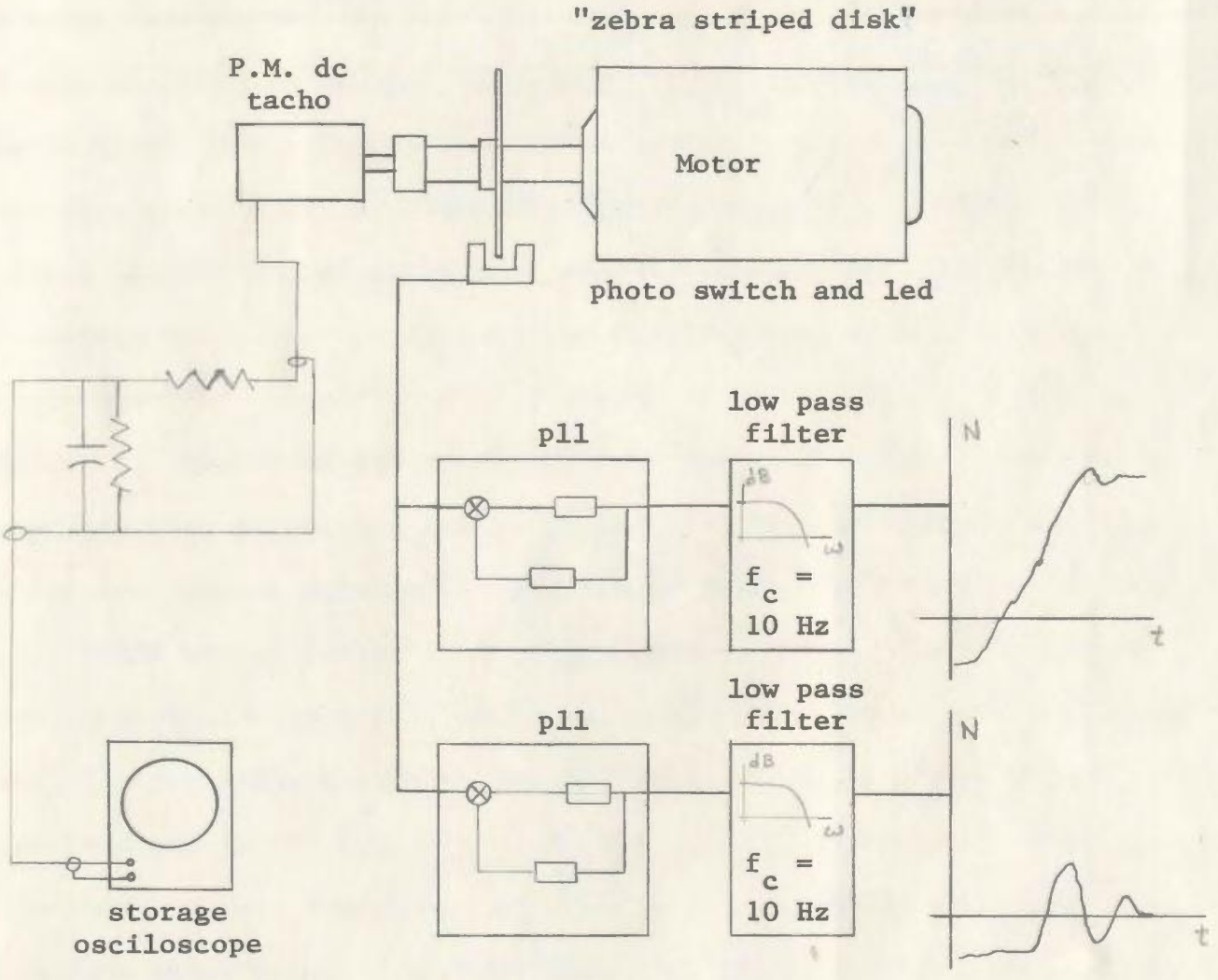

Figure 4.8 Speed measurement system for transient response

4.4.1 Run-Up Test

The run-up test consists of starting the prototypes under differing load conditions and recording the speed run-up as a function of time. These tests give some indication of the motor's ability to accelerate and synchronize various loads. Rotors 15 and 21 were tested under the following conditions: 1) the rotor was started with no connected load and only the inertia of the rotor itself, 2) the rotor was started with a small (i.e. 10%) friction load and a coupled inertia of 0.027 kg-m^2 (this is approximately 20 times the inertia of rotor 15 and exceeds 10 times the inertia of rotor 21), and 3) the rotor was started with the maximum friction load it could synchronize with a coupled inertia of approximately twice the rotor inertia. Figures 4.9 - 4.11 are pictures of the actual oscilloscope trace for each of the loading conditions described above, for rotors 15 and 21. By manipulating the input voltage and current signals it is possible to obtain a signal proportional to the rotor output power. This signal was recorded as a function of rotor speed to obtain a plot somewhat similar to a dynamic torque vs speed plot. The resulting curves for rotor 22 are shown in Figure 4.12 for a) no load run-up and b) run-up with large friction loading. Figure 4.13 is included to show the effect of line voltage on starting capability. The figure shows rotor 21 accelerating a small friction load at 1.0, 0.9 and 0.8 p.u. voltage. Finally Figure 4.14 is given to demonstrate the result of trying to accelerate a friction load beyond the motor's capability; it clearly shows the large speed pulsations which extend from approximately 1240 rpm to 1440 rpm.

a)

Rotor 15

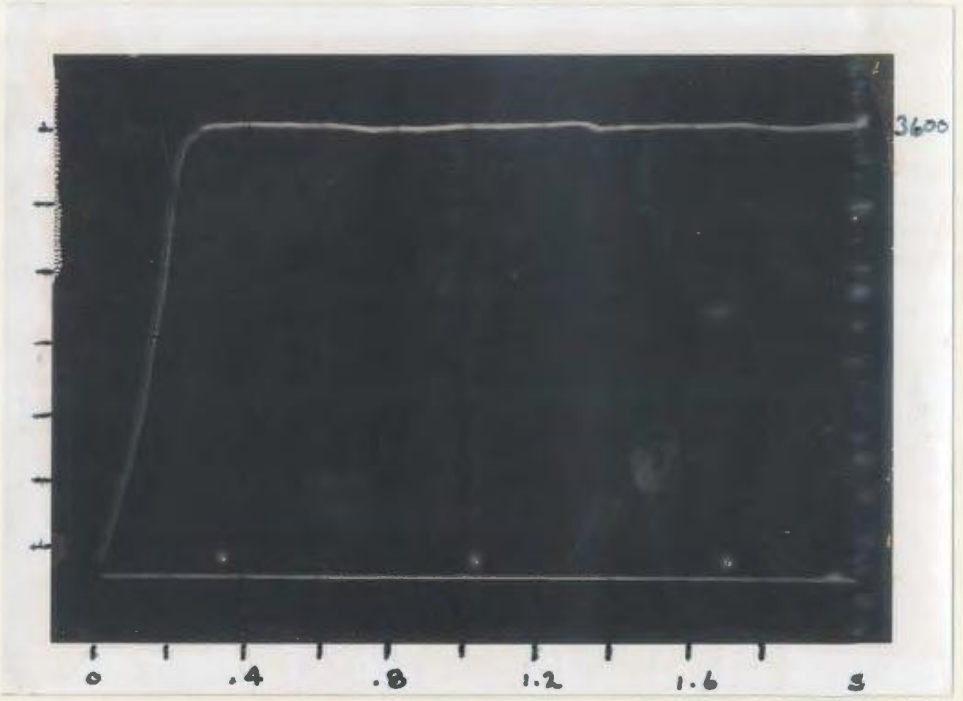

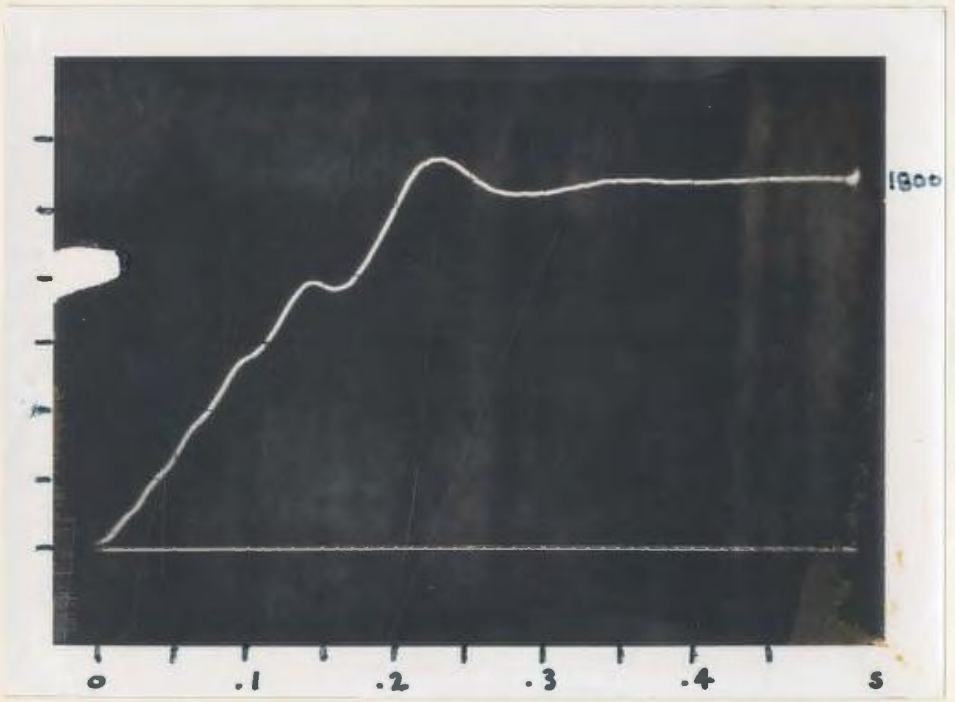

b)

Rotor 21

Figure 4.9 No load run up response

a)

Rotor 15

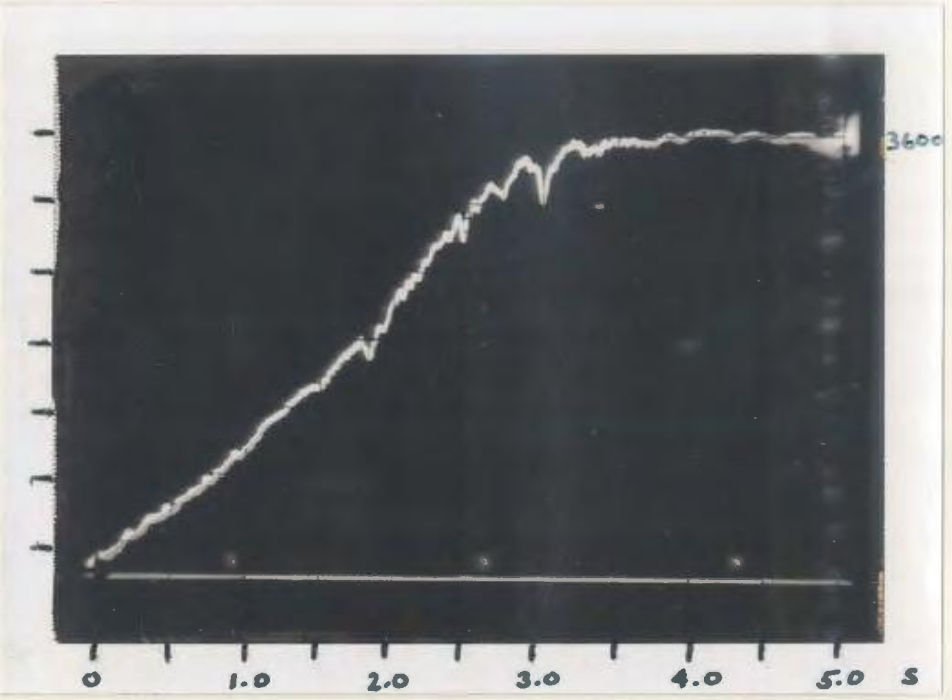

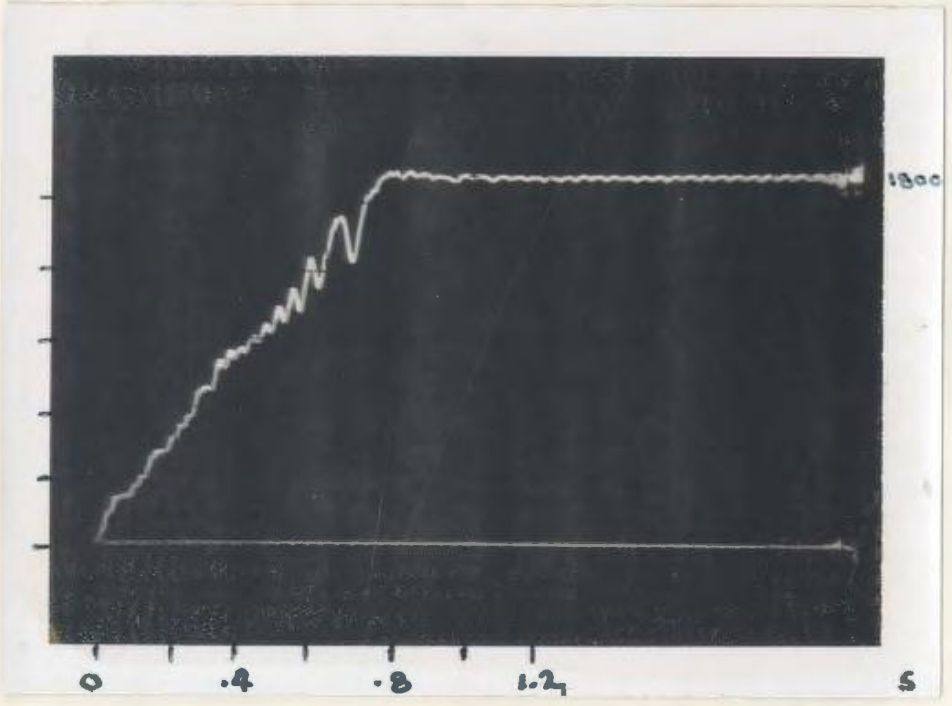

b)

Rotor 21

Figure 4.10 High inertia run up response

a)

Rotor 15

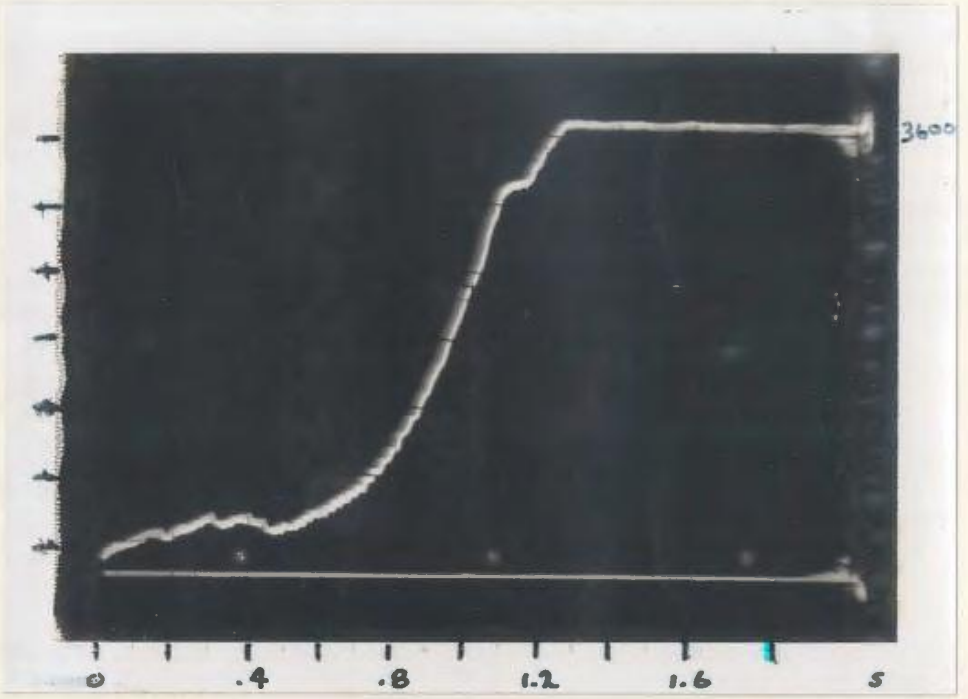

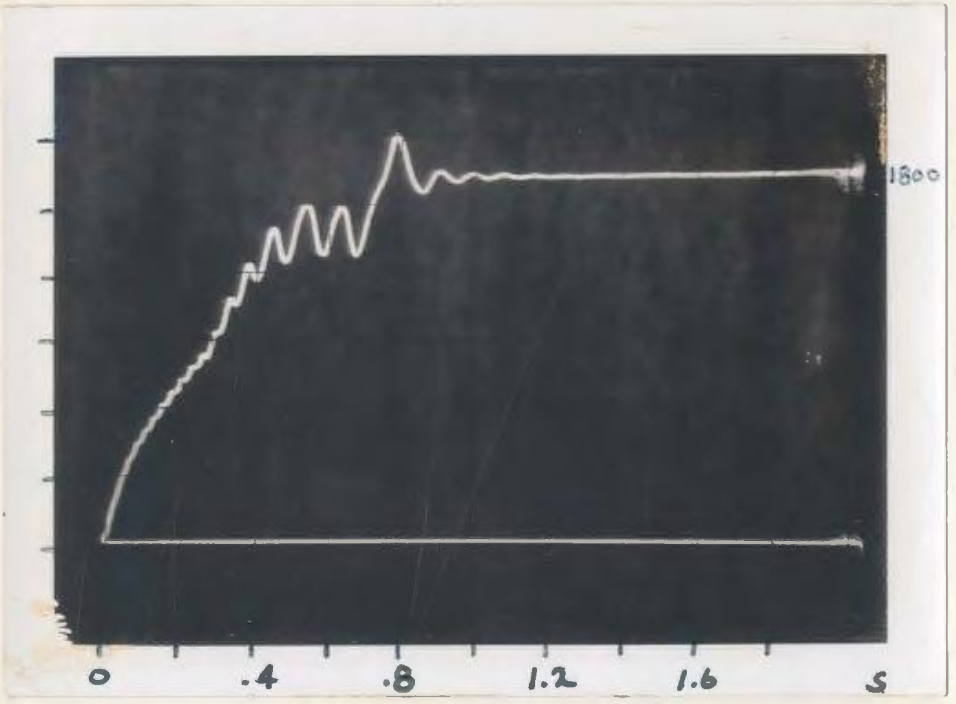

b)

Rotor 21

Figure 4.11 Large friction load run up response

a)

No load run-up,
rotor 22

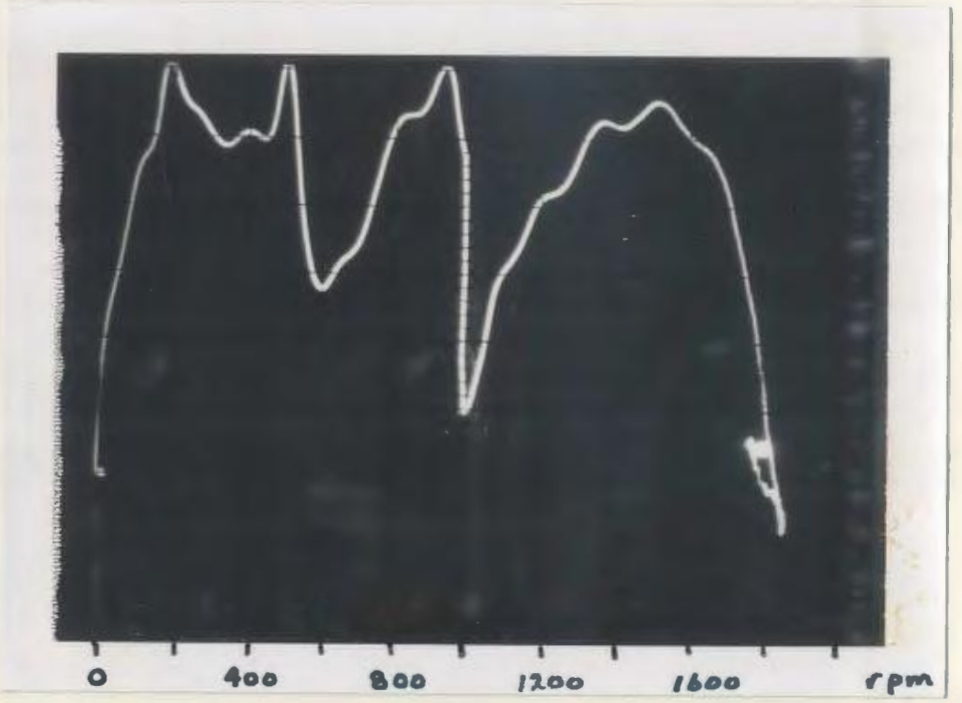

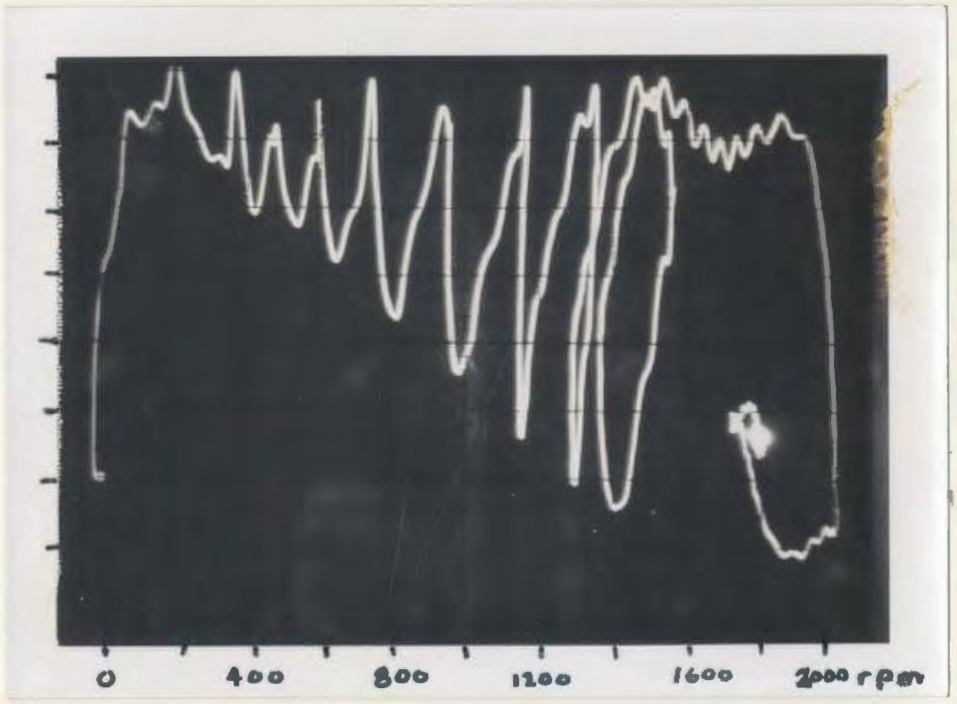

b)

Large friction load,
rotor 22

Figure 4.12 Output power versus speed characteristic

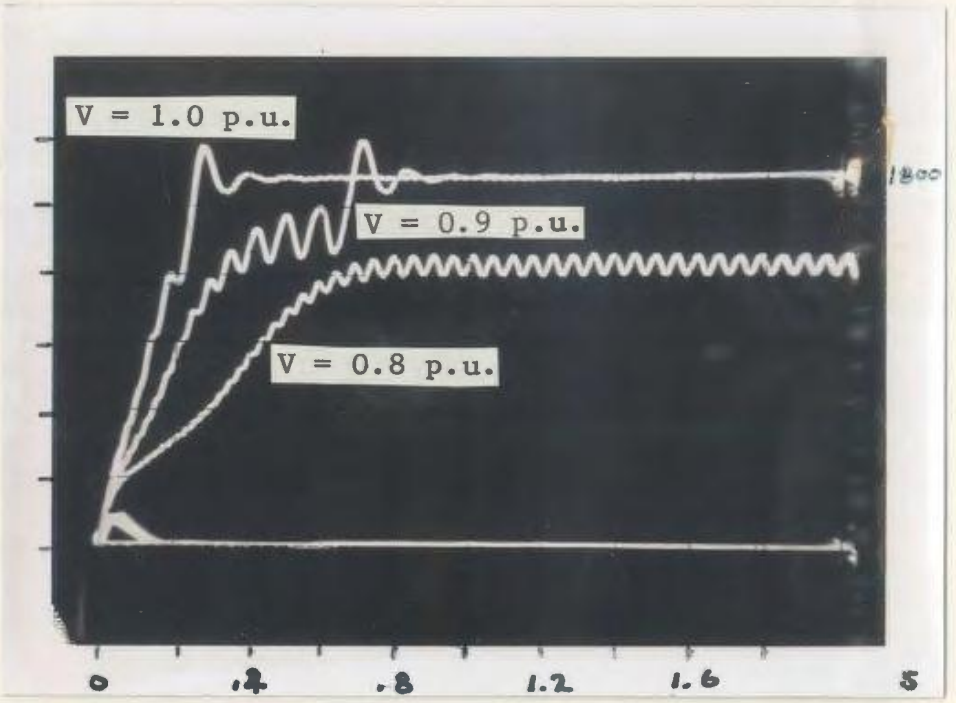

Figure 4.13

Effects of line voltage on starting

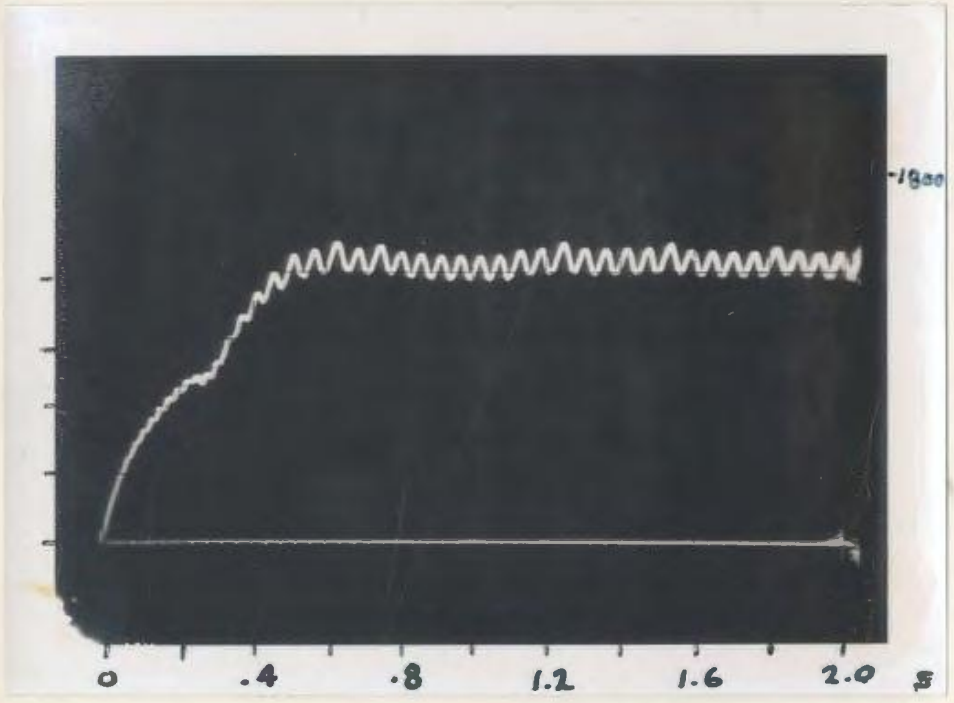

Figure 4.14

Synchronization not achieved

4.4.2 Sudden Applied Load

The sudden applied load test consists of applying a load to the motor shaft while operating at synchronous speed in steady state. The instantaneous speed variations are recorded to give an indication of the motor's operating stability. The test is repeated for removal of the load as well. The applied load consisted of a friction load of one-half the motor's rated capability. This test helps determine the effect of the starting cage as a damper winding.

a)

Load application
Rotor 22

Applied load =
19.5 lb-in

Vertical = 17.75
rpm/div

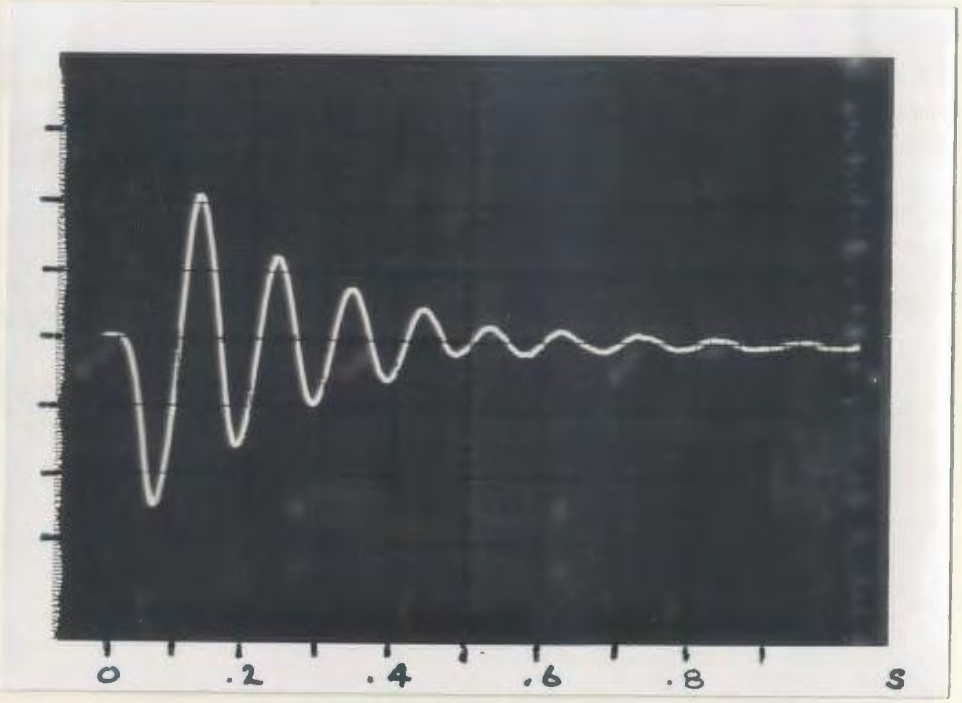

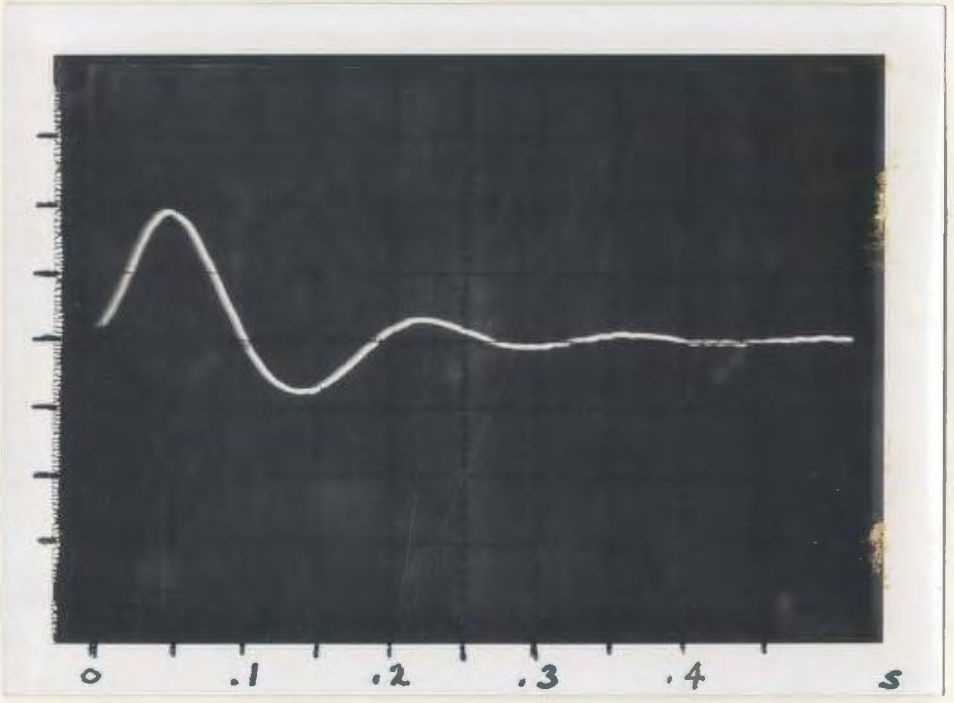

b)

Load removal
Rotor 22

Initial load =
19.5 lb-in

Vertical = 17.75
rpm/div

Figure 4.15 Sudden application and removal of load

5.0 PARAMETER VARIATION FOR DESIGN IMPROVEMENT

In this chapter the results of the previous two chapters will be compared to give a reasonable confidence in the numerical prediction routines. Having achieved that, a number of parameter variations will be attempted in order to optimize the present rotor configuration. Furthermore, the parameter studies will allow an indication of where the major effort should be placed in future design work. With the number of parameters available to the P.M. motor designer, a comprehensive parameter study would be a monumental task covering a significant time period. Therefore only the four parameters deemed most critical to the overall design will be dealt with in this work, namely, 1) the overall geometry of the magnets, 2) the steel paths available for leakage flux, 3) the rotor cage design, and 4) the effects of various magnet materials on motor performance and design.

5.1 Correlation of Predicted and Tested Results

Upon comparing the results presented in the previous two chapters, it is apparent that a high degree of correlation exists in both the transient and steady state results. Note particularly the steady state results of Table 3.5 and Table 4.5a, where the torque angle and armature current predictions are very close. Furthermore, the output efficiency and power factor stay within 5% of the actual tested results until the output power goes above full load. The predicted values of X_q also follow the pattern of saturation verified by the load test. Secondly, and most important to note from the tested results of rotor 15 is the sudden jump in power factor for the last few test points. Although this jump does not occur at the same load value in the predicted case, it

does confirm the existence of the saturation effect along the d-axis. Honsinger [35] also shows this sudden saturation but states that it occurs for currents less than the no-load value. This conclusion is true for his particular design, but, in general, the point at which saturation occurs is entirely dependent on the thickness of the bridges and the X_d/X_q ratio. By comparing the predicted and tested results for rotor 21, it is evident that the saturation effect occurs just beyond the pull-out capability and thus there is no sudden jump in power factor, as in rotor 15.

While the computed results for rotor 21 more accurately predict the pull-out capability of the motor, the overall correlation between tested and predicted values is not as good as for rotor 15. Part of the reason for this is that the winding information for the type 2 stator is not known with any confidence. Consequently the values for X_m and E_o may be incorrect, and hence the whole performance prediction is subject to question. Therefore, to keep the parameter variations which are to follow as meaningful as possible, only rotor 15 data will be used.

The transient results also give a high degree of correlation. Due to the large number of parameters and variables associated with the transient routine, a point by point correlation cannot be expected. However, the accuracy of the program may be judged by the general shape of the transient curve and the duration of the transient. Furthermore, there are many unknowns which are very difficult to determine or account for, such as the timing belt friction load as a function of belt tension, input supply unbalance, voltage fluctuations, and frequency deviations,

etc. To illustrate the correlation, Figure 4.11 shows the response of the two rotors for large friction loading. The response for rotor 15 shows a low initial acceleration but synchronizes well; on the other hand, rotor 21 starts quickly but has more difficulty in synchronizing. This is to be expected from the low rotor resistance of rotor 15 and the much higher resistance of the rotor 21 cage, and is seen in the predicted curves (see Figures 3.8 and 3.9).

5.2 Important Parameter Variations

In this section a number of important observations will be made about the design and construction of P.M. motors which have arisen from the construction of the prototypes and also from the work in the area of computer prediction of performance. The burden of proof for the observations to follow will be taken from the actual tested results, since these, by their very nature, are a more reliable source upon which to base conclusions.

5.2.1 Magnet Geometry and Waveforms

In order to present a commercially viable P.M. motor it is important to make maximum use of the magnets, primarily because the magnets, at near $25 per pound, will make up a large percentage of the total material costs. It is reasonable then to try and minimize the total magnet volume in a given rotor. Furthermore, the magnets should be of simple geometry (i.e. rectangles as opposed to arcs) such that the individual pieces of magnet are easily manufactured, and also, the magnets should be placed such that the resulting characteristics are maximized. With these constraints in mind the design of the present prototypes will be

analyzed and appropriate advantages or improvements will be noted.

In order to have the magnet volume minimized it is important to have the magnets operating at or near the maximum energy product point on the demagnetization curve. For the present design or that of Honsinger [35] this would require magnet section 1 to be twice the thickness of magnet section 2. For the ideal case of the magnets operating at the peak energy product for a fully loaded motor, this would require the magnets to be stabilized for the full demagnetizing forces which occur during start up, which can be up to six times the full load values. This poses no major problem for the linear rare earth cobalt magnets but must be considered for any other magnet type. Moreover, because of the very high coercive forces available with the modern magnet technology, the magnets can withstand very high field intensities per length of magnet in the direction of the field. This would dictate that the magnet in section 2 be extremely thin. Combining this with the very brittle character of the magnets and the rough environment of a manufacturing plant would lead to the conclusion that the rotor magnet geometry is limited, not by the electrical or magnetic properties but by the mechanical strength of the magnet material. In other words the rotor design will be limited by the minimum magnet thickness which is feasible to produce, in quantity, without fear of excessive magnet breakage. It is necessary for a magnet manufacturer to deal with this question, but a relatively good figure for initial design is a length to thickness ratio of not more than 10-12. Having determined the approximate magnet size, the stator winding may then be chosen to produce sufficient mmf to properly load the magnet. The design of a stator to

match a given rotor geometry is beyond the scope of this present work. Table 5.1 is given to compare the relative thickness required to operate the magnet near its maximum energy product.

Secondly, in order to minimize the cost of a given volume of magnet, the magnet must be produced with a simple geometry. For small motors an arc is relatively easy to produce and provides marginally more magnet area than the rectangular shape (see Figure 5.1). The drawback remains that in order to receive the benefit from the larger magnet area, the arc must be radially magnetized, which will increase the initial cost. For medium and larger motors a simple rectangular block magnet can be used to build up virtually any shape required. This not only simplifies the manufacturing process but also allows higher volume procurement which can cut overall magnet costs.

Thirdly, is the actual placement of the magnets within the rotor boundaries. It is important to note in this respect, that the quadrature axis flux must pass through the space between the rotor cage and the magnet itself. The quadrature axis reactance X_q can thus be controlled independently by variation of this important space. Table 5.2 shows the performance difference for the rectangular chord magnet and the arc magnet configurations. Another important geometrical consideration is that of the usefulness of the "pulsing" or radially aligned magnet. It is conceded that for rotors with higher numbers of poles (i.e. 6 and up) the radially oriented magnet is the only reasonable way of aligning the magnets. On the other hand, with the two pole types the pulsing contribution is relatively small. Upon examination of the open circuit waveforms presented in the previous chapter, it is apparent that the

Table 5.1 Magnet Thickness Variation

			L_2 = 0.508 cm		L_2 = 0.250 cm		L_2 = 0.101 cm	
δ	Pout	I_a	H_1	H_2	H_1	H_2	H_1	H_2
3.9	7.3	0.61	6.2	3.4	6.1	6.8	7.7	21.5
11.4	233	0.78	4.2	2.3	4.2	4.7	4.8	13.3
21.3	527	1.13	0.0	0.0	0.0	0.0	0.2	0.6
31.3	714	1.48	5.8	3.2	5.7	6.5	9.0	25.1
41.2	787	1.81	13.8	7.7	506.5	572.3	432.1	1208.5
51.3	1120	2.04	739.4	411.2	834.3	942.7	680.3	1902.8
61.2	1187	2.31	1125.7	626.0	1169.1	1321.1	949.9	2656.9

N.B. 1. The three configurations have essentially the same performance, but magnet 2 is underutilized for L_2 > 0.10 cm.

2. In order to achieve equal performance, leakage bridge thickness, T_2, must be reduced in proportion to length L_2.

$\frac{\text{magnet area}}{\text{air gap area}} = 0.875$

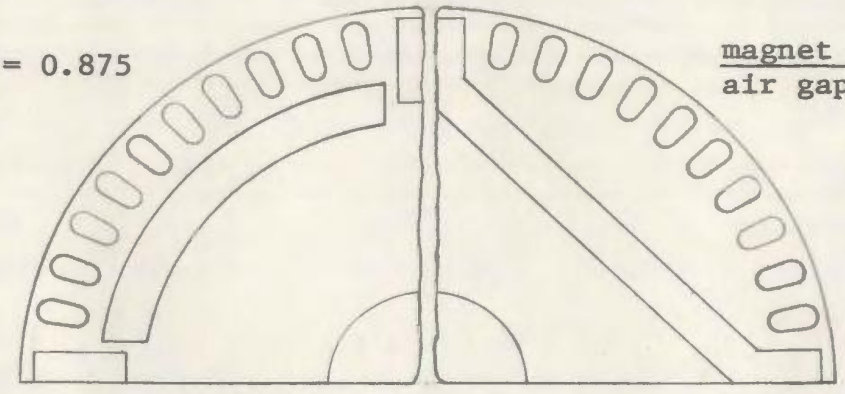

$\frac{\text{magnet area}}{\text{air gap area}} = 0.824$

Figure 5.1 Magnet area for arc and chord type magnets

Table 5.2

a) Geometry of rotor 15 with T_q increased to 0.5 cm

δ [°]	I_a [A]	Pout [W]	Efficiency [%]	Power factor	X_d [Ω]	X_q [Ω]
9.3	0.61	6.9	2.7	.413	554.0	294.9
19.2	0.82	234.6	47.8	.603	554.0	208.5
29.2	1.19	505.6	63.6	.673	554.0	164.9
39.2	1.54	653.5	66.0	.644	552.9	150.2
49.1	1.78	981.5	72.4	.767	277.9	146.3
59.1	2.05	1101.5	72.1	.748	247.3	143.8
69.1	2.30	1143.5	70.4	.710	231.7	142.4

Table 5.2 (continued)

b) Thickness T_q increased to 1.0 cm

δ [°]	I_q [A]	Pout [W]	Efficiency [%]	Power factor	X_d [Ω]	X_q [Ω]
16.5	0.62	2.3	0.9	.401	554.0	373.6
21.5	0.67	48.6	16.4	.447	554.0	346.2
31.5	0.91	254.1	49.0	.570	554.0	246.6
41.5	1.33	484.1	61.2	.597	552.6	184.8
51.5	1.55	861.6	71.8	.775	272.5	175.3
61.4	1.83	1009.8	72.4	.764	244.7	169.0
71.4	2.08	1085.5	71.5	.734	230.1	165.7
81.4	2.29	1101.1	69.7	.694	221.1	164.3

c) Thickness T_q increased to 2.0 cm. This is not a physically realizable case, but it serves to show the extent of the T_q variation.

δ [°]	I_q [A]	Pout [W]	Efficiency [%]	Power factor	X_d [Ω]	X_q [Ω]
32.6	0.65	0.5	0.2	.385	554.0	440.8
42.6	0.84	137.0	34.6	.472	552.8	326.5
52.6	1.04	566.3	67.4	.814	276.6	281.9
62.5	1.33	794.4	72.2	.833	246.3	256.5
72.5	1.60	960.0	73.6	.820	230.9	243.4
82.5	1.84	1069.7	73.5	.795	221.6	238.3
92.5	2.05	1134.2	72.6	.764	215.3	239.5
102.4	2.24	1158.2	71.2	.729	211.6	246.5
112.4	2.41	1155.4	69.4	.693	207.9	263.1

N.B. The value of δ goes beyond 90° because X_q is greater than X_d. Note also that X_q increases for large δ because I_q starts to decrease.

pulsing magnet not only adds to the fundamental component of the normalized waveform but also boosts the open circuit voltage by approximately 25%. With the increase in open circuit voltage comes the desired increase in power factor, efficiency and pull-out torque, but also a marked increase in the air gap harmonics. The increase in harmonics is due, in part, to the very short transition zone between poles (i.e. the length of section 1) and again, the solution calls for increasing the length of magnet section 1 along the circumferential direction. The waveform for rotor 22 (Figure 4.5c) shows very low harmonic content and although it has somewhat lower open circuit voltage than rotor 21 this is due primarily to improper flux barrier design. At $25 per pound the removal of the pulsing magnets could result in a cost reduction of up to $5 per rotor, a significant portion. One other consideration must be looked at while dealing with the question of the pulsing magnet, and that is the manufacturing aspect. In order to compete as a viable alternative for industrial drive requirements the P.M. motors must have smooth starting and synchronizing capability. The typical induction motor has an isotropic, skewed squirrel cage to accomplish this. Although the squirrel cage is also the most common method for starting a P.M. motor, it is the skewing effect that presents the difficulties. For maximum performance it is best if the magnets are not skewed; thus to cut an axial hole for the magnets requires increased labour costs as well as leaving a number of the rotor bars discontinuous where the magnet cuts through. When the pulsing magnet is removed, the rotor can be skewed at will with a completely isotropic rotor cage and axially aligned magnets. Some P.M. motor manufacturers have overcome this

problem altogether by skewing the stator windings, but it seems as though the most feasible alternative is to remove the pulsing magnet, except for those applications which require particularly high pull-out torques. This alternative gives away a small portion of the motor's performance capability for larger gains in cost effectiveness and manufacturing ease.

5.2.2 Effects of Leakage Paths

Again, in a study of the effects of the steel flux leakage paths surrounding the magnets, the mechanical and electrical design come into conflict. The leakage flux paths shunt otherwise useful flux away from the air gap and effectively reduce the available magnet area. From the electrical design standpoint it would be beneficial if the bridges were extremely thin or absent altogether. However the mechanical torque acting upon the rotor cage bars must be transmitted to the shaft and thus the load. It is these steel bridges which transmit the torque in most of the modern designs. Not only that, it is these bridges which hold the lamination in one piece during the manufacturing process before the squirrel cage is cast and thus solidifying the rotor. For the present design it is desirable to have the leakage bridges as thin as the mechanical design will allow. Elementary static stress analysis on rotor 21 shows that the bridge thickness could be reduced by a factor of three and still be sufficiently strong. Table 5.3 shows the effect of reducing the thickness of these bridges on the motor's performance. Note how the internal voltage "E_o" stays at very high levels and how the power factor remains leading or very near unity for a good deal of the motor's operating range.

Table 5.3 Reduction of Leakage Bridge Paths

All bridge thicknesses of rotor 15 reduced to 0.01 cm

δ [°]	I_a [A]	Pout [w]	Eff. [%]	Power factor	X_d [Ω]	X_q [Ω]	E_o [V, 1-n]
4.4	0.2	7.1	3.6	.994	172.0	230.7	325.4
11.9	0.51	307.9	61.0	.999	170.2	158.9	326.7
21.8	0.94	703.7	75.6	.994	167.4	142.9	328.9
31.8	1.36	1049.5	79.3	.980	165.1	138.2	330.6
41.8	1.75	1333.2	79.9	.958	163.4	135.9	331.9
51.7	2.12	1545.7	79.1	.926	162.1	134.7	332.9
61.7	2.45	1680.1	77.5	.887	161.4	134.1	333.4
71.7	2.76	1742.4	75.3	.842	160.6	133.6	334.0
81.6	3.03	1734.9	72.6	.791	159.9	133.4	334.5

N.B. Compare this table with Table 3.4.

By considering the flux linkage test results of Figure 4.3 it is obvious that under a small magnetizing mmf the steel bridge paths are completely unsaturated and the direct axis reactance increases markedly. As the mmf increases, the reactance values decrease. For negative values of mmf the bridges are saturated and the reactance is relatively constant. As the value of E_o or the rotor angle "δ" increases, the direction of I_d is reversed and the d-axis mmf tends to demagnitize the magnets and drive the bridges deeper into saturation. The load value at which this reversal takes place is largely dependent on the bridge thickness. Figure 5.2 uses simplified phasor diagrams to illustrate the reversal of current I_d.

A better solution to the problem of leakage flux would be to review the manufacturing process to allow the torque carrying member to be a nonmagnetic material such as aluminum, which could be cast at the same time as the rotor cage. This would replace the high permeability iron with a much lower permeability material and virtually eliminate the leakage flux, greatly improving the motor's performance capability.

5.2.3 Rotor Cage Design

Previously it was mentioned that, in order to be a useful device for industry applications, the P.M. motor must be able to accelerate and synchronize a given load. All P.M. motors to date use some type of squirrel cage winding to accomplish this purpose. The design of rotor cage windings is quite well documented [61, 62, 63] for the normal induction or synchronous machine. However additional constraints are put on the rotor cage by the presence of the magnets. Due to the nature of the constant excitation flux, a considerable break torque can be

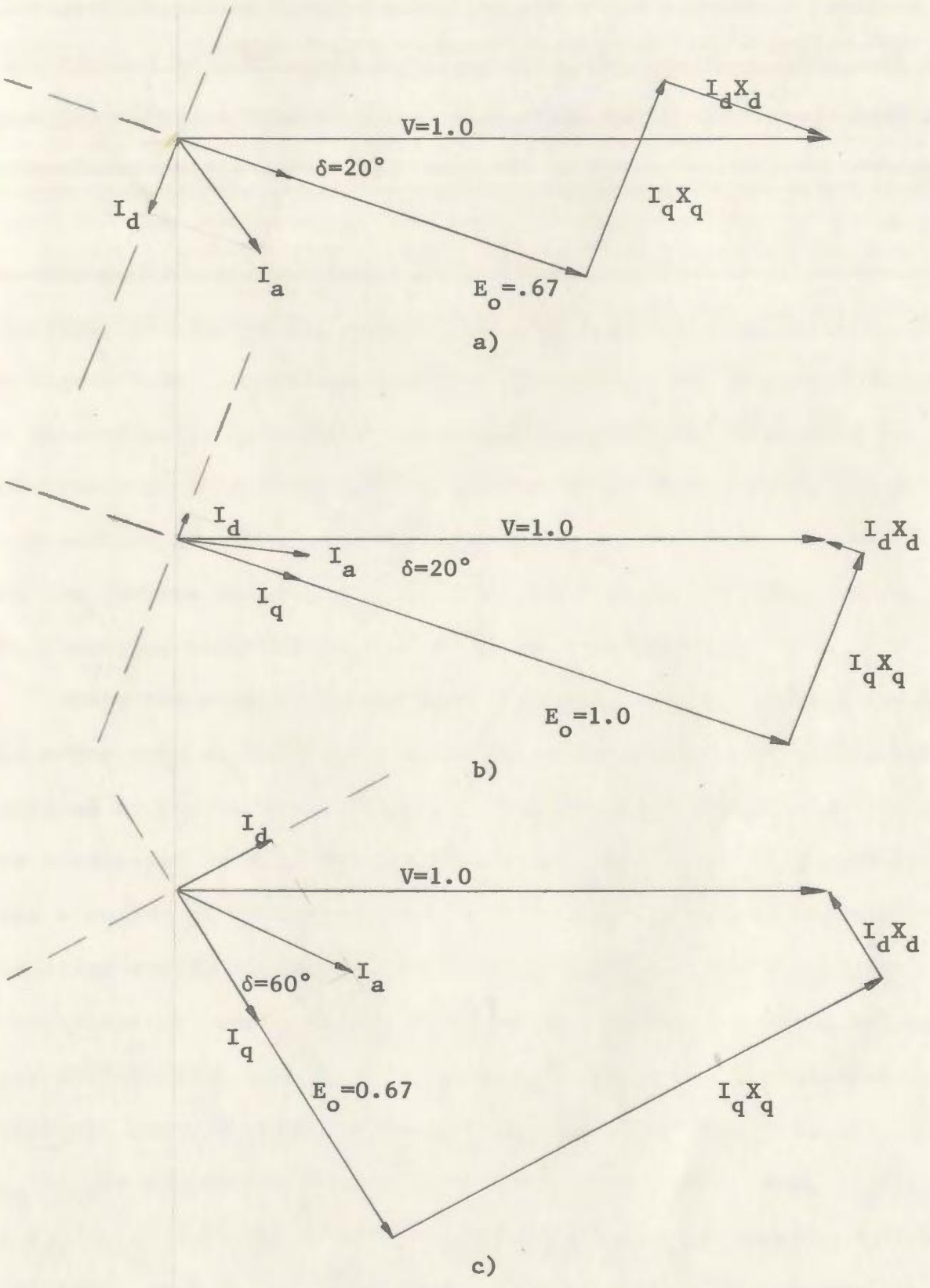

Figure 5.2 Direct axis current reversal by increasing E_o (b) and δ (c)

developed depending on the magnet material and geometry. Because of the reactive nature of the motor and source, the negative torque peaks at a relatively low speed (i.e. frequency) as is shown in Figure 5.3. This effect puts a lower limit on the resistance values for the rotor cage. If the rotor resistance is made too small (i.e. less than approximately 0.012 p.u.) then the cage torque produced cannot overcome the combined load torque and peak magnet torque and the response is similar to Figure 5.4a. On the other hand, the upper limit of rotor resistance is determined by the ability to synchronize the rotor and load. If the cage resistance is too high (i.e. above approximately 0.11 p.u.) the intersection of the load torque and motor system torque is at a speed too low for the magnets to lock into synchronism with the stator mmf. The resulting response is similar to that of Figure 5.4b.

Since the present design uses a pulsing magnet and consequently the rotor cage is no longer isotropic and the rotor resistance must be modelled by the two-axis theory, it was considered necessary to study the effects of various combinations of R_{2d} and R_{2q}. Figures 5.5-5.7 show a number of variations of the two rotor resistance figures and the resulting run-up response. The figures highlight three important conclusions: 1) small values of R_{2d} or R_{2q} (the other being normal) will give difficulties during early stages of run-up, 2) a completely isotropic rotor provides the best starting capability. As the ratio R_{2d}/R_{2q} is either increased or decreased excessively (i.e. $R_{2d}/R_{2q} < 0.05$ or $R_{2d}/R_{2q} > 2.0$) the ability to accelerate and synchronize a load diminishes, and 3) the rotor cage, although the primary means of accelerating the load, also provides stability after synchronization

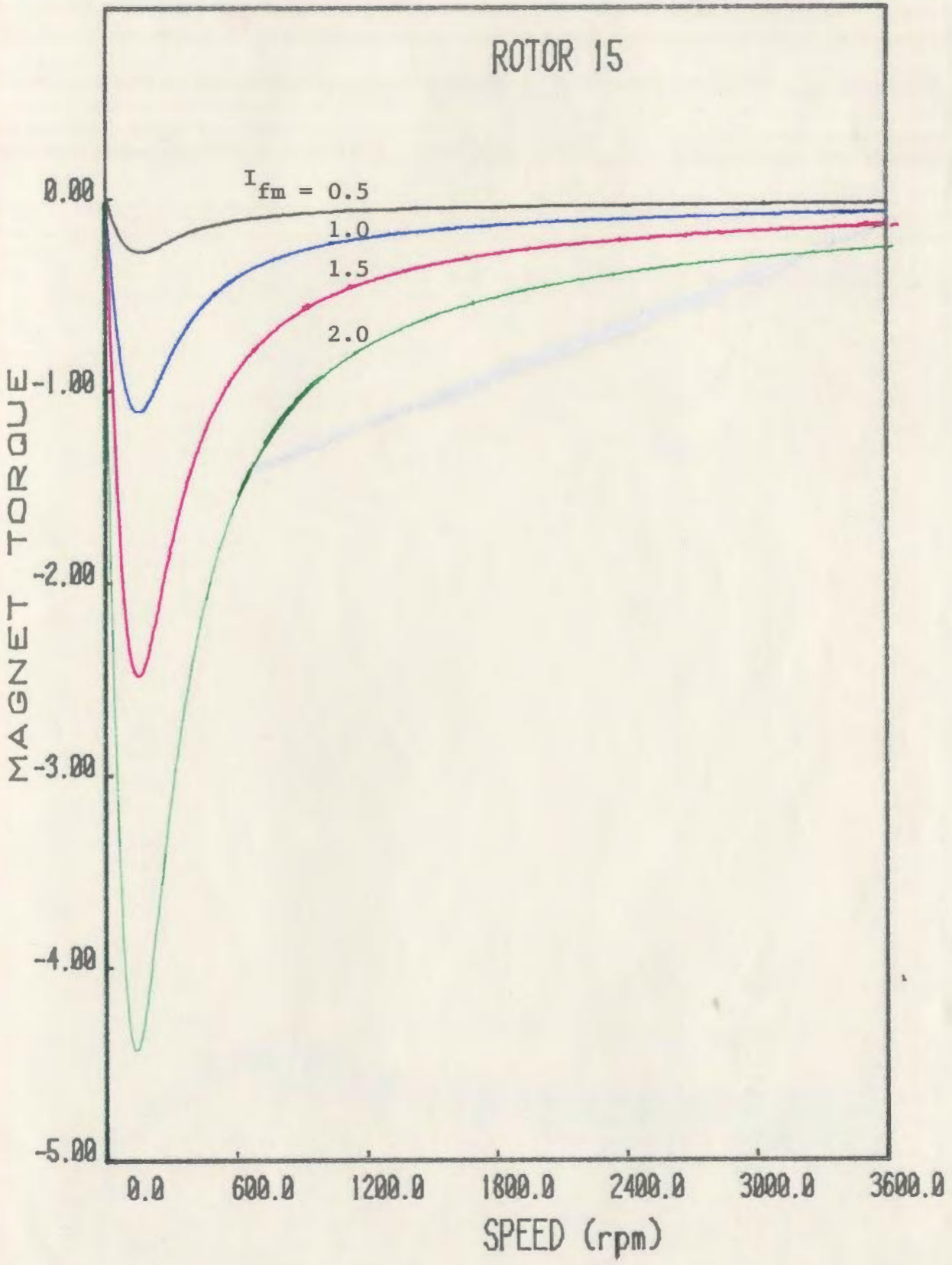

Figure 5.3 Magnet break torque as a function of increasing I_{fm}

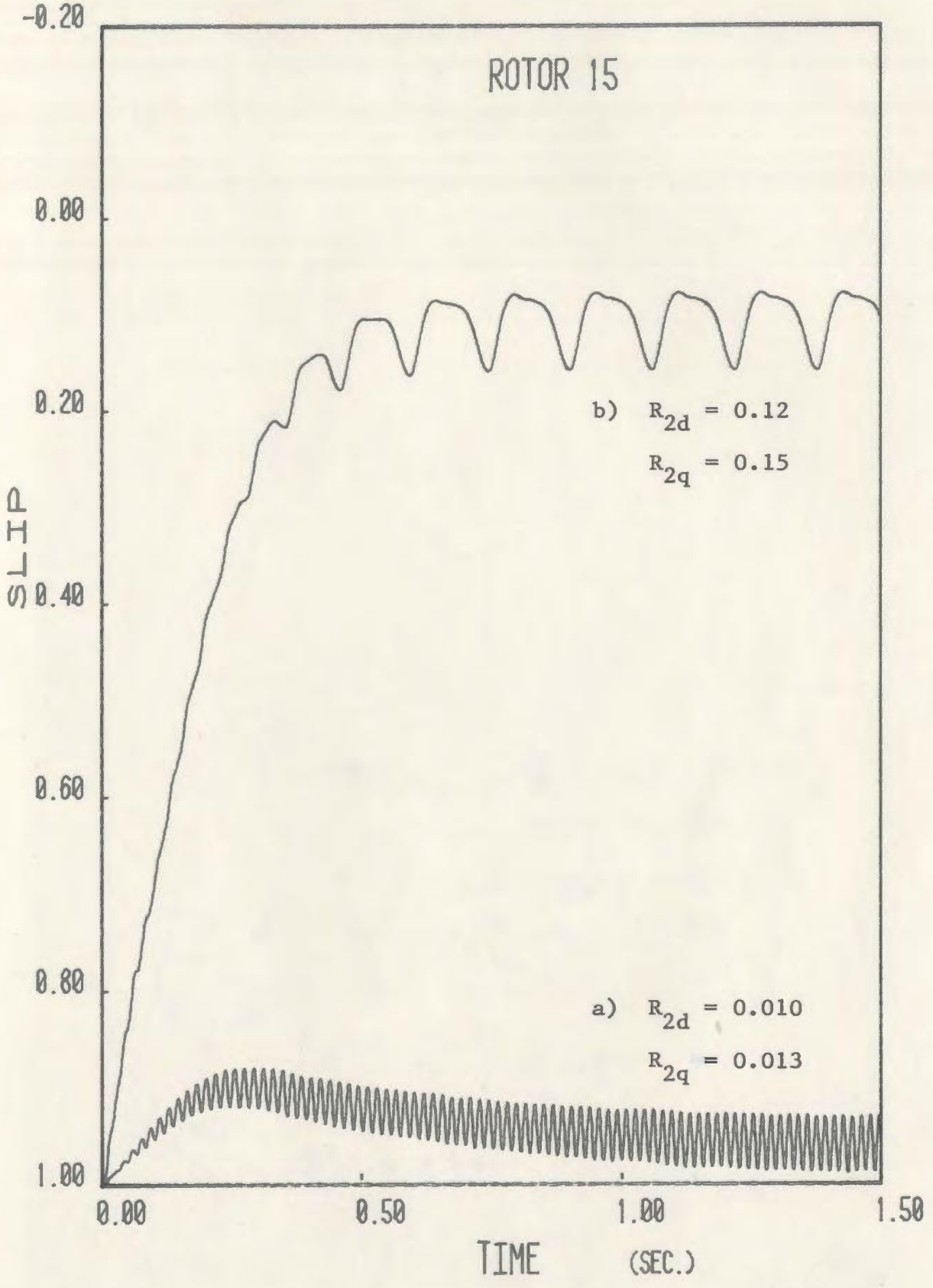

Figure 5.4 Limiting rotor resistance for load synchronization

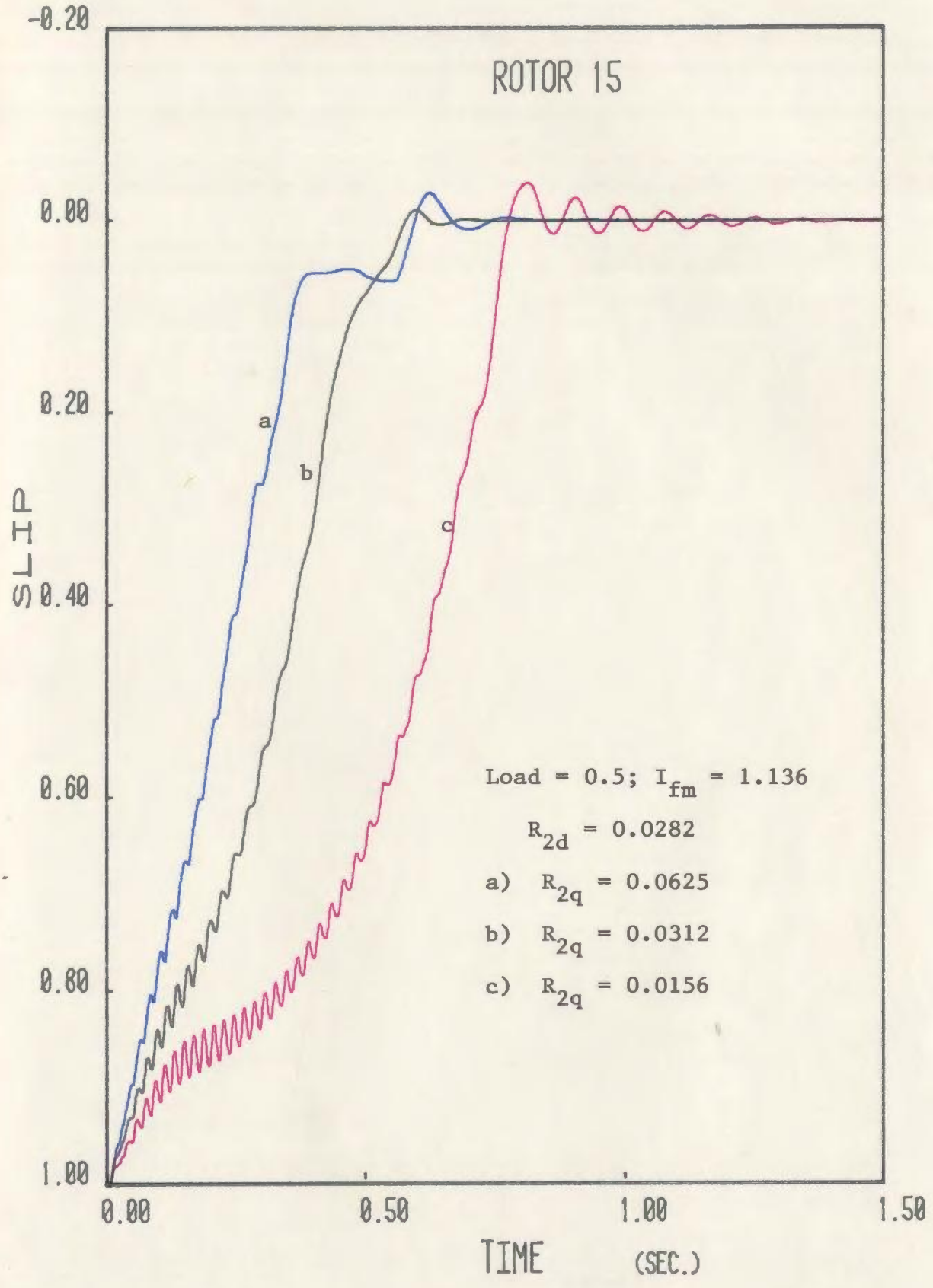

Figure 5.5 Rotor cage variations: constant R_{2d}

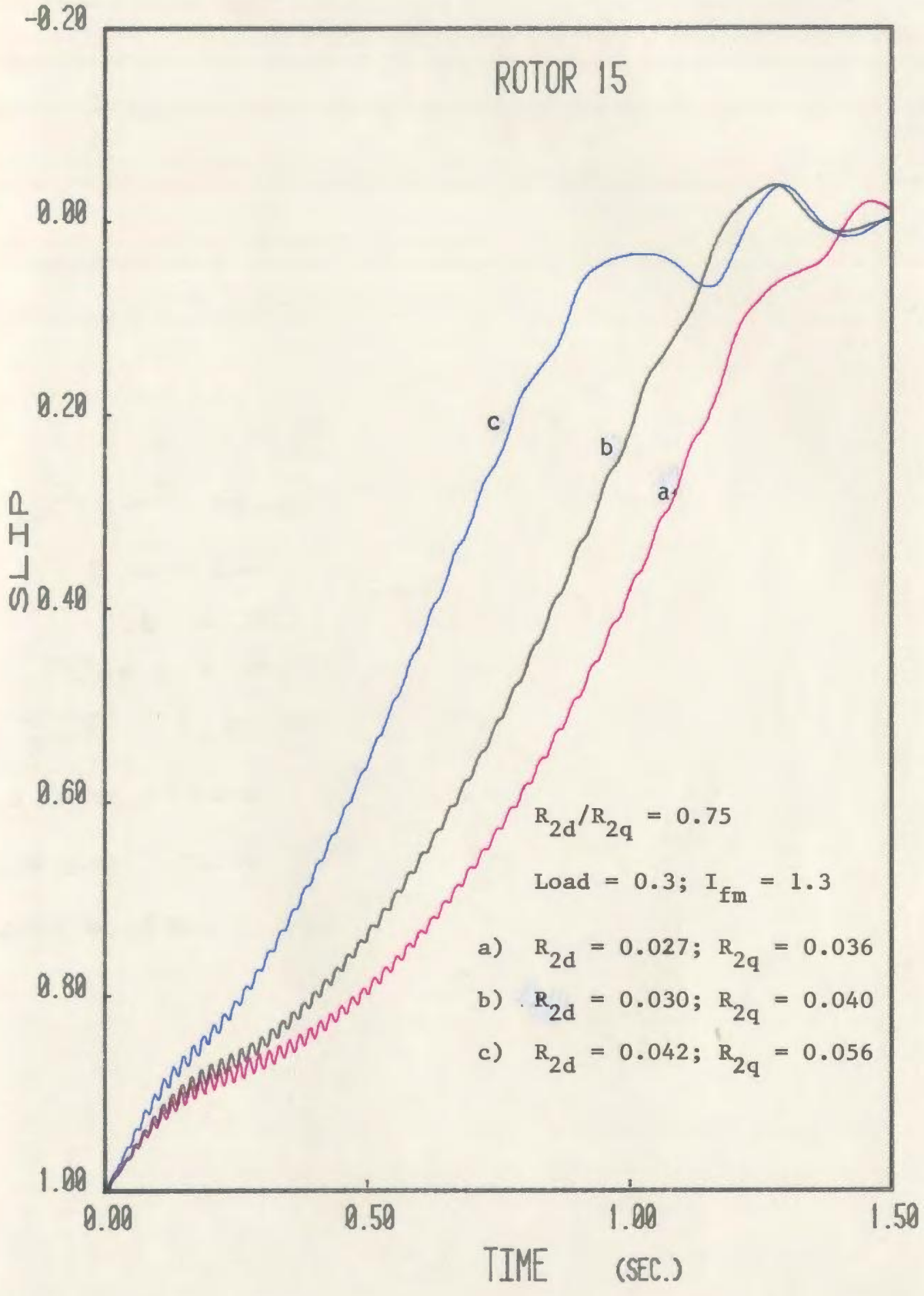

Figure 5.6 Rotor cage variations: constant R_{2d}/R_{2q}

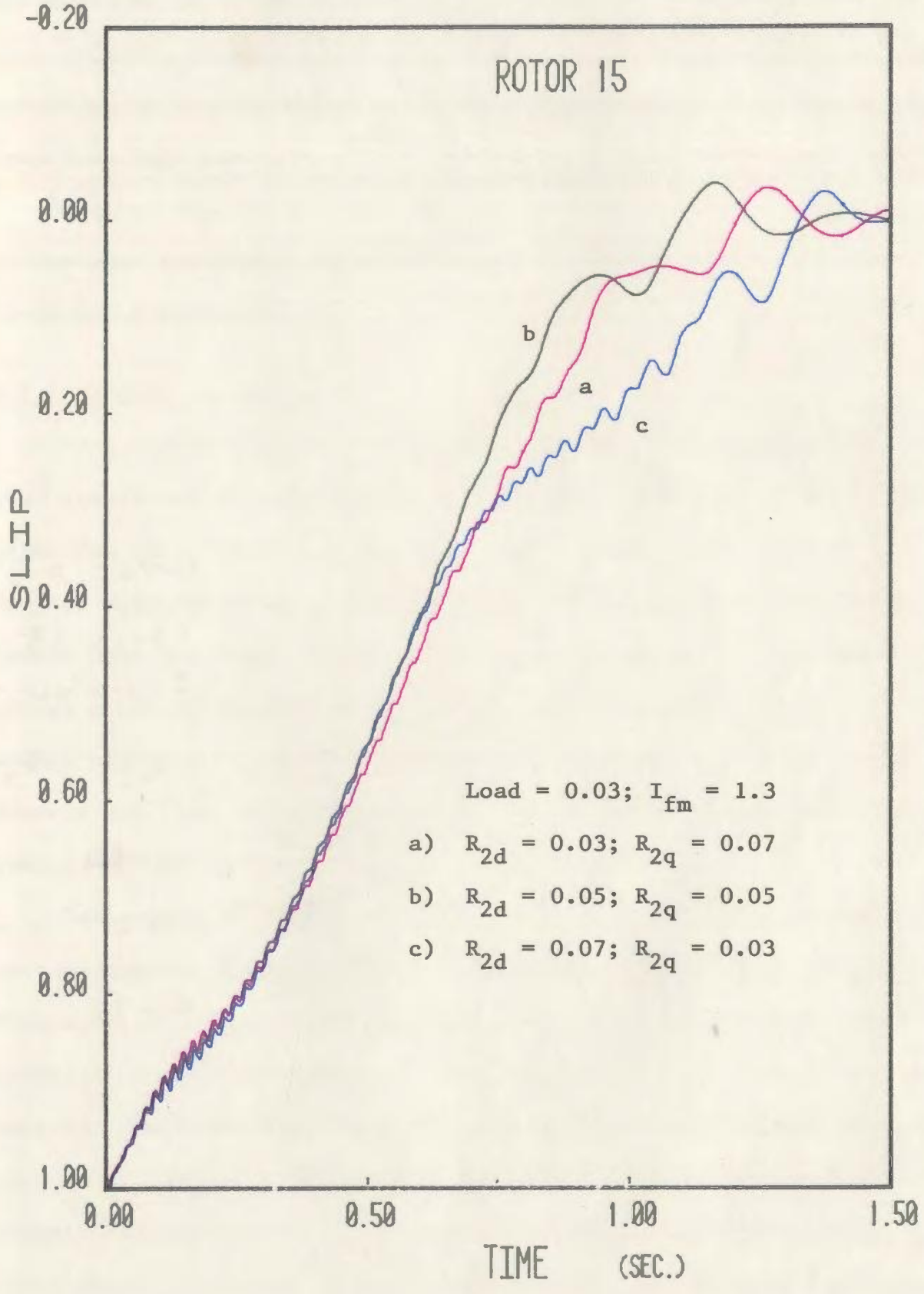

Figure 5.7 Rotor cage variations: increasing R_{2d}/R_{2q}

for fluctuating loads. Figure 5.8 is included to show the motor response to a suddenly applied load for various resistance combinations. Acceptable reduction in hunting action is achieved by designing R_{2d} and R_{2q} to be less than 0.05 p.u.

Further support for statement two above is given by Chalmers [64] in his work relating to Goerges effect in conventional wire wound synchronous machines.

5.2.4 Magnet Materials

Even the first serious P.M. motor designers were quick to indicate that the future of P.M. devices was largely dependent on the magnet materials which would become commercially available. Merrill [13] further suggested that the magnet property of residual flux density must remain near the level of the ALNICO types (i.e. $B_r \simeq 1.2T$) and the energy product improved by increased coercive force. It appears as though sufficient coercive force has been achieved with the rare earth magnets and that increased residual flux densities would be the most useful advance in the present state of technology.

Concerning the ferrite and the much heralded manganese-aluminum-carbon magnets, it is sufficient to say that these types, though much less expensive than the rare earth types, will not overtake the rare earths in motor applications. These magnets, while having sufficient coercive force for motor applications, are not used extensively primarily because of the low residual flux density. Furthermore, the ferrite magnets have been shown to have a severe temperature dependence [32], which tends to degrade the motor performance as the motor heats up under load.

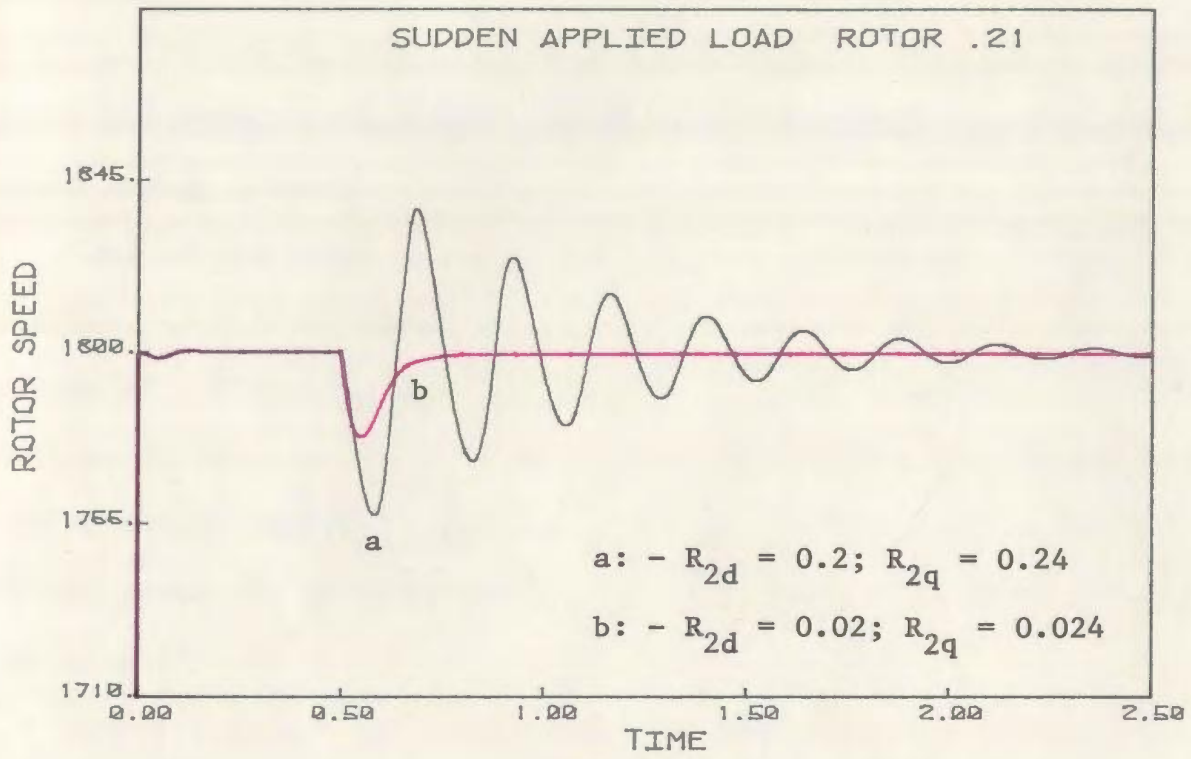

a)

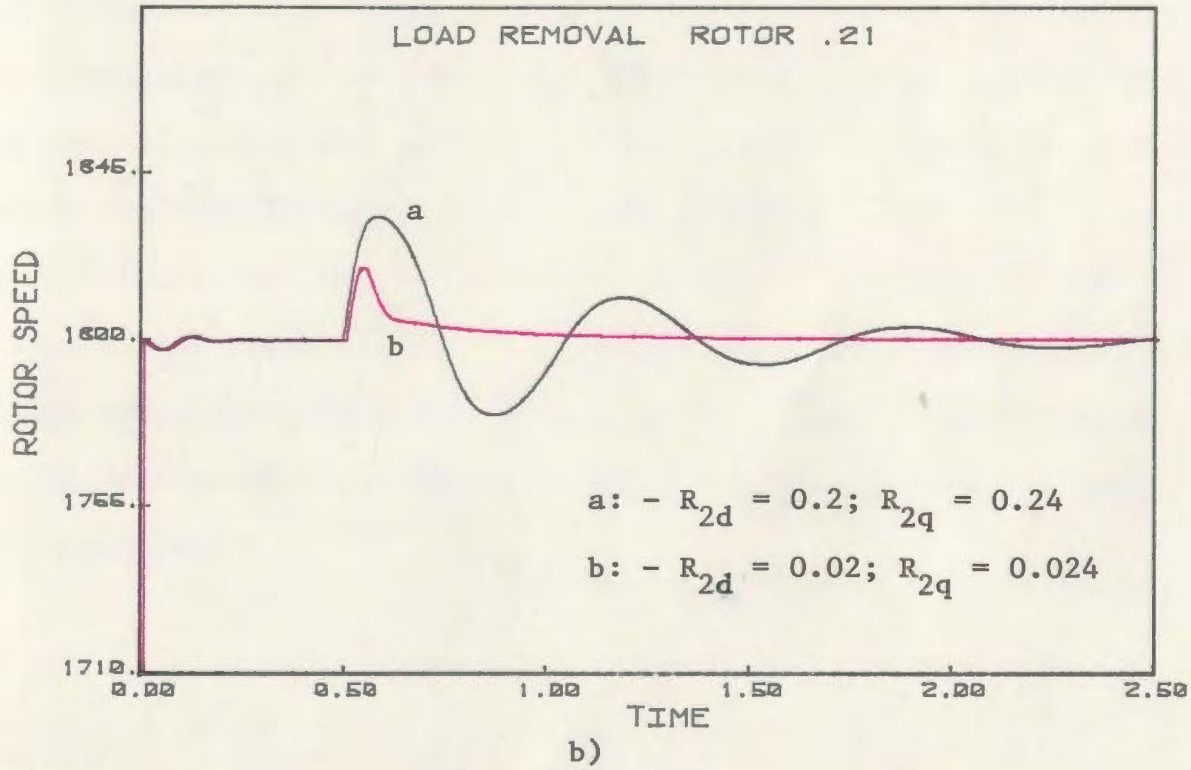

b)

Figure 5.8 Sudden load application and removal

5.3 Design Features

In concluding this chapter it is necessary to review some of the important design features of the prototype models in relation to the total design process.

One of the first criteria for judging P.M. motors, as mentioned earlier, is that of power factor. Volkrodt [16] stated that a power factor of .80 should be obtainable for a motor, when its open circuit voltage is greater than 0.4 per unit. Considering the prototypes were not optimized designs, it is important to note that both rotors 15 and 21 had power factors in excess of .80 for loads less than their pull-out capability.

Another factor in determining the value of a motor is the pull-out capability. Upon comparing each of the prototypes with the equivalent induction motor rating, all of the P.M. motor prototypes have a pull-out torque at least twice the rated value, with rotor 21 having a pull-out capability of 4.25 times the rated value. This suggests that with an overall (rotor and stator) optimized design a four pole, 1 hp P.M. motor could be manufactured in a smaller frame size.

Finally, one of the "raison d'etre" of P.M. motors is the increased power factor times efficiency product. Again it is noteworthy that for these unoptimized prototypes, both rotors 21 and 22 have power factor efficiency products in the order of 5% higher than the equivalent induction motor.

6.0 CONCLUSIONS

6.1 General Conclusions

This work has presented various aspects of the design, manufacture, and tested results of P.M. synchronous motors of the interior type. Complete transient equations have been presented and subsequently reduced to predict steady state behavior as well. Furthermore, the equations and techniques for determining various machine parameters such as E_o, X_d and X_q have been presented to aid the designer in optimizing a particular design. Four prototype models have been assembled with complete results presented which shows acceptably close agreement to the theoretically predicted results. Finally, a series of studies have been undertaken to determine the effects of varying some critical parameters on the overall motor performance and design. These parameter variation studies should be most useful for motor design engineers and also serve to give insight into what direction further research efforts should take.

A number of important conclusions have been drawn from the present work which should be of interest to the designers and users of P.M. motors alike. The major conclusions are listed in point form as follows:

[1] Permanent magnet motors can be built to operate with very high power factors and efficiencies. In fact, it has been shown [49] that the energy usage coefficient (i.e. power factor x efficiency product) of a P.M. motor can be 30-40% higher than that of a similar induction motor. The unoptimized prototypes assembled for this work achieved energy usage coefficients of approximately 5% greater than the induction motor counterpart.

[2] The two axis reactances, X_d and X_q, of a P.M. motor are almost independent of each other. The direct axis reactance is primarily controlled by the leakage paths around the magnet ends, while the quadrature axis reactance is primarily controlled by the steel path between the magnets and the rotor cage. The X_q/X_d ratio can, therefore, be controlled by proper design. The design of reference [35] has an X_q/X_d ratio greater than unity while the prototypes of this work have ratios near or slightly less than unity. Standard wire wound synchronous machines have X_q/X_d ratios as low as 0.5.

[3] It appears as though the design which has an X_q/X_d ratio larger than unity provides the highest values of power factor and efficiency for equal magnet volumes. However, this is accompanied by a maximum torque angle (δ) greater than 90° and a decreased stiffness coefficient (i.e. $dT/d\delta$). This contributes to a decrease in the motor's operating stability.

[4] One critical feature of P.M. motor design is the geometry and material used for the bridges surrounding the magnets, which are used to transfer the electromagnetic cage torque to the shaft. The prototypes reported here used the rotor steel for these bridges and consequently, a large component of the total magnet flux was lost to leakage. It was determined that the thickness of these bridges could be reduced by a factor of three and still be able to withstand the mechanical forces generated at 200% overload. In general, the steel bridges should be as thin as mechanically possible. However, a far

better solution is to use a nonmagnetic material to surround the magnets and carry the generated torques, thus virtually eliminating all magnetic leakage. To achieve this will require new manufacturing techniques and modified rotor designs, which will not only enhance the motor performance but should also reduce the costs of the rotor laminations.

[5] In order to meet low per unit cost requirements, it is important to use a minimum of magnet material. The parameter variations reported here show that the magnet thickness, in the direction of magnetization, can be reduced by a factor of approximately five. The one condition on this statement is that the leakage flux must, at least, remain constant as the magnet thickness decreases. This is somewhat difficult to achieve using steel leakage bridges, but is considerably easier when using nonmagnetic materials. It is the large coercive forces available in the rare earth cobalt magnets and the linearity of the demagnetization curve which make these magnet volume reductions possible. However, because of the brittleness of the magnet material, the reduction in thickness is somewhat limited by the mechanical strength of the magnet.

[6] Since motor steels are designed to be operated at flux density levels of 0.7 to 1.0 T., for reasonable core loss, it is important that the magnet area (Br for rare earth cobalt magnets is $\simeq$ 0.85 T) be equal to the air gap area for proper working fluxes.

[7] The rotor cage must be designed to overcome the large brake torque, produced by the permanent field excitation, as well as to accelerate the load to a speed where the magnets can lock into synchronism. This requires a rotor resistance in the range $0.012 \leq R_2 \leq 0.05$ per unit, in order to meet the starting requirements and to provide ample damping torque.

6.2 Recommendations for Further Study

It is proposed that the areas in which further investigations are required are mostly practical in nature with the implementation of the P.M. motor on an industrial scale in mind. The present work dealt only with the rotor and its optimization but it is necessary to investigate the complete motor including the stator winding. Secondly, a need has arisen to determine new manufacturing processes which can be used to improve the design of the P.M. motor. Included in this are the leakage bridge paths and the concept of skew. Finally, improved methods of predicting the motor steady state performance must be completed. This will encompass the use of finite element techniques to determine the flux distribution within the motor and consequently to predict the values of E_o, X_d and X_q.

References

[1] Underhill, E.M. (ed.). "Permanent Magnet Handbook." Crucible Steel Co. of America, 1957.

[2] Andrews, L.D. (ed.). "Testing and Measurement of Permanent Magnets." Standards and Engineering Committee of Magnetic Materials Producers Association, July 1977.

[3] Sibley, S.F. "Cobalt Supply and Availability in Relation to Demand for Magnetic Materials." Conf. on Magnetism of the M.M.P.A., Jan. 10, 1980.

[4] Binns, K. J., Jabbar, M.A. "High-Field Self-Starting Permanent-Magnet Synchronous Motor." Proc. IEE., Vol. 128, Pt. B, No. 3, May 1981, pp. 157-160.

[5] Richter, E. "Power Density Considerations for Permanent Magnet Machines." Electric Machines and Electromechanics, Vol. 4, 1979, pp. 21-32.

[6] Volkrodt, W. "Machines of Medium-High Rating with a Ferrite Magnet Field." Siemens Review, XLIII (1976), No. 6, pp. 249-254.

[7] Rahman, M.A. "Permanent Magnet Synchronous Motors--A Review of the State of Design Art." Proc. ICEM., Athens, Greece, Sept. 15-17, 1980, Pt. 1, pp. 312-319.

[8] Merrill, F.W. "ALNICO Materials for Small Motor and Generator Fields." Electrical Manufacturing (New York, NY), Vol. 39, March 1947, pp. 78-83, 180-190.

[9] Saunders, R.M., Weakly R.H. "Design of Permanent Magnet Alternators." Trans. of AIEE, Vol. 70, Pt. II, 1951, pp. 1578-1581.

[10] Brainard, M.W. "Synchronous Machines with Rotating Permanent-Magnet Fields." Part I, Trans. of AIEE, Vol. 71, Pt. III, Aug. 1952, pp. 670-676.

[11] Strauss, F. "Synchronous Machines with Rotating Permanent-Magnet Fields." Part II, Trans. of AIEE, Vol. 71, Pt. III, 1952, pp. 887-893.

[12] Hershberger, D.D. "Design Considerations of Fractional Horsepower Size Permanent-Magnet Motors and Generators." Trans. of AIEE, Vol. 72, June 1953, pp. 581-585.

[13] Merrill, F.W. "Permanent-Magnet Excited Synchronous Motors." Trans. of AIEE, Vol. 73, Feb. 1955, pp. 1754-1759.

[14] Alger, P.L. Discussion on "Permanent-Magnet Excited Synchronous Motors." Trans. of AIEE, Vol. 73, Feb. 1955, pp. 1759-1760.

[15] Douglas, J.F.H. "Current Loci of Permanent Magnet Synchronous Motors." Trans. of AIEE, Vol. 78, Pt. III, 1959, p. 76.

[16] Volkrodt, W. "Polradspannung, Reaktanzen und Ortskurve des Stromes der mit Dauermagneten Erregten Synchronmaschine." Electrotechnische Zeitschrift, Vol. 83, July 1962, pp. 517-522. (In German)

[17] Cahill, D.P.M., Adkins, B. "The Permanent-Magnet Synchronous Motor." Proc. IEE, Vol. 109, Pt. A, No. 48, 1962, pp. 483-491.

[18] Binns, K.J., Jabbar, M.A., Barnard, W.R. "Computation of the Magnetic Field of Permanent Magnets in Iron Cores." Proc. IEE, Vol. 122, No. 12, Dec. 1975, pp. 1377-1381.

[19] Binns, K.J., Barnard, W.R., Jabbar, M.A. "Hybrid Permanent Magnet Synchronous Motors." Proc. IEE, Vol. 125(3), Mar. 1978, pp. 203-208.

[20] Binns, K.J., Kurdali, A. "Permanent Magnet A.C. Generators." Proc. IEE, Vol. 126(7), July 1979, pp. 690-696.

[21] Binns, K.J., Jabbar, M.A., Parry, G.E., Russell, S.W. "A Variable Speed Drive Using a Permanent Magnet A.C. Motor."

[22] Binns, K.J., Jabbar, M.A. "Dynamic Performance of a Permanent Magnet Synchronous Motor." IEE Conf. on Small Electrical Machines." Publication No. 136, March 1976, pp. 78-81.

[23] Binns, K.J., Jabbar, M.A., Parry, G.E. "Choice of Parameters in the Hybrid Permanent Magnet Synchronous Motor." Proc. IEE, Vol. 125(8), Aug. 1979, pp. 741-744.

[24] Binns, K.J., Molyneux, D.C., Barnard, W.R. "Some Aspects of the Development of a High Performance Permanent Magnet Synchronous Motor." IEE Conf. on Small Electrical Machines, Publication No. 136, Mar. 1976, pp. 76-77.

[25] Binns, K.J.: "Alternating current electric machine," British Patent 1 263 300.

[26] Binns, K.J., Barnard, W.R.: "Permanent magnet rotor for synchronous electric machine," British Patent 1 324 147.

[27] Binns, K.J.: "Permanent magnet rotor for synchronous electric machines," British Patent 1 359 548.

[28] Binns, K.J.: "High output stabilised permanent-magnet machine," British Patent 1 437 348.

[29] Boules, N., Weh, H. "Field Analysis for a High-Power, High-Speed, Permanent Magnet Synchronous Machine of the Disk Construction Type." Electric Machines and Electromechanics, Vol. 5, 1980, pp. 25-37.

[30] Boules, N., Weh, H. "Machine Constants and Design Considerations of a High-Power, High-Speed, Permanent Magnet Disc Type Synchronous Machine." Electric Machines and Electromechanics, Vol. 5, 1980, pp. 113-123.

[31] Boules, N. "Impact of Slot Harmonics on Losses of High-Speed Permanent Magnet Machines with a Magnet Retaining Ring." Electric Machines and Electromechanics, Vol. 6, 1981, pp. 527-539.

[32] Miyashita, K., Yamashita, S., Tanabe, S., Shimozu, T., Sento, H. "Development of a High Speed 2-pole Permanent Magnet Synchronous Motor." Trans. IEEE, PAS-99, No. 6, 1980, pp. 2175-2183.

[33] Honsinger, V.B. "Performance of Polyphase Permanent Magnet Machines." Trans. IEEE, PAS-99, 1980, pp. 1510-1516.

[34] Honsinger, V.B. "Permanent Magnet Machines: Asynchronous Operation." Trans. IEEE, PAS-99, 1980, pp. 1503-1509.

[35] Honsinger, V.B. "The Fields and Parameters of Interior Type A.C. Permanent Magnet Machines." Trans. IEEE, PAS-101, 1982, pp. 867-875.

[36] Miller, T.J.E. "Methods for Testing Permanent Magnet Polyphase A.C. Motors." IEEE IAS Conf. Record No. 81CH1678-2, 1981, pp. 494-499.

[37] Miller, T.J.E. "Transient Performance of Permanent Magnet A.C. Machines." IEEE IAS Conf. Record No. 81CH1678-2, 1981, pp. 500-503.

[38] Richter, E. "Rare Earth-Cobalt Permanent Magnets for Electrical Machines of Medium to Large Power Ratings." Goldschmidt Infomiert, Vol. 48, 1979, pp. 50-57.

[39] Campbell, P., Rosenberg, D.J., Stanton, D.P. "The Computer Design and Optimization of Axial-Field Permanent Magnet Motors." Trans. IEEE, Pass-100, April 1981, pp. 1490-1497.

[40] Campbell, P., Chari, M.V.K., D'Angelo, J. "Three-Dimensional Finite Element Solution of Permanent Magnet Machines." Intermag Conf., Grenoble, France, 1981.

[41] D'Angelo, J., Chari, M.V.K., Campbell, P. "Three Dimensional Finite Element Solution for a Permanent Magnet Axial-Field Machine." Trans. IEEE, PAS-102, Jan. 1983, pp. 83-92.

[42] Borger, W.U. "Transient Performance of Permanent Magnet Synchronous Motors." Wright-Patterson Air Force Base, Ohio, 1982.

[43] Borger, W.U. "Single Phase Permanent Magnet Synchronous Motors." Ph.D. Dissertation, Univ. of Dayton, Dayton, Ohio, 1981.

[44] Rahman, M.A. "High Efficiency Permanent Magnet Synchronous Motors." IEEE, IAS Conf. Record No. CH1484-5/79, 1979, pp. 561-564.

[45] Rahman, M.A., Little, T.A., Dash, P.K. "Computer Simulation of the Dynamic Performance of Permanent Magnet Synchronous Motors." IEEE IAS Conf. Record No. 81CH1678-2, 1981, pp. 511-514.

[46] Gumaste, A.V., Slemon, G.R. "Steady State Analysis of a Permanent Magnet Synchronous Motor Drive with Voltage Source Invertor." Trans. IEEE, IAS-17, No. 2, 1981, pp. 143-151.

[47] Slemon, G.R., Gumaste, A.V. "Steady State Analysis of a Permanent Magnet Synchronous Motor with Current Source Inverter." IEEE IAS Conf. Record No. 81CH1678-2, 1981, pp. 683-690.

[48] Adkins, B., Harley, R.G. "The General Theory of Alternating Current Machines." Chapman and Hall, London, 1975.

[49] Fitzgerald, A.E., Kingsley, C. Jr., Kusko, A. "Electric Machinery." McGraw-Hill, 3rd ed., 1971.

[50] Rafian, M., Laughton, M.A. "Aspects of Induction and Synchronous Motors Analysis using Dynamic Phase Co-ordinate Theory." Proc. IEE, Vol. 126(8), 1979, pp. 749-758.

[51] Isaacson, E., Keller, H.B. "Analysis of Numerical Methods." Wiley, 1966.

[52] Frölich, O. Elektrotech Zeitschrift, Vol. 2, 1881, pp. 134-141.

[53] King, T.L., Novotny, D.W. Discussion on "Performance of Polyphase Permanent Magnet Machines." Trans. IEEE, PAS-99, 1980, pp. 1503-1509.

[54] ANSI/IEEE Std. 112-1978. Standard Test Procedures for Polyphase Induction Motors and Generators.

[55] IEEE Std. 115. Test Procedure for Synchronous Machines.

[56] ANSI/IEEE Std. 86-1975. IEEE Standard Definitions of Basic Per Unit Quantities for Alternating Current Rotating Machines.

[57] BS 4296:1968 British Standard Methods for Determining Synchronous Machine Quantities.

[58] Pospisil, J.V. "Practical Verification of Motor Speed-Torque Characteristics." Trans. IEEE, PAS-97, 1978, pp. 1011.

[59] Matsch, L.W. "Electromagnetic and Electromechanical Machines." IEP, New York, 1977, p. 439.

[60] Jones, C.V. "The Unified Theory of Electrical Machines." Butterworths, London, 1967.

[61] Alger, P.D. "The Nature of Polyphase Induction Machines." John Wiley and Sons, New York, 1951.

[62] Jains, C.G. "Design, Operation and Testing of Synchronous Machines." Asia Publishing House, New York, 1966.

[63] Veinott, C. "Theory and Design of Small Induction Motors." McGraw-Hill, 1959.

[64] Chalmers, B.J., Agarwal, A.K. "Importance of direct and quadrature axis-damper impeadances in starting performance of salient-pole motors." Proc. IEE, Vol. 113, No. 4, April 1966, pp. 663-667.

APPENDIX A

COMPUTER PROGRAMS

```
C
C
C       TRANSIENT PERFORMANCE OF PERMANENT MAGNET SYNCHRONOUS MOTORS
C
C
C       XD       DIRECT ARMATURE REACTANCE
C       XQ       QUADRATURE ARMATURE REACTANCE
C       XMD      DIRECT MAGNETIZING REACTANCE
C       XMQ      QUADRATURE MAGNETIZING REACTANCE
C       X2D      DAMPER WINDING REACTANCE
C       X2Q      DAMPER WINDING REACTANCE
C       IFM      EQUIVALENT FIELD CURRENT
C       WO       RATED ANGULAR SPEED
C       R1       STATOR RESISTANCE
C       RC       CORE LOSS RESISTANCE
C       V        VOLTAGE
C       R2D      CAGE RESISTANCE
C       R2Q      CAGE RESISTANCE
C       IC1      INERTIA CONSTANT
C       X1       LEAKAGE REACTANCE FOR STATOR
C       X2       LEAKAGE REACTANCE FOR CAGE
C       TL       LOAD TORQUE
C       TH       HYSTERESIS TORQUE
C       ID       DIRECT AXIS CURRENT
C       IQ       QUADRATURE AXIS CURRENT
C       I2D      CAGE DIRECT AXIS CURRENT
C       I2Q      CAGE QUADRATURE AXIS CURRENT
C       TM       MOTOR TORQUE  (TMOT)
C       TMAG     MAGNET TORQUE
C       TCAGE    CAGE TORQUE
C       W        SPEED (RADIANS/SECOND)
C       EO       MAGNET EXCITATION
C
C
      COMMON /BLOCK/UU,VV,XL,YL,XU,YU,RXL,RYL,RXU,RYU
      REAL IC1,ID,IQ,I2D,I2Q,IDM,IQM,IFM
      DIMENSION XN(10),X(10),FX(10),Q(10,4),ABSC(2100),ORD(2100)
      DIMENSION ABS2(2100)
C
C     INPUT MOTOR PARAMETERS
C
      TYPE*,'PLOT LABELS?  TYPE 1 FOR NO  2 FOR YES'
      ACCEPT*,PLO
      TYPE*,'PLOT LOAD TORQUE?  1=NO  2=YES'
      ACCEPT*,LT
      TYPE*,'H'
      ACCEPT*,H
      XD=0.31560
      TYPE*,'TL,R2D,R2Q'
      ACCEPT*,TL,R2D,R2Q
      V=1.0
      XQ=0.645
      XMD=0.2642
      XMQ=0.5934
```

```
      X2D=0.3186
      X2Q=0.6475
      IFM=1.936
      W0=377.0
      R1=0.0589
      IC1=0.0064
      X1=0.0516
      X2=0.0516
C
C     INITIALIZE VARIABLES FOR INTEGRATION ROUTINE
C
      TH=0.0
      TLL=0.0
      TM=0.0
      TMAG=0.0
      TCAGE=0.0
      TN=0.0
      NN=6
      DO 15 K=1,NN
      XN(K)=0.0
   15 CONTINUE
      W=0.0
      SLIP=1.0
      ID=0.0
      IQ=0.0
      I2D=0.0
      I2Q=0.0
      I=0
      II=1
C
C     CALCULATE Q-AXIS SATURATED REACTANCE
C
      XSM=XQ
      XSQ=.5*XQ
C
C     SET PLOT PARAMETERS
C
      XL=0.0
      YL=0.0
      XU=12.0
      YU=9.0
      RXL=0.0
      RYL=1.0
      RXU=2.5
      RYU=-0.2
      CALL TRANS(TN,SLIP)
      ABSC(II)=UU
      ORD(II)=VV
C
C     RKG ROUTINE STARTS
C
   99 CONTINUE
      L=1
      I=I+1
```

```
      T=TN
      DO 777 K=1,NN
      X(K)=XN(K)
 777  CONTINUE
      GO TO 42
10    DO 161 K=1,NN
      Q(K,L)=H*FX(K)
  161 CONTINUE
      T=TN+H/2.
      DO 252 K=1,NN
      X(K)=XN(K)+Q(K,L)/2.
  252 CONTINUE
      L=2
      GO TO 42
20    DO 251 K=1,NN
      Q(K,L)=H*FX(K)
  251 CONTINUE
      T=TN+H/2.
      DO 352 K=1,NN
      X(K)=XN(K)+Q(K,L)/2.
  352 CONTINUE
      L=3
      GO TO 42
30    DO 351 K=1,NN
      Q(K,L)=H*FX(K)
  351 CONTINUE
      T=TN+H
      DO 452 K=1,NN
      X(K)=XN(K)+Q(K,L)
  452 CONTINUE
      L=4
      GO TO 42
40    DO 451 K=1,NN
      Q(K,L)=H*FX(K)
  451 CONTINUE
      GO TO 7
C
C     EVALUATE DERIVATIVES
C
42    DO 9 M=1,NN
      FX(M)=0.0
    9 CONTINUE
      FX(1)=WO-X(2)
      FX(2)=(1./IC1)*(TM-TLL)
      FX(3)=-V*WO*SIN(X(1))-WO*R1*ID+X(2)*X(4)
      FX(4)=V*WO*COS(X(1))-WO*R1*IQ-X(2)*X(3)
      FX(5)=-WO*R2D*I2D
      FX(6)=-WO*R2Q*I2Q
      GO TO (10,20,30,40),L
C
C     CALCULATE NEXT TIME STEP
C
7     DO 8 K=1,NN
      XN(K)=XN(K)+(1./6.)*(Q(K,1)+2.*Q(K,2)+2.*Q(K,3)+Q(K,4))
```

```
    8     CONTINUE
C
C         CALCULATION OF MASUREABLE QUANTITIES
C
          DEL1=XD*X2D-XMD*XMD
          DEL2=XQ*X2Q-XMQ*XMQ
          EO=XMD*IFM
          ID=(X2D*(XN(3)-EO)-XMD*(XN(5)-EO))/DEL1
          I2D=(-XMD*(XN(3)-EO)+XD*(XN(5)-EO))/DEL1
          I2Q=(-XMQ*XN(4)+XQ*XN(6))/DEL2
          IQ=(X2Q*XN(4)-XMQ*XN(6))/DEL2
          AC=SQRT(ID*ID+IQ*IQ)
          CC=SQRT(I2D*I2D+I2Q*I2Q)
C
C         MAGNET CURRENTS
C
          WR=XN(2)
          W=WR
          G=WR/WO
          D3=R1*R1+XD*XQ*G*G
          IDM=-XMD*IFM*XQ*G*G/D3
          IQM=-G*R1*XMD*IFM/D3
          PMC=SQRT(IDM*IDM+IQM*IQM)
C
C         TORQUE CALCULATIONS
C
          TMAG=(EO*IQM+IDM*IQM*(XD-XQ))
          TCAGE=XN(5)*I2Q-XN(6)*I2D
          TM=XN(3)*IQ-XN(4)*ID
          SLIP=(1.-WR/WO)
          TN=TN+H
          IF(IQ.GT..5)XQ=XSM-.154*IQ
          IF(XQ.LT.XSQ)XQ=XSQ
          XMQ=XQ-X1
          X2Q=XMQ+X2
          TLL=TL*((1.-SLIP)*(1.-SLIP))
          NUM=INT(((2.5/H)/2100.)+1)
          IF(((I/NUM)*NUM).NE.I)GO TO 98
          II=II+1
          CALL TRANS(TN,SLIP)
          ABSC(II)=UU
          ORD(II)=VV
   98     CONTINUE
          IF(TN-2.5)99,99,100
  100     CONTINUE
C
C         OUTPUT PLOTTING SECTION
C
          CALL PLOTS
          CALL XYPLOT(1.5,.75,-3)
          IF(PLO.EQ.1.0)GO TO 105
          CALL GRAFIC
          CALL LABLE
   105    CONTINUE
```

```
      CALL XYPLOT(0.0,0.0,-3)
      DO 110 K=1,II
      CALL XYPLOT(ABSC(K),ORD(K),2)
110   CONTINUE
      IF(LT.EQ.1.)GO TO 130
      CALL XYPLOT(0.0,0.0,-3)
      DO 120 M=10,II,10
      CALL XYPLOT(ABSC(M),ABS2(M),2)
120   CONTINUE
130   CONTINUE
      CALL DUMP
      CALL PLEXIT
      STOP
      END
C
C  THIS SUBROUTINE DRAWS THE X AND Y AXIS FOR THE GRAPH
      SUBROUTINE GRAFIC
      COMMON /BLOCK/UU,VV,XL,YL,XU,YU,RYL,RXL,RXU,RYU
      DO 23,J=1,3
      KL=J-1
      CALL XYPLOT(XL-.01*KL,YL-.01*KL,3)
      CALL XYPLOT(XU+KL*.01,YL-.01*KL,2)
      CALL XYPLOT(XU+KL*.01,YU+KL*.01,2)
      CALL XYPLOT(XL-KL*.01,YU+KL*.01,2)
      CALL XYPLOT(XL-KL*.01,YL-KL*.01,2)
23    CONTINUE
      CALL DUMP
C  PLOTTING X AXIS LABELS
      DO 55,NO=1,26,5
      RNO=NO/10.0
      CALL TRANS(RNO,1.0)
      CALL NUMBER(UU-0.25,-0.3,.14,0.0,RNO,'(F5.2)',5)
      CALL SYMBOL(UU,0.05,0.05,7,0.0,-1)
55    CONTINUE
      CALL DUMP
C  PLOTTING Y AXIS LABELS
      CALL XYPLOT(1.5,.75,3)
      DIN=1.0
16    CONTINUE
      CALL TRANS(1.0,DIN)
      CALL NUMBER(-0.6,VV,.14,0.0,DIN,'(F5.1)',5)
      CALL SYMBOL(0.05,VV,0.05,8,0.0,-1)
      CALL DUMP
      DIN=DIN-0.1
      IF(DIN.GT.RYU)GO TO 16
      RETURN
      END
C
C
C  THIS SUBROUTINE TRANSFORMS XY COORDINATES FOR PLOTTING
      SUBROUTINE TRANS(X,Y)
      COMMON /BLOCK/UU,VV,XL,YL,XU,YU,RXL,RYL,RXU,RYU
      UU=((XU-XL)*(X-RXL)/(RXU-RXL))+XL
      VV=((YU-YL)*(Y-RYL)/(RYU-RYL))+YL
```

```
      RETURN
      END
C
C
C  THIS SUBROUTINE LABELS THE GRAPH COORDINATES. IT MUST BE
C  CHANGED WHEN THE PARAMETERS ARE CHANGED
      SUBROUTINE LABLE
      CALL SYMBOL(5.6,-0.7,0.2,'TIME',0.0,4)
      CALL SYMBOL(-0.6,3.5,0.2,'SLIP',90.0,6)
      CALL SYMBOL(6.0,6.5,.2,'RUN UP CURVE  ROTOR #21',0.0,23)
      CALL DUMP
      RETURN
      END
```

```
C
C       THIS PROGRAM CALCULATES THE STEADY STATE PERFORMANCE
C       OF A GENERAL PERMANENT MAGNET SYNCHRONOUS MOTOR
C
C
      REAL IA,ID,IQ,KF,KL,KL1,KW,LMD,LMQ,LS,L1,L2,L3,L4,M
      REAL LDQ,IDC,IQC,I1C,ICD,ICQ,ICD1,ICQ1
      REAL KX,KR
      REAL LQ,N
      DATA POUT1,BR1,BR2,U11,U21/.0,6150.,6150.,1.014,1.014/
      DATA M,DELTA,PI,MM/3.0,0.0,3.14159,0/
      TYPE*,'NRN'
      ACCEPT*,NRN
C
C       MAGNET GEOMOTRY
C
      TYPE*,'L1,L2,L3,L4,LQ '
      ACCEPT*,L1,L2,L3,L4,LQ
      TYPE*,' T1,T2,T3,T4,TQ'
      ACCEPT*,T1,T2,T3,T4,TQ
      TYPE*,' HM1,HM2'
      ACCEPT*,HM1,HM2
C
C            MOTOR CONSTANTS
C
      TYPE*,' G,D,LS,N,KW,P'
      ACCEPT*,G,D,LS,N,KW,P
      TYPE*,' X1,PFW,R1,RC,V'
      ACCEPT*,X1,PFW,R1,RC,V
      TYPE*,'CX'
      ACCEPT*,CX
C
C            LEAKAGE CONSTANTS
C
      TYPE*,' KL,BQ,'
      ACCEPT*,KL,BQ,
C
C     CALCULATIONS     **************
C
C           MAGNET RELUCTANCE
C
      RM1=L1/(U11*2*LS*HM1)
      RM2=L2/(U21*2*LS*HM2)
      RM=(2*RM1*RM2)/(RM1+(2*RM2))
C
C            AIR GAP RELUCTANCE
C
      AG=PI*D*LS/P
      RG=G/AG
C
C            MOTOR CONSTANTS
C
      RPM=120.*60/P
      B=2*RG/RM
```

```
      PHIR=2*LS*(HM1*BR1+HM2*BR2)
      KF=SIN((P*L1)/(2*D))/((P*L1)/(2*D))
      XM=120.*CX*CX*PI*(1.6*M*LS*D/G)*((N*KW/P)**2)*1E-8
C
C     PRINT INPUT PARAMETERS
C
      WRITE(6,1)NRN
      WRITE(6,2)M,P,RPM
      WRITE(6,3)
      WRITE(6,4)N,KW,R1,X1
      WRITE(6,5)
      WRITE(6,6)G,D,LS
      WRITE(6,7)
      WRITE(6,8)L1,L2,L3,L4,LQ
      WRITE(6,9)T1,T2,T3,T4,TQ
      WRITE(6,11)HM1,HM2,BR1
      WRITE(6,12)
      WRITE(6,13)
      WRITE(6,14)
C
C     START ITERATION     **********
C
 10   CONTINUE
      CD=(1-(0.611/(1+(B*KL))))
      CQ=(1-(0.611/(1+BQ)))
      XMD=XM*CD
      XD=XMD+X1
      XMQ=XM*CQ
      XQ=XMQ+X1
C
C          CORE LOSS CORRECTION FACTORS
C
      AD=XMD/RC
      AQ=XMQ/RC
      E=(AD*AQ)/(1+AD*AQ)
C
C          ADJUSTED PARAMETERS
C
      XDC=XD-E*XMD
      XQC=XQ-E*XMQ
      R1C=R1+E*RC
      KR=(R1C-AQ*XDC)/(1+AD*AQ)
      KX=(XQC+AQ*R1C)/(1+AD*AQ)
C
C          ADJUSTED AXIS CURRENTS
C
      E0=((216.*N*KW*PHIR*KF)/(1+B*KL))*1E-8
      C2=XDC*XQC+R1C*R1C
      IDC=(V*(XQC*COS(DELTA)-R1C*SIN(DELTA))-KX*E0)/C2
      IQC=(V*(R1C*COS(DELTA)+XDC*SIN(DELTA))-KR*E0)/C2
      I1C=SQRT((IDC*IDC+IQC*IQC))
C
C          INTERNAL VOLTAGE
C
```

```
      PHI=DELTA+ATAN2(IDC,IQC)
      EIREAL=V-I1C*R1*COS(PHI)-I1C*X1*SIN(PHI)
      EIIM=I1C*R1*SIN(PHI)-I1C*X1*COS(PHI)
      EI=SQRT((EIREAL*EIREAL+EIIM*EIIM))
      DELTAI=DELTA+ATAN2(EIIM,EIREAL)
C
C           CORE LOSS CURRENTS
C
      ICD=(-EI)*(SIN(DELTAI))/RC
      ICQ=EI*((COS(DELTAI))/RC
C
C           NORMAL AXIS CURRENTS
C
      ID=IDC-ICD
      IQ=IQC-ICQ
C
C           FIND ACTUAL LEAKAGE FACTOR
C
      FDM=(0.9*M*ID*N*KW)/P
      H1M=(B*PHIR*RM/L1)/(1+(B*KL))
      H1A=(1.6*FDM/L1)/(1+(B*KL))
      H1=ABS(H1M-H1A)
C
C           FIND PERMEABILITY AND IRON RELUCTANCE
C
      U1=1+(20000/(3.2+H1))
      IF(H1.LT.8.0)U1=2000.
      H2=(H1*L1)/(2*L2)
      U2=1+(20000/(3.2+H2))
      IF(H2.LT.8.0)U2=2000.
      U3=1.0
      H4=H2*L2/L4
      U4=1+(20000/(3.2+H4))
      IF(H4.LT.8.0)U4=2000.
      RL=1/(2*LS*((U1*T1/L1)+(U2*T2/L2)+(U3*T3/L3)+(U4*T4/L4)))
      KL1=1+RM/RL
C
C           FIND Q-AXIS RELUCTANCE
C
      FMQ=(0.9*M*N*KW*IQ)/P
      HQ=(1.6*FMQ)/(LQ*(1+BQ))
      UQ=1+(20000/(3.2+HQ))
      IF(HQ.LT.4.0)UQ=2000.
      RQ=LQ/(LS*UQ*TQ)
      BQ=2*RG/RQ
C
C           CHECK TOLERANCE
C
      TYPE*,KL,KL1
      IF(ABS(KL-KL1).LT.0.01)GO TO 20
      KL=KL1+0.3*(KL-KL1)
      GO TO 10
   20 CONTINUE
C
```

```
C      OUTPUT DATA      ############
C
         DEL=0.087
         DEL=0.0435
         WC=M*(ICD*ICD+ICQ*ICQ)*RC
         PE=M*(IQ*EO+ID*IQ*(XMD-XMQ))
         IF(PE.LT.PFW)DEL=0.0065
         IF(PE.LT.PFW)GO TO 25
         PIN=M*V*I1C*COS(PHI)
         POUT=PE-PFW
         IF(POUT.LT.POUT1)MM=MM+1
         IF(MM .GT.3)GO TO 30
         POUT1=POUT
         EFF=POUT/PIN
         PF=COS(PHI)
         D=DELTA*180/PI
         DI=DELTAI*180/PI
         T=((POUT/746.)*5254.)/(7200./P)
         SF=1+B*KL
C
C        OUTPUT SECTION
C
         WRITE(6,15)D,I1C,POUT,T,EFF,PF,XD,XQ,EO
         IF(ABS(DELTA-2.5).LT.0.01)GO TO 30
   25    DELTA=DELTA+DEL
         GO TO 10
   30    CONTINUE
C
C      OUTPUT FORMATTING       ##############
C
    1    FORMAT('1',35X,'ROTOR NO. ',I3)
    2    FORMAT(' ',' V=575.0 ',' M=',F3.1,'  F=60.0',',  HP=1.0',
        1  '  POLES=',F4.1,'  RPM=',F6.1)
    3    FORMAT(' ',30X,'WINDING INFORMATION')
    4    FORMAT(' ',' N='F5.1,'  KW=',F5.3,'  R1=',F5.2,
        1  '  X1=',F5.2)
    5    FORMAT(' ',30X,'MOTOR GEOMETRY')
    6    FORMAT(' ','G=',F6.4,'  D=',F8.3,'  LS=',F5.2)
    7    FORMAT(' ',30X,'MAGNET GEOMETRY')
    8    FORMAT(' ','L1=',F5.3,'  L2=',F5.3,'  L3=',F5.3,'  L4=',
        1  F5.3,'  LQ=',F6.3)
    9    FORMAT(' ','T1=',F5.3,'  T2=',F5.3,'  T3=',F5.3,
        1  '  T4=',F5.3,'  TQ=',F5.3)
   11    FORMAT(' ','HM1=',F5.3,'  HM2=',F5.3,'  BR1=BR2=',F6.1,
        1  '  HC=7300.0'/)
   12    FORMAT(' ',30X, 'MOTOR PERFORMANCE')
   13    FORMAT(' ','DELTA   ','   IA   ','  POUT   ','  TORQ  ',
        1  ' EFF   ','   PF   ','  XD   ','   XQ   ','  EO   ')
   14    FORMAT(' ','------  ','------  ',' ------  ','------  ',
        1  '------  ','------  ','------  ','------  ','------')
   15    FORMAT(' ',F6.2,2X,F8.2,2X,F7.1,2X,F5.2,2X,F5.3,2X,
        1  F5.3,2X,F6.2,2X,F6.2,2X,F6.2)
         STOP
         END
```

APPENDIX B

DETAILED TEST RESULTS

Table A-1. Measured Starting Torque

Rotor 15		Rotor 16	
Voltage [v]	Torque [lb-in]	Voltage [v]	Torque [lb-in]
208.0	3.2	159.0	2.1
253.0	6.5	245.0	5.2
335.0	8.2	315.0	10.4

Rotor 21		Rotor 22	
Voltage [v]	Torque [lb-in]	Voltage [v]	Torque [lb-in]
200.3	6.8	181.0	5.9
248.7	9.7	270.6	11.8
317.8	14.6		
374.7	22.2		

Table A-2. Measured Pull-out Torque

Voltage [v]	Rotor 15 [lb-in]	Rotor 16 [lb-in]	Rotor 21 [lb-in]	Rotor 22 [lb-in]
250	8	7.8	21	22
300	11.8	11.6	30	27
350	15.6	15.0	40	36
400	20.6	19.0	51	44
450	25.2	22.6	-	-
500	30.0	26.9	-	-
550	35.0	31.8	-	-

Table A-3. Measured Moment of Inertia

a) Rotor type I (typical)

Rotor weight - 5.938 lb.	Unbalance length - 1.00 in.
Unbalance weight - 0.625 lb	Unbalance width - 0.75 in.
Rotor diameter - 2.697 in.	Length a (see fig.) - 0.344 in.
Shaft diameter - 0.687 in.	Length b (see fig.) - 1.724 in.

Average period of oscillation - 0.8006 sec.
Calculated moment of inertia - 1.407×10^{-3} kg-m^2

b) Rotor type II (typical)

Rotor weight - 8.188 lb.	Unbalance length - 1.00 in.
Unbalance weight - 0.906 lb.	Unbalance width - 1.10 in.
Rotor diameter - 4.141 in.	Length a (see fig.) - 0.312 in.
Shaft diameter - 0.624 in.	Length b (see fig.) - 2.571 in.

Average period of oscillation - 0.8544 sec.
Calculated moment of inertia - 3.092×10^{-3} kg-m^2

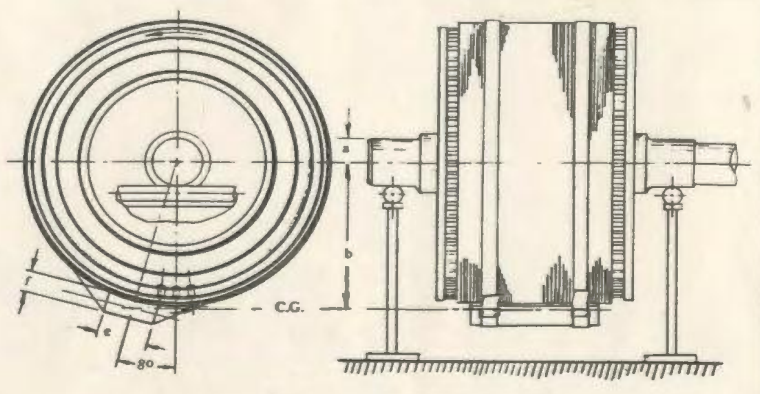

RECTANGULAR UNBALANCE ADDED TO INDUCTION ROTOR

Table A-4. No load tests results

a) Type I (The angle δ is given an arbitrary scale)

Voltage	Rotor 15			Rotor 16		
	I_a	P_T	δ	I	P_T	δ
[V]	[A]	[w]	[°]	[A]	[w]	[°]
575	.680	142.5	72	.792	155.5	39
500	.412	98.8	75	.477	106.7	48
450	.333	82.0	77	.367	88.3	51
400	.279	72.5	78	.300	75.0	49
350	.200	62.7	78	.249	61.3	48
300	.123	58.8	75	.198	53.1	47
250	.202	64.8	70	.123	48.8	47
200	.406	79.5	65	.192	49.2	48
150	.725	107.9	56	.453	57.0	54

b) Type II (the angle δ is given an arbitrary scale)

Voltage	Rotor 21			Rotor 22		
	I_a	P_T	δ	I_a	P_T	δ
[V]	[A]	[w]	[°]	[A]	[w]	[°]
575	1.172	196.0	44	1.099	178.5	95
500	-	-	-	0.666	107.5	95
450	0.480	89.8	45	0.500	81.0	94
400	0.319	67.8	47	0.388	63.3	93
350	0.152	59.3	46	0.281	51.2	90
300	0.184	60.0	47	0.133	41.4	87
250	-	-	-	0.187	38.2	86
200	-	-	-	0.536	51.1	87
150	-	-	-	0.947	77.8	90

Table A-5. Rotor 15 flux linkage test

I [A d.c.]	$\int_0^t (V_A - V_B)dt$	K	flux linkage (ψ)	$X_d = \left[\frac{R_3 - R_4}{R_4}\right]\left[\frac{\psi}{I}\right](\omega)$ [Ω]
0.2	0.128	0.5	0.064	181.6
0.4	0.198	1	0.198	234.4
0.6	0.200	2	0.400	323.6
0.8	0.257	2	0.514	304.3
1.0	0.302	2	0.604	286.5
1.2	0.068	10	0.680	268.4
1.4	0.074	10	0.740	250.3
-0.2	0.111	0.5	0.055	131.4
-0.4	0.130	1	0.130	153.9
-0.6	0.098	2	0.196	154.7
-0.8	0.119	2	0.238	140.9
-1.0	0.139	2	0.278	131.7
-1.2	0.037	10	0.370	146.0
-1.35	0.039	10	0.390	136.8

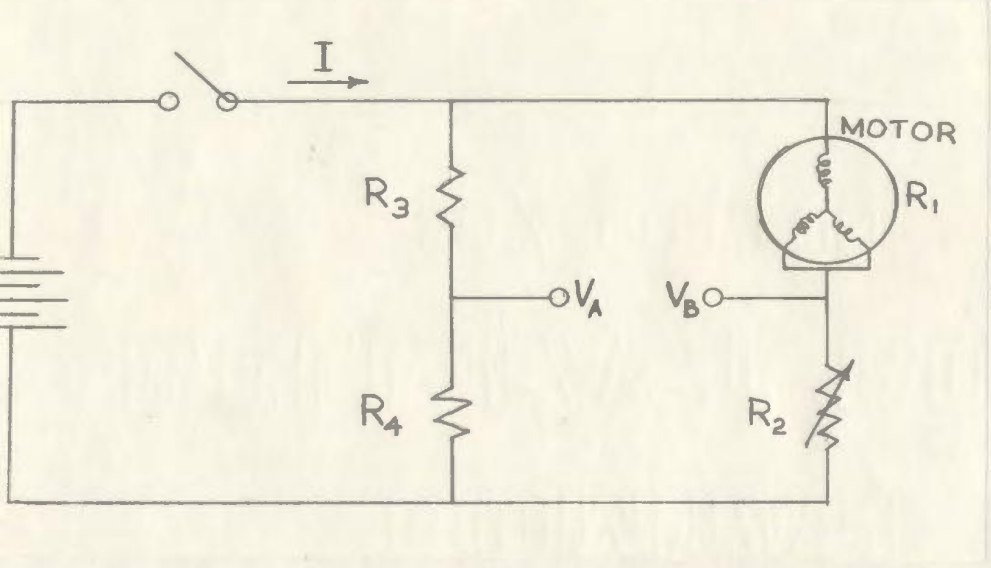

R_3 = 306 Ω

R_4 = 1194 Ω

R_1 ≃ 23 Ω

R_2 = 75-123Ω

APPENDIX C

INSTRUMENT SCHEMATICS AND COMPONENT VALUES

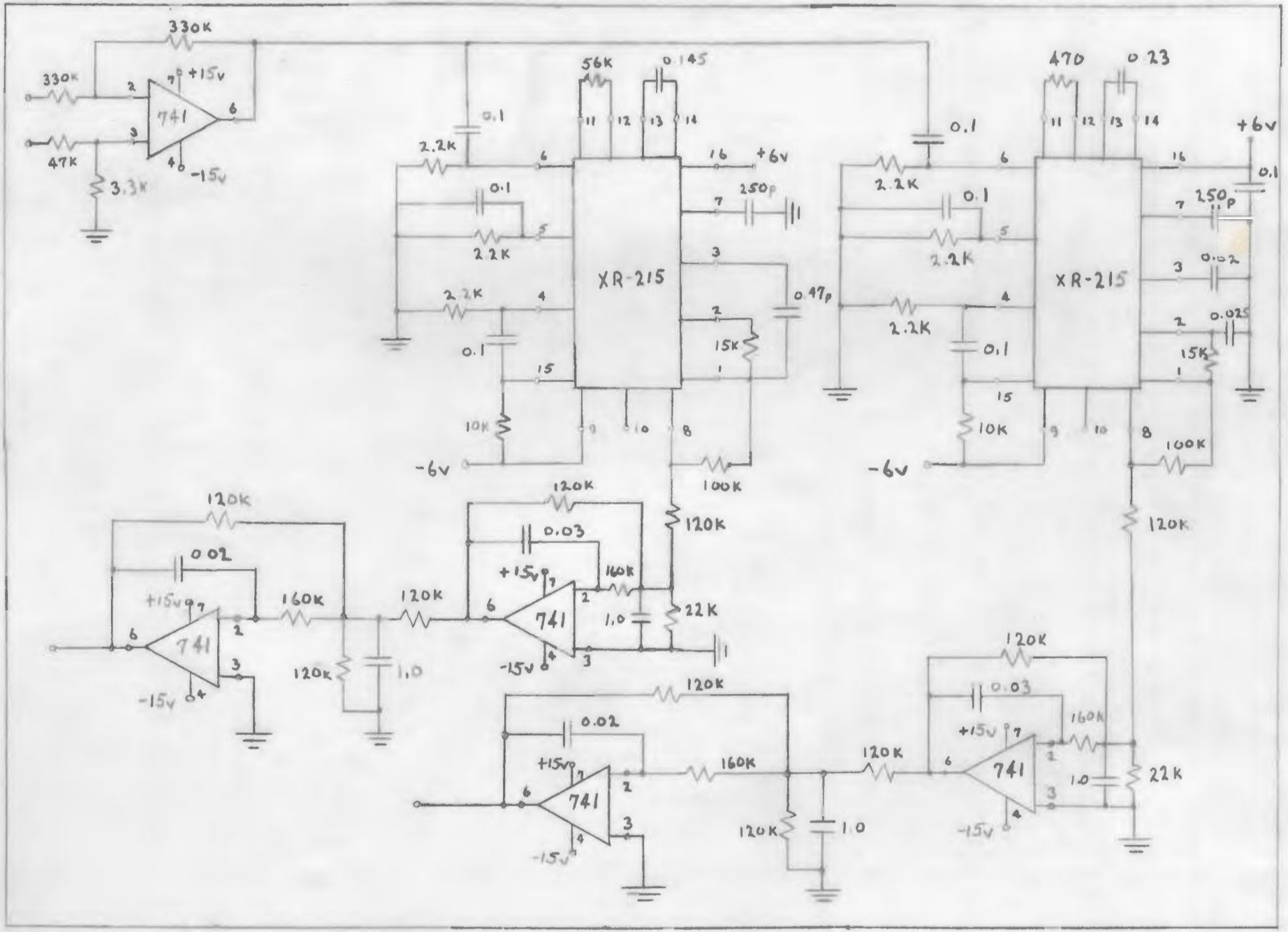
330K
330K
+15v
741
47K
3.3K
-15v
56K
0.145
0.1
2.2K
+6v
250p
XR-215
0.47p
15K
10K
-6v
100K
470
0.23
0.02
0.025
120K
0.03
160K
22K
1.0
0.002

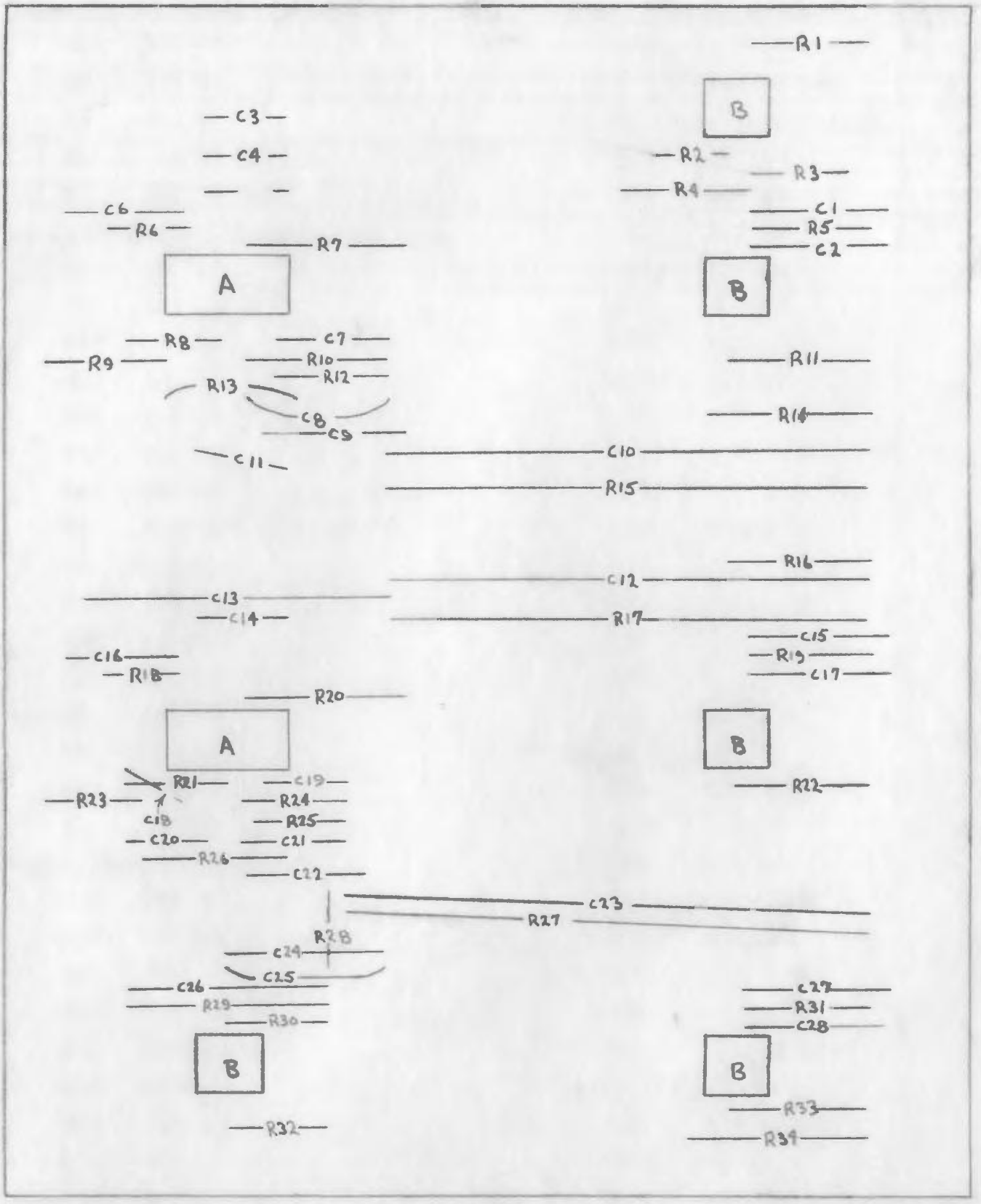
R1
B
C3
C4
R2
R3
R4
C6
R6
C1
R5
C2
R7
A
B
R8
C7
R9
R10
R12
R11
R13
C8
R14
C9
C10
C11
R15
R16
C12
C13
C14
R17
C15
C16
R19
R18
C17
R20
A
B
R21
C19
R22
R23
R24
C18
R25
C20
C21
R26
C22
C23
R27
R28
C24
C25
C26
C27
R29
R31
R30
C28
B
B
R33
R32
R34

Input Pulse Shaping Buffer

R1	330 kΩ
R2	330 kΩ
R3	3.3 kΩ
R4	47 kΩ
B	741 op amp

Small Deviation Phase-Locked Loop

R6	10 kΩ
R7	5.6 kΩ
R8	2.2 kΩ
R9	15 kΩ
R10	2.2 kΩ
R12	2.2 kΩ
R13	100 kΩ
C3	0.02 μF
C4	0.025 μF
C5	0.1 μF
C6	0.1 μF
C7	250 μF
C8	0.1 μF
C9	0.1 μF
C11	0.47 μF
A	XR-215

Small Deviation Filter 1

R16	120 kΩ
R17	22 kΩ
R19	120 kΩ
R22	160 kΩ
C12	1.0 μF
C15	0.02 μF
C17	0.01 μF
B	741 op amp

Small Deviation Filter 2

R5	120 kΩ
R11	160 kΩ
R14	120 kΩ
R15	120 kΩ
C1	0.01 μF
C2	0.01 μF

Small Deviation Filter 2 (cont)

C10	1.0 μF
B	741 op amp

Run Up Phase-Locked Loop

R18	10 kΩ
R20	470 kΩ
R21	2.2 kΩ
R23	15 kΩ
R24	2.2 kΩ
R25	2.2 kΩ
R26	100 kΩ
C13	0.1 μF
C14	0.23 μF
C16	0.1 μF
C18	0.025 μF
C19	250 μF
C20	0.02 μF
C21	0.1 μF
C22	0.1 μF
A	XR-215

Run Up Filter 1

R28	120 kΩ
R29	22 kΩ
R30	120 kΩ
R32	160 kΩ
C24	0.02 μF
C25	0.01 μF
C26	1.0 μF
B	741 op amp

Run Up Filter 2

R27	120 kΩ
R31	120 kΩ
R33	160 kΩ
R34	120 kΩ
C23	1.0 μF
C27	0.01 μF
C28	0.01 μF
B	741 op amp